(9)

AD-A145 981

ADVANCED LPI INTERCEPT DETECTOR RESEARCH

Axiomatix

DTIC FILE COPY

DTIC
ELECTE
SEP 26 1984
S D
B

84 7 23 038

ADVANCED LPI INTERCEPT DETECTOR RESEARCH

FINAL REPORT

Contract No. N00014-82-C-0585

Prepared for

Office of Naval Research

Prepared by

Dr. Andreas Polydoros

With Contributions From

Dr. J. K. Holmes
Dr. K. T. Woo

Axiomatix
9841 Airport Blvd., Suite 912
Los Angeles, California 90045

Axiomatix Report No. R8403-1
March 26, 1984

TABLE OF CONTENTS

APPENDICES

LIST OF FIGURES

1.0 OVERVIEW

This report constitutes the first phase of research conducted by Axiomatix wherein our aim was to derive, evaluate and compare various detector structures whose purpose is to intercept a spread-spectrum communication transmitter. The transmitter under surveillance employs a variety of modulation/spreading/transmission techniques which are invariably assumed to emit the message-bearing signal in deep background noise or interference. Thus, the challenging task of the intercepting detector is to reveal as best he can any transmission of the unfriendly spread waveform in the presence of a strongly obscuring noisy environment.

Naturally, the degree of success achieved by the interceptor when detecting the presence of the communicator's spread signal depends on the amount of information available to him regarding the structure of that signal. At one extreme, the interceptor's most fortunate situation would be to acquire the spreading code itself ("crack" the code). This being too demanding, he must settle for less, such as approximate knowledge of the signal's carrier center frequency, code rate, code epoch, spreading bandwidth, etc., or a subset thereof. At the other extreme, he might know almost nothing*; in which case, he could resort to a simple energy discriminator device ("radiometer") since it is, on many occasions, a low-SNR asymptotically optimal detector. In this report, our main interest is to investigate the possibility that the interceptor could do better by optimally processing whatever information is available to him between the two extremes cited above.

The detectability of the primary candidates for low-probability-of-intercept (LPI) waveforms, such as direct-sequence (DS), frequency-hopping (FH), time-hopping (TH) and their hybrids, is customarily related to two factors: (1) performance level of the interceptor's detector whose only function is to monitor† the communicated messages and, (2) amount of signal processing (i.e., complexity) associated with such performance. Thus, the exploitability of a spread-spectrum waveform is measured in terms of the complexity required of the interceptor's receiver, so that it can perform such surveillance, as well as in terms of the level of its power spectral density (PSD) and the resulting probability of intercept.

---

*Approximate spectral band location is a minimum prerequisite for any interceptor.

†Intercepting/jamming combinations would also be of interest at a more advanced stage of study.

In subsequent sections, it will be shown that the detectability (exploitability) of a spread signal is greatly dependent on the interceptor's knowledge regarding the form of both the waveform and the interference. In other words, one should know not only the spreading format used (plus, possibly, some other parameters*), but it is also very helpful to be able to identify the kind of background noise or interference involved. Although most of this report deals with white Gaussian noise as the dominant form of (omnipresent) interference, a case is made in the final section about the impact of nonwhite (random tones, in particular) interference. It will be shown in Sections 3 through 5.1 that, when white noise is the only deterrent, the gains achieved by intelligent processing of the received waveform can vary from modest to significant (always as compared to the performance of a radiometer), depending on the scenario at hand. However, when random interfering tones are present and a DS or a hybrid FH/DS is detected, those gains become impressive (many tens of decibels, for example). For details, see section 5.2.

In searching for those structures which perform the aforementioned tasks, we start from the optimal solutions, as derived from applying the optimal likelihood-ratio rule. The results assume a good deal of knowledge about the signal parameters (although never the spreading code itself) and could thus become rather academic in most practical situations. Furthermore, they typically suffer from the common symptom of prohibitive implementational complexity. Thus, it is important to consider suboptimal structures and evaluate their relative loss with respect to the (unattainable) optimal performance. This has indeed been the spirit which permeated the present work.

The report is organized as follows: In section 2, we classify the various receivers and briefly lay the theoretical groundwork for evaluating the forthcoming detector structures. In Sections 3. 4 and 5, we develop the theory for DS, TH and FH signals, respectively†. This is also the order by which the relative gains from sophisticated receivers seem to increase when faced by white noise. In particular, a two-reception, synchronous, coherent DS detector can result in a gain of up to 4.5 dB in signal-to-noise ratio (SNR) above the radiometer. Each of the three aforementioned features of this detector contributes approximately 1.5 dB; however, each also imposes strenuous conditions on the

---

*See Section 2 for a detailed discussion.

†Let us note that the hybrid FH / DS of section 5.2 can also be thought of as a DS signal in colored interference.

system implementation. This kind of modest relative benefit must be attributed to the "noise-like" appearance of a high-rate DS code, which makes it hard to distinguish from wideband thermal noise. On the other hand, TH or FH can look spectrally different from DS, so that higher gains can be expected; this is documented in Sections 4 and 5. We note, however, that those gains are typically associated with excessive complexity; in which case, implementation becomes the cardinal issue. This prompted us to investigate suboptimal, but still very efficient, schemes which are suggested by today's technology (e.g., real-time autocorrelation devices). The application of such novel ideas in Section 5 has established conditions (both by analysis and simulation), under which one can anticipate significant-to-impressive gains over the radiometer, even in the presence of white noise. It is shown in Section 5 that a proper measure of performance improvement (defined in section 5.1) is proportional to γ_H^2, where γ_H is the hop SNR of an FH system. The proportionality constant depends on algorithmic parameters, but is independent of the assumed tactical scenario. Thus, by properly translating γ_H into physical parameters (i.e., transmitter/intercepter distance, signal power, antenna gains, etc.), one can arrive at certain threshold values in the proximity of which the signal becomes highly detectable. Although this would be the bottom line of a global interception analysis, this task will not be undertaken here, as it is highly scenario dependent.

In conclusion, the findings of this report can serve as broad analytical guidelines for the determination and evaluation of a variety of detectors in the context of LPI interception. They also serve to motivate a further pursuit of techniques which, in light of today's (and tomorrow's) technology, emerge as very appealing, sophisticated and promising alternatives to the simplistic solutions of the past.

2.0 DETECTOR CLASSIFICATION AND PERFORMANCE MEASURES

In this section, we first classify a variety of receivers which an interceptor could employ to detect the presence of a wideband (spread) signal imbedded in white and/or nonwhite interference. Furthermore, we discuss some approximate measures of performance upon which the assessment for any detector's merit is based. We should note here that such measures give a quantitative feeling of what can be expected from certain detectors but do not provide any indication of the structure's implementational complexity, which is definitely an important parameter. Therefore, a total evaluation of the system effectiveness should incorporate that as a separate, but indispensable, consideration.

The classification attempted here is summarized in Figure 2.1. Wideband detectors can first be classified as optimal or suboptimal. We term "optimal" those structures which result from a straightforward application of the generalized likelihood ratio theory to this problem and invoke a number of assuptions regarding the signal structure. For instance, optimal solutions typically assume knowledge of certain parameters (code rate or hopping rate, SNR, carrier frequencies, etc.) and average over the unknown ones (timing epochs, true hopping or code sequences, etc.). Since, however, optimal structures are often hard to implement, one resorts to "suboptimal" solutions whereby either one (or more) assumptions are removed or certain "atypical" nonlinearities, such as the $\ell n \cosh(\cdot)$ function, are substituted by simpler ones as, for instance, a square-law device.

A second classification results from the nature of the spread-spectrum signal for which the intercepting device is designed, so it can be a DS, FH, TH or hybrid detector. Also, DS and TH detectors can be coherent or noncoherent, depending on whether or not the carrier phase is known. FH detectors are assumed to be noncoherent from hop to hop due to the nature of the communicating channel and the transmitter wideband FH synthesizers.

The presence or absence of timing (epoch) information about the spreading code distinguishes detectors as synchronous or asynchronous. It is clear that timing is initially unavailable since the detector does not even know if the signal is there; hence, asynchronous structures naturally attract more practical interest. However, synchronous and/or coherent detectors will also be considered--not only because they provide useful upper bounds in performance--but also because of the conceptual possibility of improved detector structures,

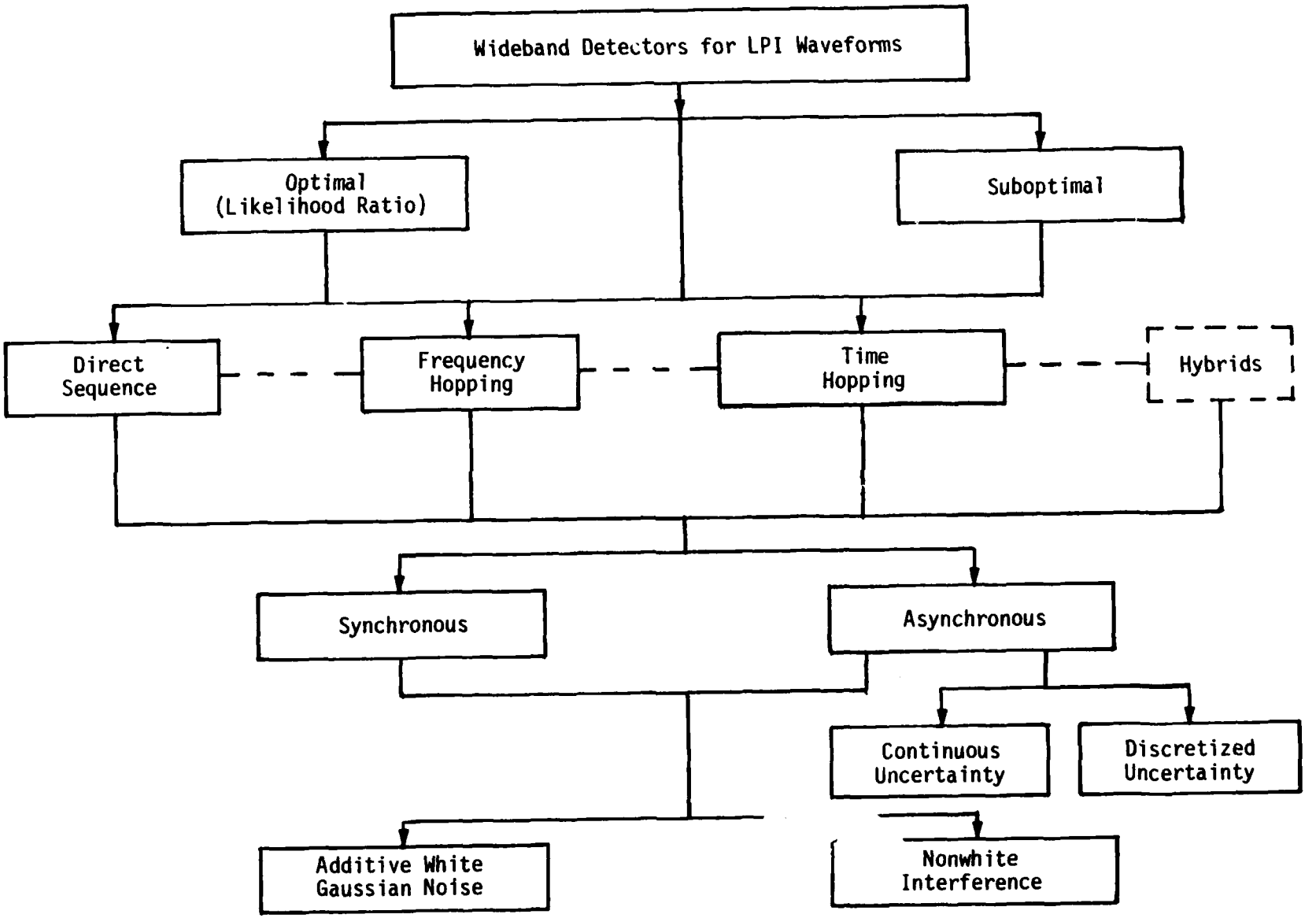

Figure 2.1. Classification of LPI Detectors

aided by the recursive estimation of pertinent parameters [8]. Furthermore, by quantizing the continuous-epoch uncertainty region into an adequate finite number of points, matched-detector structures can be devised that are synchronized to each of those levels and whose outputs are combined to yield the final decision variable. Thus, since the maximum code-epoch uncertainty equals a chip time*, one concludes that good nonsynchronous detectors can be constructed from combinations of a few synchronous ones. More discussion on this topic is provided in later sections.

Finally, we classify the detectors according to whether they expect to operate in the presence of white (and typically Gaussian, such as thermal noise) or nonwhite interference. The maximum-likelihood approach renders itself to the first case most easily, while its formulation is cumbersome for the second. Accordingly, the theory is fairly mature for AWGN interference, while it is still at the exploratory level for scenarios which call for more complicated interference forms.

Let us now briefly discuss analytical ways for measuring performance in the present context. It is well known [3] that, under the common detection-performance criteria (most notably, the Neyman-Pearson philosophy), generalized likelihood ratios yield optimal hypothesis-testing solutions, and performance is measured by the resulting pair of detection and false-alarm probabilities (P_D, P_{FA}). Furthermore, it can be shown that, in many cases of practical interest, the overall likelihood ratio (LR) can be expressed as the product of individual LR's due to the statistical independence of successive code chips (random DS code) or hopping slots (TH or FH). When the true model for the problem does not allow for such assumptions (as in the case of a random, but fixed, carrier phase), the resulting LR is too complicated for either analysis or implementation†. The performance of such decision schemes is assessed by bounding arguments (see the following sections) so that the product LR can always be thought of as the analytical cornerstone. Since the log-likelihood ratio (LLR) is not only theoretically equivalent, but also more convenient to implement than an LR (it turns products into sums), it will serve as our point of departure.

The number of terms entering the summation of the LLR is typically large--it equals the total number of chips (DS) or time slots (TH) or frequency slots (FH) observed. Therefore, it is reasonble to conclude, via a central-limit

*This clearly assumes a purely random code sequence for which a full chip time shift corresponds to another realization of the same stochastic process.

†In addition, it can be argued that the superposition of random data on DS or TH, such as PSK modulation, invalidates the notion of a constant carrier phase.

type of argument, that the distribution of the resulting LLR is approximately Gaussian under either hypothesis. This constitutes the basic assumption upon which performance is derived in this report. In other words, the pair (P_D, P_{FA}) is expressed in terms of the Gaussian integral function

$$Q(x) = \frac{1}{\sqrt{2\pi}} \int_x^\infty \exp\left\{-z^2/2\right\} dz \tag{2-1}$$

and its inverse $Q^{-1}(\cdot)$; furthermore, using the approximation that the LLR possesses the same variance under either hypothesis, it is easily shown that performance is quantified by the distance d, defined as

$$d = Q^{-1}\left[P_{FA}\right] - Q^{-1}\left[P_D\right] \tag{2-2}$$

which is a function of the decision rule and the system parameter values.

Peterson et al [3, section 4.9] have invoked the Gaussian assumption about the LLR in order to show that d^2 is equal to the difference of the means of the LLR under the two hypothesis (hence, the notion of distance) and is also equal to its variance. Most important, d can be related to the original product LR Λ via*

$$d^2 = \ell n\left(\mathscr{E}\left\{\Lambda\middle|^2 H_0\right\}\right) = \ell n\left(1 + \mathrm{var}\left\{\Lambda\middle|H_0\right\}\right) \tag{2-3}$$

where the second equality results from the fact that $\mathscr{E}\left\{\Lambda\middle|H_0\right\} = 1$ for every LR. Therefore, (2-3) measures the performance of any LLR†, which could include arbitrary memoryless nonlinearities (indeed, the optimal ones). Since many of them are hard to implement, however, it is of interest to examine the penalty in performance incurred when going from optimal to suboptimal decision rules just by simplifying (or approximating) those nonlinearities. Clearly, the suboptimal rules are also associated with some distance d, as per (2-2), which we shall denote by d_{appr} (approximate) as opposed to the "exact" distance d_{ex} derived from (2-3). The other approximations nonwithstanding, the difference between d_{appr} and d_{ex} should signify the loss paid for implementational simplicity. In addition, d_{appr} will serve as the yardstick when comparing the approximate rules resulting from various other assumptions (or the lack thereof).

*Here, $\mathscr{E}\{\cdot\}$ and $\mathrm{var}\{\cdot\}$ stand for the statistical mean and variance, respectively.

†Always within the Gaussian assumption.

3.0 DETECTION OF DIRECT-SEQUENCE SIGNALS IN THE PRESENCE OF AWGN

In this section, we consider and analyze wideband detectors for DS waveforms. It will be assumed throughout that the receiver has knowledge of the carrier frequency and code rate and that the code is biphase modulating the carrier. For the carrier phase, the two possibilities of it being known (coherent detection) and unknown (noncoherent detection) are examined separately in sections 3.1 and 3.2, respectively. A common assumption in both of these sections is that the detectors are synchronous, i.e., the code chip-timing epoch is known. In most practical situations, this is rather unrealistic; the synchronous results can then be thought of as upper bounds on the performance of any asynchronous detector. Furthermore, by quantizing the continuous-epoch uncertainty region into an adequate finite number of points, matched-detector structures can be devised which are synchronized to each of these levels and whose outputs are combined to yield the final decision variable. More discussion on the cost of asynchronism is given in section 3.3. Section 3.4 discusses some gains derived from combining two independent receptions, ranks the performance of the aforementioned detectors and compares them to that of the radiometer.

In order to introduce some notation, let the high-rate, ±1-valued random spreading code c(t) be represented by

$$c(t) = \sum_{n=-\infty}^{\infty} c_n \, p(t - nT_c - \varepsilon T_c) \qquad (3\text{-}1)$$

where p(t) is a unit pulse of duration T_c seconds and $\{c_n\}_{-\infty}^{\infty}$ is a sequence of independent, identically distributed) (iid) random variables (rv's), with $Pr\{c_n = 1\} = Pr\{c_n = -1\} = 0.5$. Furthermore, the chip epoch is modeled by the rv ε, uniformly distributed over (0,1). The waveform observed by the detector is therefore given by

$$r(t) = \begin{cases} \sqrt{2S}\, c(t) \cos(\omega_0 t + \phi) + n(t) & (H_1) \\ n(t) & (H_0) \end{cases} \qquad (0 \leq t \leq T) \qquad (3\text{-}2)$$

where S, ω_0 and ϕ are the average signal power, carrier radian frequency and carrier phase, respectively, under H_1, and n(t) is bandpass AWGN with one-sided power spectral density (PSD) of N_0 W/Hz. The observation time is T seconds, which we assume to be an integer multiple of the chip time, i.e., $T = NT_c$; N a positive integer. Such an assumption is the least restrictive since, in practice, N is generally a large number (of the order of hundreds or higher). However, a somewhat stronger restriction is embedded in (2), namely, the assumption that, under hypothesis H_1, the signal is present during the whole observation interval. That excludes the possibility of the signal either starting or ending at any random time in (0,T). Still, such a formulation is important because it provides meaningful and fairly simple comparative conclusions which (a) would otherwise be obscured by mathematical complexities and, (b) can be argued to extend to more general models.

In terms of the above notation, a synchronous detector implies that ε is identically zero, while a coherent one means that ϕ is known. The detector for which ϕ is unknown but constant over the observation interval (0,T) will be called carrier noncoherent*. For computational purposes, we also consider the *fictitious chip-noncoherent* detector, where phase is assumed to change randomly from chip to chip. Although this is totally unrealistic, it is discussed here because its readily derived performance serves as a very useful lower bound to the performance of the optimal, carrier-noncoherent receivers, which are difficult to analyze.

3.1 Synchronous Coherent Detectors

When both the random phase ϕ and random chip epoch ε are assumed known, the detector is asked to perform the following composite hypothesis testing problem: Decide between the alternatives H_0 and H_1, where

$$r(t) = \begin{cases} \sqrt{S}\, c(t) + n_I(t) & (H_1) \\ n_I(t) & (H_0) \end{cases} \qquad (0 \leq t \leq NT_c) \qquad (3\text{-}3)$$

Hypothesis H_1 is composite because it contains all possible patterns that the code can assume in NT_c seconds. Although we consider only random codes (in

*This clearly assumes that the observation duration is well within the coherence time of the spread-spectrum channel.

which case, there are exactly $M = 2^N$ such patterns), some of the steps below would also be valid for deterministic codes. The subscript I in $n_I(t)$ indicates that only the inphase component of the noise contributes, with a flat two-sided PSD of $N_0/2$ W/Hz. At this point, we should emphasize that the problem formulation is reminiscent of, but not identical to, the M-ary communication problem of detecting the presence of one of $M = 2^N$ possible waveforms embedded in noise. In the latter case, we know a priori that one of the signals is present, but we don't know which one it is. In the current case, our only interest is detecting the presence of <u>any</u> one of the M equilikely candidate waveforms without identifying it.

Starting with classical well-known results about detectors designed to minimize the probability of error [3], it follows that the optimal detector performs a generalized likelihood ratio threshold comparison. Specifically, the generalized likelihood ratio is

$$\Lambda(r(t)) = \sum_{i=1}^{2^N} \frac{f\left(r(t)|H_1, c_i(t); 0 \leq t \leq T\right)}{f\left(r(t)|H_0\right)} \underset{H_0}{\overset{H_1}{\gtrless}} \Lambda_0 \tag{3-4}$$

where $f(r(t)|H_i)$ indicates the conditional likelihood functional of the hypothesis H_i, given the observation $r(t); 0 \leq t \leq T$, and $c_i(t)$ is the <u>i</u>th pattern out of the 2^N total possible. For the case of AWGN, the generalized likelihood ratio in (3-4) reduces to the following form:

$$\Lambda(r(t)) = \frac{\exp\left\{-N\gamma_c\right\}}{2^N} \sum_{i=1}^{2^N} \exp\left\{\frac{2\sqrt{S}}{N_0} \int_0^{NT_c} r(t)\, c_i(t)\, dt\right\}$$

$$= \frac{\exp\left\{-N\gamma_c\right\}}{2^N} \sum_{i=1}^{2^N} \exp\left\{\frac{2\sqrt{S}}{N_0} \sum_{j=1}^{N} r_j\, c_{ij}\right\} \underset{H_0}{\overset{H_1}{\gtrless}} \Lambda_0 \tag{3-5}$$

where

$$\gamma_c = \frac{ST_c}{N_0} \tag{3-6}$$

is the predetection (or chip) SNR, c_{ij} is the jth chip of the ith pattern, and r_j is given by

$$r_j \triangleq \int_{(j-1)T_c}^{jT_c} r(t)\, dt \tag{3-7}$$

The expression in (3-5) can be further simplified using certain symmetries and identities. Indeed, it is shown in Appendix A that (3-5) is expressible as

$$\Lambda(r(t)) = \prod_{i=1}^{N} \exp\{-\gamma_c\} \cosh\left(\frac{2\sqrt{S}}{N_0} r_j\right) \underset{H_0}{\overset{H_1}{\gtrless}} \Lambda_0 \tag{3-8a}$$

or, equivalently,

$$\ell n\Lambda(r(t)) = -N\gamma_c + \sum_{i=1}^{N} \ell n \cosh\left(\frac{2\sqrt{S}}{N_0} r_j\right) \underset{H_0}{\overset{H_1}{\gtrless}} \ell n\, \Lambda_0 \tag{3-8b}$$

We note that (3-8) could have been derived directly based on the statistical independence of successive chips and the AWGN (see [6]). The somewhat different approach preferred here, however, is more easily generalized to models where successive chips are not independent (c.f. section 3.2).

A structure implementing the rule (3-8) is shown in Figure 3.1 with $f(x) = \ell n \cosh(x)$. Its operation is as follows: A time-synchronized, chip-by-chip, coherent integration of the received waveform r(t) results in a sequence of rv's r_i, each of which is separately processed by the memoryless nonlinearity $f(\cdot)$, then summed over the desired length of N chips to produce the decision statistic. Let us notice that the optimal $f(\cdot)$ is an even function, which can be be interpreted as the receiver's attempt to compensate for his lack of knowledge regarding the sign of each integrated code chip.

The mean under H_1 of the random argument of the $\ell n \cosh(\cdot)$ function in (3-8b) is $2\gamma_c$, which is also its variance under H_0. Therefore, for typical predetection SNR values below -10 dB or so, the approximation $\ell n \cosh(x) \approx x^2/2$ is applicable; in which case, (3-8) reduces to the approximate (suboptimal) rule

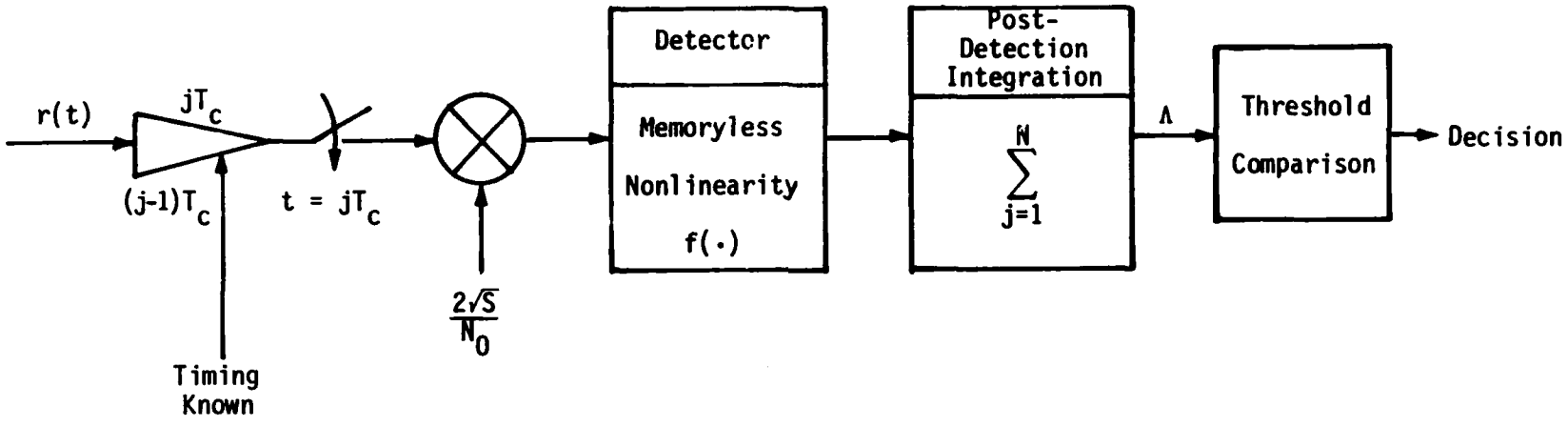

Figure 3.1. Optimal Synchronous-Coherent Receiver for the Detection of Direct-Sequence Waveforms

$$\Lambda' = \sum_{j=1}^{N} r_j^2 \underset{H_0}{\overset{H_1}{\gtrless}} \Lambda_0' \tag{3-9}$$

Since the aforementioned approximation of the $\ell n \cosh(x)$ function becomes increasingly tight as $x \to 0$, it follows that (3-9) is asymptotically optimal as $\gamma_c \to 0$.

Within the theoretical framework of Section 2, the performance of (3-9) is easily derived. The mean and variance of Λ' are given by (for proof, see Appendix B)

$$\mathcal{E}\{\Lambda' | H_k\} = N(N_0 T_c)\left(\tfrac{1}{2} + \gamma_c \delta_{k1}\right) \qquad (k=0,1) \tag{3-10a}$$

and

$$\mathrm{var}\{\Lambda' | H_k\} = N(N_0 T_c)^2 \left(\tfrac{1}{2} + 2\gamma_c \delta_{k1}\right) \tag{3-10b}$$

respectively, where δ_{k1} is the Kronecker delta

$$\delta_{k1} = \begin{cases} 1 , & k=1 \\ 0 , & k=0 \end{cases} \tag{3-10c}$$

Therefore, P_D and P_{FA} are related by

$$P_D \approx Q\left[\frac{Q^{-1}[P_{FA}] - a\sqrt{N}\gamma_c}{\sqrt{1 + b\gamma_c}}\right] \tag{3-11}$$

with

$$\boxed{a = \sqrt{2} \; ; \; b = 4} \qquad \text{(Synchronous coherent detector)} \tag{3-12a}$$

Since $b\gamma_c$ is typically much less than 1, (3-11) can be combined with (2-2) to yield

$$d_{appr} \approx a\sqrt{N}\gamma_c \tag{3-12b}$$

We note that performance is dictated by the product $\sqrt{N}\,\gamma_c$, which is typical of schemes employing post-detection integration. In contrast, detection of a known waveform would involve the factor $\sqrt{N\gamma_c}$ (see section 3.5); the losses in performance due to the generalized test (since the signal pattern is unknown) for low values of SNR are evident by comparison.

Equation (3-11) has been plotted in Figure 3.2 for various values of N and P_{FA}. In terms of the overall observation time T and the null-to-null spread-spectrum bandwidth $W_s = 2T_c^{-1}$ Hz, (3-12) can be rewritten to establish the required $(S/N_0)_{req}$ in order to achieve the performance level d_{appr} as

$$\left(\frac{S}{N_0}\right)_{req} \approx \left(\frac{1}{2}\right)\sqrt{\frac{W_s}{T}}\, d_{appr} \tag{3-13}$$

On the other hand, the distance d_{ex} for the exact rule (3-8) can also be derived. Let $y_j \triangleq 2\sqrt{S}\, r_j/N_0$. Under H_0, y_j is a zero-mean Gaussian rv with variance $\sigma_y^2 = 2\gamma_c$. Using the fact that $\mathcal{E}\{\cosh(y_j)\} = \exp\{\sigma_y^2/2\}$ in conjunction with (3-8a) and (2-3) results in

$$d_{ex} = \sqrt{N\ \ell n\ \cosh(2\gamma_c)} \tag{3-14}$$

For small x, $\ell n\ \cosh(x) \approx x^2/2$, which, upon substitution in (3-14), verifies that $d_{ex} \to d_{appr}$ of (3-12) as $\gamma_c \to 0$. In conclusion, approximate rule (3-9) is well suited for the low-predetection SNR range of interest.

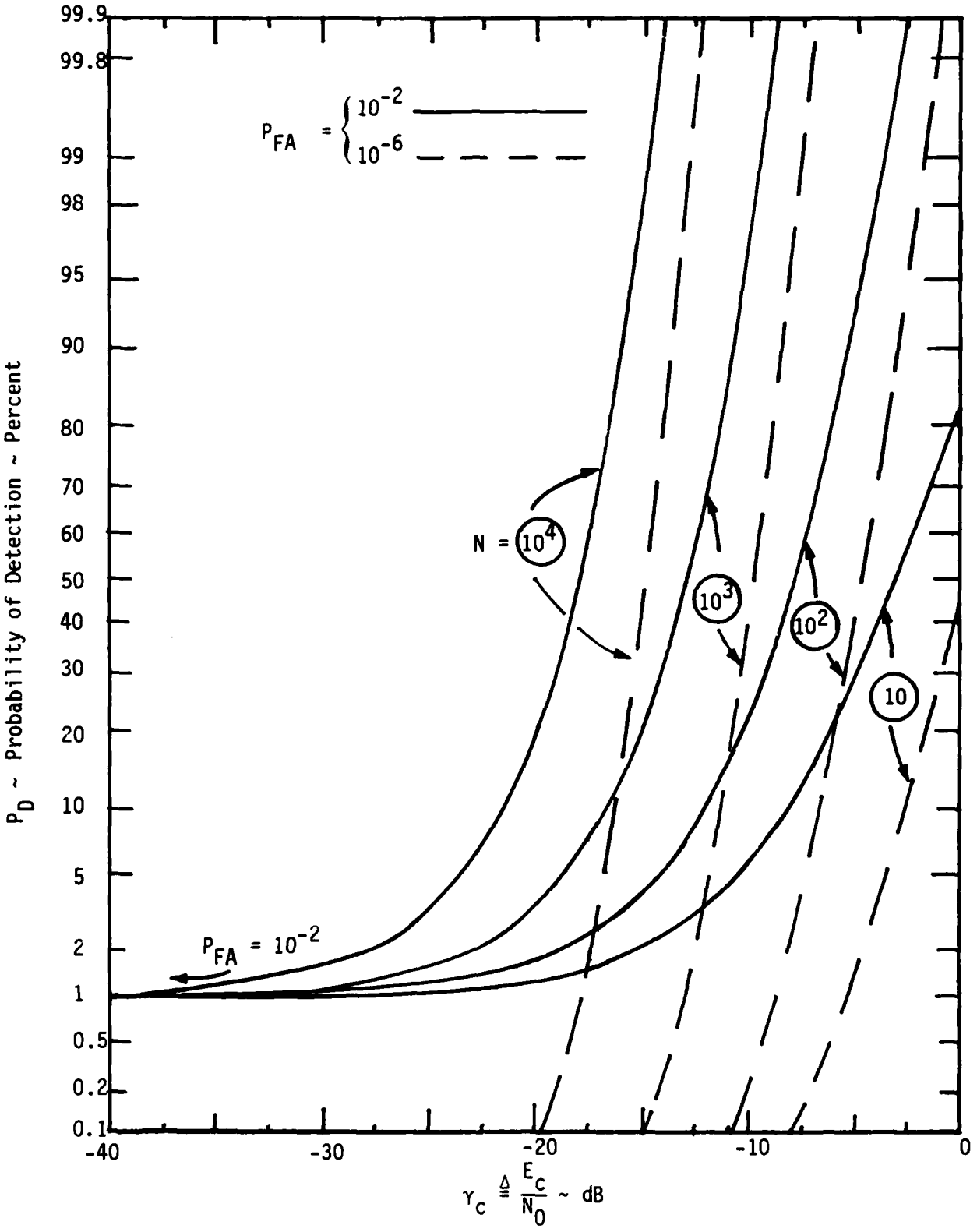

Figure 3.2. Performance of Synchronous-Coherent Detector for False-Alarm Probabilities of 10-2 and 10-6 and Various Values of N

3.2 Synchronous Noncoherent Detectors

Let us now relax the unrealistic assumption that the carrier phase of the DS waveform is known by the interceptor, but still retain the assumption of a known code epoch. When the observation interval is smaller than the coherence time of the channel, the carrier phase ϕ can be modeled as an rv, uniformly distributed in $(0,2\pi)$, resulting in the aforementioned carrier-noncoherent system. In addition, a fictitious chip-noncoherent system will be considered whereby the phase is assumed to change randomly from chip to chip. The reason for discussing such a totally hypothetical signal is twofold: (1) it can be shown that the optimal decision rule for a carrier-noncoherent system is asymptotically equivalent to the decision rule of the chip-noncoherent system (hence, their corresponding performances also coincide asymptotically) as the SNR γ_c decreases to zero; (2) more important is the fact that the performance of the chip-noncoherent structure is easily obtained (within the Gaussian approximation), in sharp contrast to the unwieldy analysis of the optimal carrier-noncoherent system. Thus, the (unobtainable) performance of the latter can be nicely bracketed between the (obtainable) performance of the former, which serves as an asymptotically tight lower bound*, and the upper bounding performance of the synchronous coherent detector in the previous section (3.1).

Let us first consider a carrier-noncoherent system. Under the usual narrowband assumption $\omega_0 \gg 2\pi/T$, the resulting decision rule is

$$\Lambda = \exp\{-N\gamma_c\} \sum_{i=1}^{2^N} I_0\left(\frac{2\sqrt{S}}{N_0} R_i\right) \underset{H_0}{\overset{H_1}{\gtrless}} \Lambda_0 \tag{3-15}$$

where $I_0(\cdot)$ is the zeroth-order modified Bessel function and R_i is the ith correlation envelope

$$R_i = \sqrt{e_{I_i}^2 + e_{Q_i}^2} \; ; \; i=1,2,\ldots,2^N \tag{3-16}$$

*Since a chip-noncoherent detector utilizes less statistical information than a carrier-noncoherent detector, it is inferior to the latter for all SNR values.

In (3-16),

$$e_{a_i} = \sum_{j=1}^{N} r_{a_j} c_{ij} \triangleq \underline{r}_a \cdot \underline{c}_i \; ; \; a=I,Q \tag{3-17}$$

with

$$\begin{bmatrix} r_{I_j} \\ r_{Q_j} \end{bmatrix} \triangleq \sqrt{2} \int_{(j-1)T_c}^{jT_c} r(t) \begin{bmatrix} \cos \omega_0 t \\ \sin \omega_0 t \end{bmatrix} dt \; ; \; j=1,\ldots,N \tag{3-18}$$

As mentioned, the optimal rule (3-15)-(3-18) is hard to mechanize. Instead, suppose that the received waveform r(t) is represented under H_1 by

$$r(t) = \sqrt{2S} \sum_{j=-\infty}^{\infty} c_j \, p\left(t - jT_c\right) \cos\left(\omega_0 t + \phi_j\right) + n(t) \tag{3-19}$$

where $\left\{\phi_j\right\}$ is a sequence of statistically independent uniform phases, thus modeling the aforementioned chip-noncoherent system. It is then straightforward to show (see Appendix C) that the optimal decision rule is

$$-N\gamma_c + \sum_{j=1}^{N} \ell n \; I_0\left(\frac{2\sqrt{S}}{N_0} r_j\right) \underset{H_0}{\overset{H_1}{\gtrless}} \Lambda_0 \tag{3-20}$$

where r_j is the envelope of the jth chip

$$r_j = \sqrt{r_{I_j}^{\,2} + r_{Q_j}^{\,2}} \tag{3-21}$$

with r_{I_j}, r_{Q_j} as per (3-18). An implementation of (3-20) is shown in Figure 3.3. Again, under the small-argument approximation $\ell n I_0(x) \simeq x^2/4$, it follows that (3-20) reduces to the suboptimal rule

$$\Lambda' = \sum_{j=1}^{N} r_j^{\,2} \underset{H_0}{\overset{H_1}{\gtrless}} \Lambda_0' \tag{3-22}$$

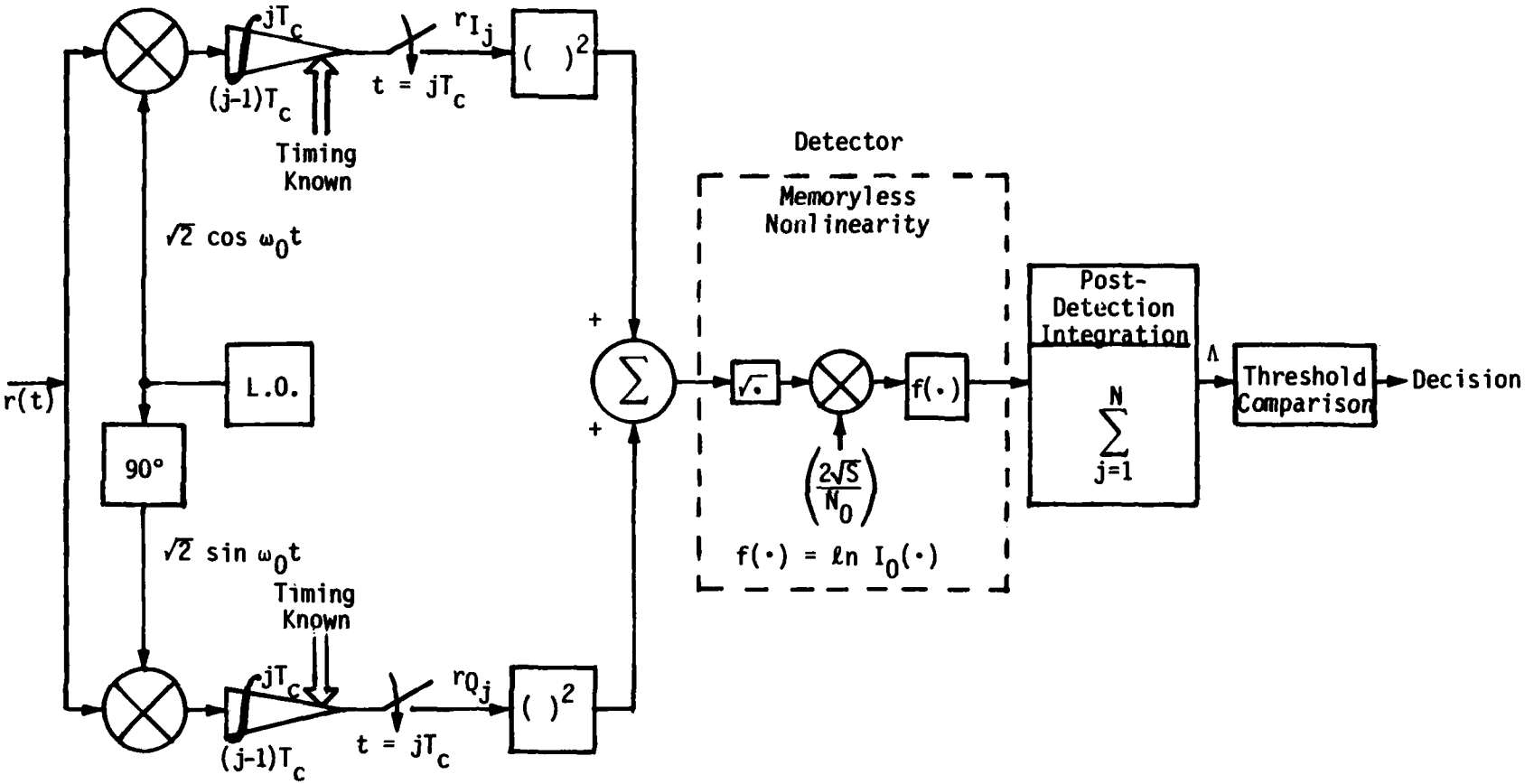

Figure 3.3. Optimal Synchronous Chip-Noncoherent Detector for Direct-Sequence Waveforms

We note that the rule (3-22) is formally identical to (3-9), the difference being that here r_j corresponds to a noncoherent chip integration.

Although the distance d_{ex} for the exact rule (3-20) can be derived (see Section 4 for a closely related case), we shall be content with d_{appr} of (3-22) in view of the low-SNR conclusions of the previous section. Using the Rayleigh (under H_0) or Rician (under H_1) nature of r_j, it is easily shown that (see Appendix D)

$$\mathcal{E}\left\{r_j^2 \middle| H_k\right\} = (N_0T_c)\left[1 + \gamma_c\ \delta_{k1}\right] \tag{3-23a}$$

and

$$\text{var}\left\{r_j^2 \middle| H_k\right\} = (N_0T_c)^2\left[1 + 2\gamma_c\ \delta_{k1}\right] \tag{3-23b}$$

Combining (3-22) and (3-23) and employing the Gaussian assumption results in (3-11) (or (3-12b)), where now

$$\boxed{a = 1\ ;\ b = 2} \qquad \text{(Synchronous chip-noncoherent detector)} \tag{3-24}$$

Equivalently,

$$\left(\frac{S}{N_0}\right)_{req} \approx \frac{1}{\sqrt{2}}\sqrt{\frac{W_s}{T}}\ d_{appr} \tag{3-25}$$

which reveals a loss factor of $\sqrt{2}$, or 1.5 dB with respect to the coherent detector. This is the penalty paid for the lack of coherency. Furthermore, since the performance of the carrier-noncoherent system is bracketed between the coherent (upper bound) and the chip-noncoherent (lower bound) ones that differ by only 1.5 dB, it is concluded that any implementational complexity beyond that of rule (3-22) is not justified from a practical standpoint.

3.3 Asynchronous Detectors

We shall now explore the possibility of removing the rather stringent requirement of epoch synchronization. In other words, we shall derive optimal and suboptimal structures that do not assume knowledge of the chip epoch ε (see (3-1)); furthermore, we shall estimate the (approximate) penalty in performance compared to the previously discussed synchronous detectors. For reasons which were explained before, attention will be given to totally coherent and totally (chip) noncoherent detectors. These are the chip-by-chip processors which readily render themselves to asynchronous alternatives.

In subsection 3.3.1, Continuous-Epoch Uncertainty, we discuss structures which utilize analog filters in order to perform averaging over the continuous rv ε, uniformly distributed in $(0,T_c)$. Thus, the final system output, which is a continuous function of time, provides, after proper sampling, the theoretically optimal answer to the generalized (i.e., average over ε) likelihood ratio test for discriminating between H_0 and H_1. The derivation presented here follows some basic steps from Krasner's work [4] in a somewhat more simplified and expanded manner. In subsection 3.3.2, Quantized-Epoch Uncertainty, we explore suboptimal structures that result from a quantization of the epoch uncertainty region and are much easier to implement than the optimal detector. In particular, the two-point quantization scheme is discussed and analyzed in detail. It will be argued that different interpretations of that analysis could serve as upper and lower bounds on the performance of the optimal continuous uncertainty detector in subsection 3.3.1.

3.3.1 Continuous-Epoch Uncertainty

For the sake of clarity, let us consider the coherent case first. Most of the following steps carry over without change to the chip-noncoherent decision rule (3-22) as well.

The starting point is the coherent likelihood ratio (3-8a), additionally conditioned on the random offset ε. Following a procedure identical to the development of section 3.1 yields the expression

$$\Lambda(r(t)|\varepsilon) = \prod_{j=1}^{N} \left[\cosh(r_j(\varepsilon)) \exp\{-\gamma_c\}\right] = \exp\{-N\gamma_c\} \prod_{j=1}^{N} \cosh(r_j(\varepsilon)) \qquad (3\text{-}26)$$

for the aforementioned conditional likelihood ratio. In equation (3-26), $r_j(\varepsilon)$ indicates the coherent integration of the received waveform $r(t)$ in the jth chip interval, as per (3-7), where the integration limits have now been adjusted to reflect the conditioning on an assumed value of the offset ε:

$$r_j(\varepsilon) = \int_{(j-1)T_c+\varepsilon}^{jT_c+\varepsilon} r(t)\, dt \tag{3-27}$$

In the following, the constant factor $\exp\{-N\gamma_c\}$ will be denoted by K_Λ, for simplicity. Let us note that the final decision rule (3-8b) for the synchronous case results immediately from (3-26) for $\varepsilon = 0$ once we rewrite the latter in the equivalent form

$$\Lambda(r(t)|\varepsilon) = K_\Lambda \exp\left\{\ell n\left(\prod_{j=1}^{N} \cosh\left(r_j(\varepsilon)\right)\right)\right\} = K_\Lambda \exp\left\{\sum_{j=1}^{N} \ell n \cosh\left(r_j(\varepsilon)\right)\right\} \tag{3-28}$$

and use the monotonicity of the function $\exp(\cdot)$. It will soon be clear that, from an implementational viewpoint, (3-28) is more convenient to work with than (3-26).

The overall conditional likelihood ratio $\Lambda(r(t))$ is formed by averaging the conditional one, i.e., $\Lambda(r(t)|\varepsilon)$, with respect to ε, which is assumed uniformly distributed in $(0,T_c)$:

$$\begin{aligned}\Lambda(r(t)) &= \mathscr{E}_\varepsilon\, \Lambda(r(t)|\varepsilon) = K_\Lambda \int_0^{T_c} \exp\left\{\sum_{j=1}^{N} \ell n \cosh\left(r_j(\varepsilon)\right)\right\} d\varepsilon \\ &= K_\Lambda \int_0^{T_c} \exp\left\{\sum_{j=1}^{N} \ell n \cosh\left(\int_{(j-1)T_c+\varepsilon}^{jT_c+\varepsilon} r(\tau)d\tau\right)\right\} d\varepsilon \end{aligned} \tag{3-29}$$

Although the above decision rule is optimal from a theoretical standpoint, it is not immediately clear exactly how it can be implemented in practice without resorting to various approximations, such as quantizing the range of ε, etc. One possible way will now be illustrated which employs appropriate analog filters and devices.

First, let us define the waveform y(t) as

$$y(t) = \int_{t-T_c}^{t} r(\tau)\, d\tau \tag{3-30}$$

The above function is easily mechanized as the output corresponding to an input r(t) of a linear filter matched to the chip square pulse

$$p(t) = \begin{cases} 1 , & 0 \leq t \leq T_c \\ 0 , & \text{otherwise} \end{cases} \tag{3-31}$$

(see (3-1)) since, indeed,

$$\int_{t-T_c}^{t} r(\tau)\, d\tau = \int_{-\infty}^{\infty} r(\tau)\, p(t-\tau)\, d\tau$$

It is clear from (3-29) that the argument of the $\ell n \cosh(\cdot)$ function is just the value of y(t) at time $t = jT_c+\varepsilon$. Thus, we can rewrite (3-29) as

$$\Lambda(r(t)) = K_\Lambda \int_0^{T_c} \left\{ \sum_{j=1}^{N} \ell n \cosh\left(y\left(jT_c+\varepsilon\right)\right) \right\} d\varepsilon \tag{3-32}$$

The next step is to somehow create the summation in the exponent of (3-32) as the outcome of a linear-filtering operation whose input is $\ell n \cosh(y(t))$. Such a sum of equispaced (by T_c) samples of the input function arises at the output f(t), with proper sampling, of a filter whose impulse response is a sequence of equispaced delta functions:

$$h(t) = \sum_{m=0}^{N-1} \delta\left(t - mT_c\right) \tag{3-33}$$

Indeed, when the output waveform

$$f(t) = h(t) \circledast \ell n \cosh(y(t)) = \int_{-\infty}^{\infty} \left(\sum_{m=0}^{N-1} \delta(\tau - mT_c) \right) \ell n \cosh(y(t-\tau)) d\tau$$

$$= \sum_{m=0}^{N-1} \ell n \cosh\left(y(t - mT_c)\right) \tag{3-34}$$

of such a filter is sampled at $t = kT_c + \varepsilon$, it equals

$$f\left(kT_c+\varepsilon\right) = \sum_{m=0}^{N-1} \ell n \cosh\left(y((k-m)T_c+\varepsilon)\right) \tag{3-35}$$

or, changing variables $j = k - m$,

$$f\left(kT_c+\varepsilon\right) = \sum_{j=k-N+1}^{k} \ell n \cosh\left(y\left(jT_c+\varepsilon\right)\right) \tag{3-36}$$

Clearly, then, the exponent of (3-32) arises exactly when $k = N$, i.e., when $f(t)$ is sampled at $t = NT_c+\varepsilon$.

Before proceeding, let us note that an impulse response as per (3-33) corresponds to a tapped-delay-line filter whose (N-1) delay elements are T_c seconds each (see Figure 3.4(a)). Such an implementation, however, bears the restriction that it is not recursive, i.e., higher values of N require more delay elements. An alternative structure is shown in Figure 3.4(b) which employs a single delay element in the feedback path. Ideally, such a filter would provide an infinite series of delta functions, thus alleviating the need to specify N. Typically, however, stability considerations dictate the insertion of a gain $\alpha < 1$ in the feedback loop; the available maximum N is then practically restricted by the infinte-impulse-response (IIR) filter memory.

Returning to (3-36) and combining it with (3-32), one recognizes that the desired likelihood ratio statistic is, in fact, the time average of the function $\exp\{f(t)\}$ over the interval $\left[NT_c,(N+1)T_c\right]$. Again, such an average is

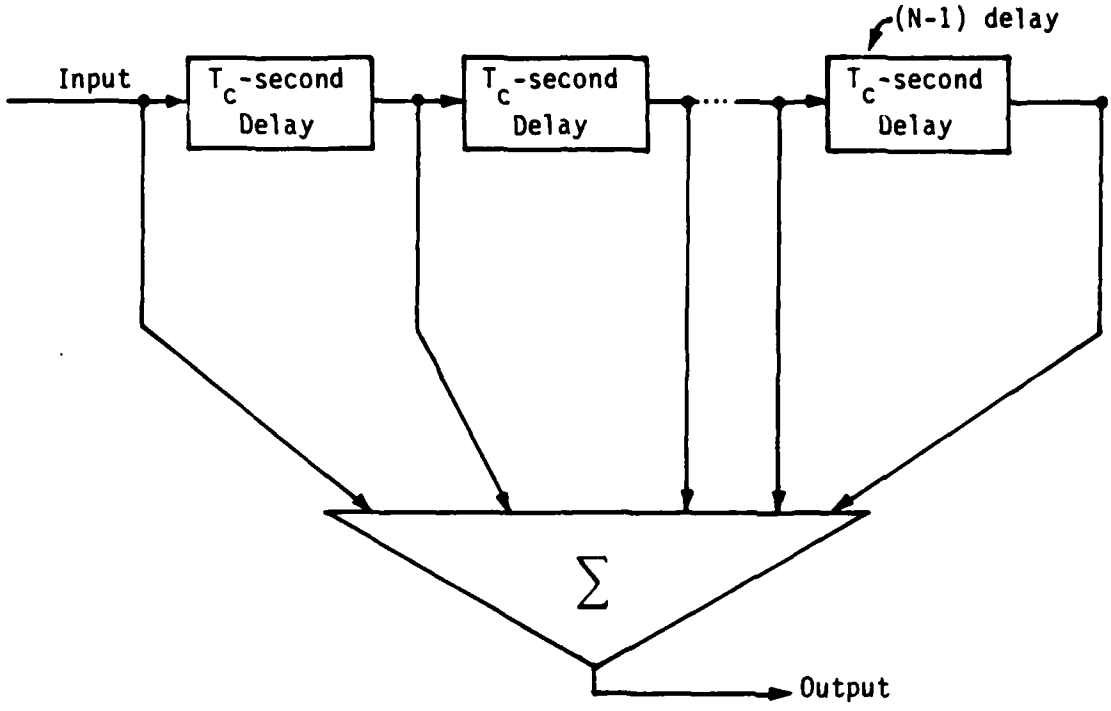

(a) Tapped-Delay Line with (N-1) Delay Elements

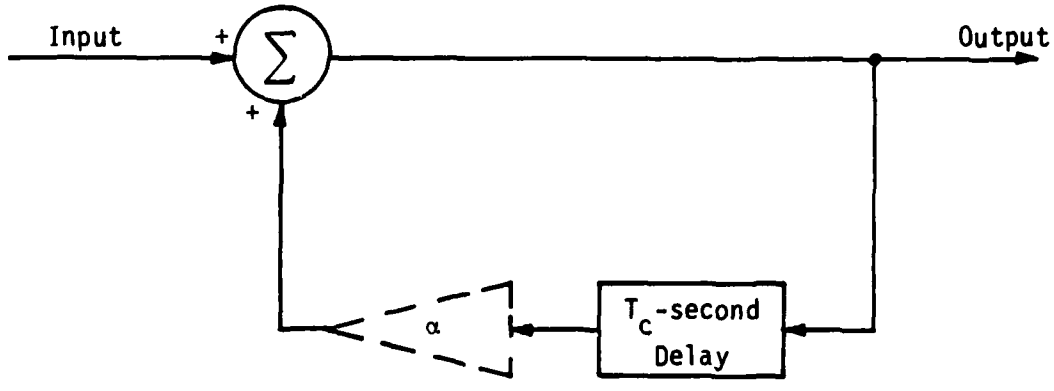

(b) Alternative Implementation through an Infinite-Impulse-Response Filter

Figure 3.4. Filters Providing h(t) of (3-33) as an Impulse Response

created by sampling at $t = (N+1)T_c$ the output of a filter whose impulse response is a unit pulse, T_c seconds long. Figure 3.5 provides a possible implementation of such a "moving-average" filter. Finally, the detector compares the output sample at $t = (N+1)T_c$ to a threshold and produces a decision. The overall scheme is depicted in Figure 3.6.

Several observations can be made here. First, a practical scheme would avoid the $\ell n \cosh(\cdot)$ and $\exp(\cdot)$ nonlinearities since they are hard to construct and replace them by a single square-law device operating on $y(t)$, i.e., the following approximation of (3-32) could be used:

$$\Lambda(r(t)) \approx K_\Lambda \int_0^{T_c} \left[\sum_{j=1}^{N} y^2 (jT_c + \varepsilon) \right] d\varepsilon \qquad (3\text{-}37)$$

The basis for such a simplification is the previously used fact that, for low SNR, $y(t)$ is a small quantity; in which case, the approximations $\ell n \cosh y(t) \approx 1 + y^2(t)$ and $\exp(f(t)) \approx 1 + f(t)$ can be employed. Furthermore, let us note that the chip pulse shape need not be rectangular. An arbitrary (but chip-time limited) shape can be accommodated by designing the very first filter of Figure 3.6 to be matched to that particular shape. All other elements remain the same.

Finally, it can be shown that the arguments and detector structures of this subsection apply directly to the chip-noncoherent case, provided that the first nonlinearity $\ell n \cosh(\cdot)$ of Figure 3.6 is replaced by $\ell n\, I_0(\cdot)$ and the initial chip-matched filtering at the input of that figure is done noncoherently. This can be accomplished by the noncoherent chip-envelope detector comprising the predetection integration of Figure 3.3, once the inphase and quadrature integrate-and-sample type filters are replaced by analog matched filters with a continuous-time output.

3.3.2 Quantized-Epoch Uncertainty

A step towards reducing the complexity of the previous detector is to quantize the epoch uncertainty region of T_c seconds into a (small) finite number of alternatives, i.e., points. This is equivalent to assuming that the epoch rv can take on only those values and accordingly develop the optimal or near-optimal detector for the resulting finite hypothesis problem. The quality

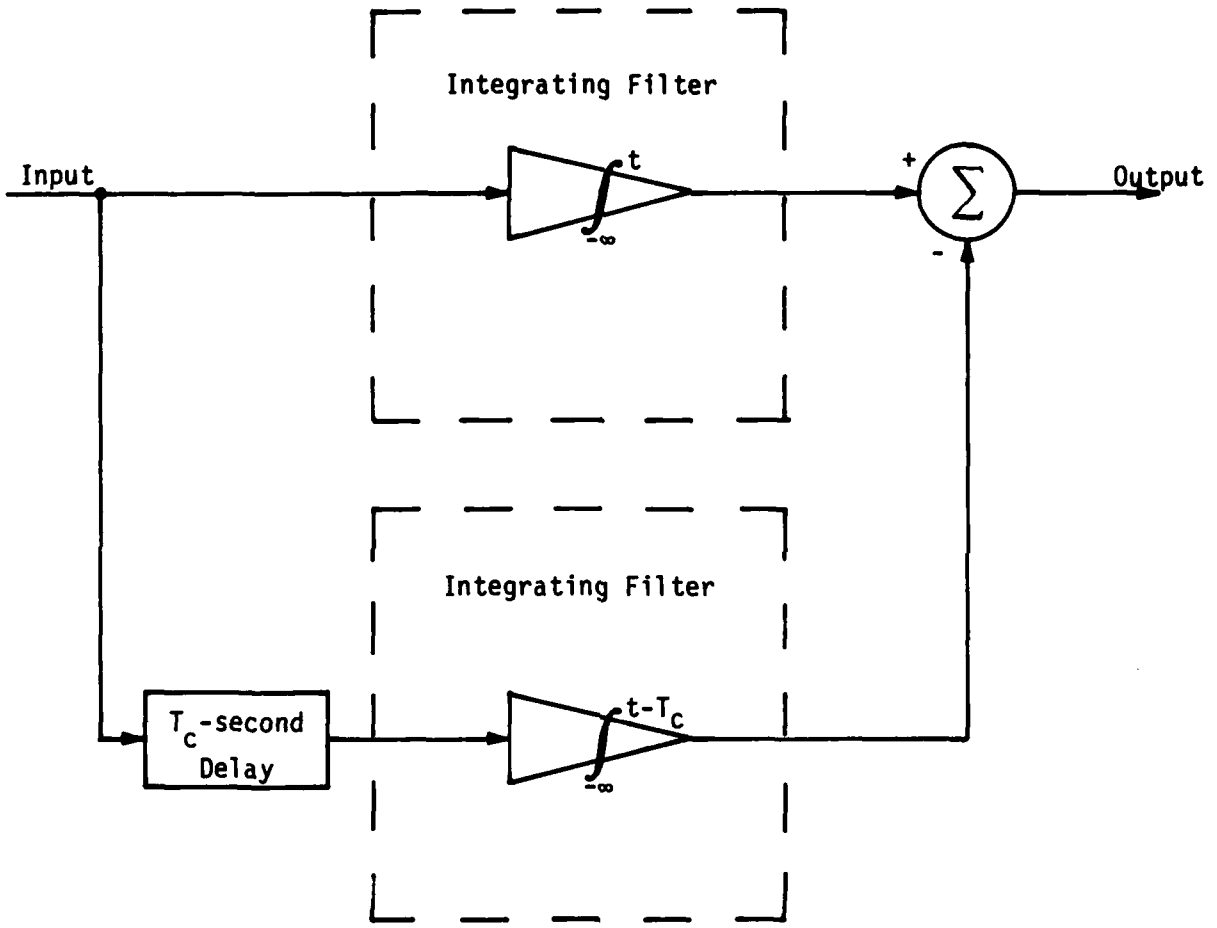

Figure 3.5. Moving Average Filter with a Square-Pulse Impulse Response

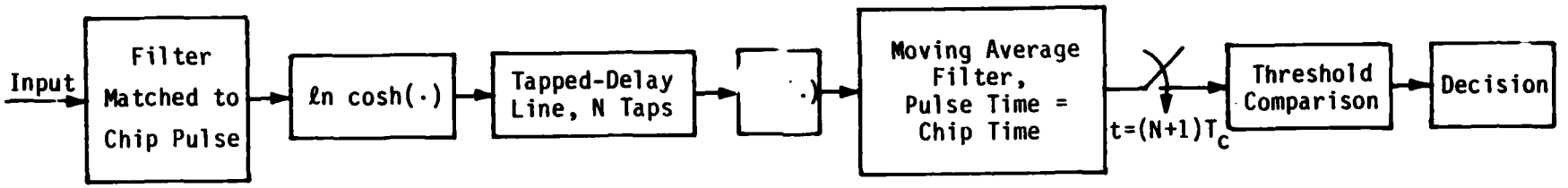

Figure 3.6. Optimal, Continuous-Epoch Uncertainty, Likelihood Ratio Detector for the Coherent Case

(as well as the complexity) of such an approximation will obviously increase with the number of points considered. It will soon be clear, however, that the simplest case of only a two-point quantization, which will be the one we analyze herein, provides quite an adequate performance with respect to the ideal (synchronous) detector; thus, higher level quantization and complexity might even be undesirable from a practical viewpoint. In addition, a suitable interpretation of this analysis can simultaneously serve as a bounding technique (upper and lower) for the optimal, continuous-epoch uncertainty detector of the previous subsection, whose exact analysis is intractable.

Let us assume that the two points comprising the epoch uncertainty* are ε_0 and $\varepsilon_{1/2}$, corresponding to the offsets $\varepsilon = 0$ and $\varepsilon = 1/2$ in (3-1). That is to say, the incoming code chips are likely to arrive either in perfect synchronization ($\varepsilon = 0$) or half a chip off ($\varepsilon = 1/2$) with respect to the local chip timing reference, and they are both equally probable to occur. A variation of the optimal-likelihood ratio (3-28) for the coherent case, adapted for the above scenario, would imply that the decision rule should be

$$\left(\frac{1}{2}\right)\left[\exp\left\{\sum_{j=1}^{N} \ell n \cosh\left(r_j(\varepsilon_0)\right)\right\} + \exp\left\{\sum_{j=1}^{N} \ell n \cosh\left(r_j(\varepsilon_{1/2})\right)\right\}\right]\exp\left\{-N\gamma_c\right\} \underset{H_0}{\overset{H_1}{\gtrless}} \Lambda_0 \qquad (3\text{-}38)$$

where

$$r_j(\varepsilon_0) = \int_{(j-1)T_c}^{jT_c} r(\tau)d\tau \quad ; \quad r(\varepsilon_{1/2}) = \int_{(j-1)T_c+T_c/2}^{jT_c+T_c/2} r(\tau)d\tau \qquad (3\text{-}39)$$

Clearly, the chip-noncoherent detector would form the envelopes r_j in place of the coherent integrations (3-39); otherwise, the development is analogous.

We should note here that the two NT_c-second observation intervals for the two corresponding exponential terms of (3-38) are slightly off by half a chip. For large N, such "edge effects" are insignificant and will be neglected in the following†.

---

*So, at this point, the epoch uncertainty is assumed to be discrete by nature, not by quantization.

†For that purpose, small adjustments will be made for convenience without explicit acknowledgement.

The familiar small SNR approximation applied to (3-38) yields the suboptimal rule:

$$\Lambda' = \sum_{j=1}^{N} r_j^2(\varepsilon_0) + \sum_{j=1}^{N} r_j^2(\varepsilon_{1/2}) \underset{H_0}{\overset{H_1}{\gtrless}} \Lambda_0' \tag{3-40}$$

Let r_{j1} and r_{j2} indicate the coherent integrations during the first and second halves of the jth chip interval, respectively, i.e.,

$$r_{j1} = \int_{(j-1)T_c}^{(j-1/2)T_c} r(\tau)d\tau \quad ; \quad r_{j2} = \int_{(j-1/2)T_c}^{jT_c} r(\tau)d\tau \tag{3-41}$$

Then (3-40) can be rewritten in terms of (3-41) as

$$\Lambda' = \sum_{j=1}^{N} \left(r_{j1} + r_{j2}\right)^2 + \sum_{j=1}^{N} \left(r_{j2} + r_{j+1,1}\right)^2 \underset{H_0}{\overset{H_1}{\gtrless}} \Lambda_0' \tag{3-42a}$$

or, expanding terms, neglecting edge effects $\left(\text{i.e., substituting } r_{N+1,1}^2 \text{ with } r_{1,1}^2\right)$, and dividing by 1/2, we get

$$\Lambda' = \sum_{j=1}^{N} r_{j1}^2 + r_{j2}^2 + r_{j2}\left(r_{j1} + r_{j+1,1}\right) \underset{H_0}{\overset{H_1}{\gtrless}} \Lambda_0' \tag{3-42b}$$

Figure 3.7 shows a possible implementation of rule (3-42).

An examination of the decision rule (3-42b) reveals the source of inferiority of the asynchronous coherent detector in comparison with its synchronous counterpart, namely, rule (3-9). The latter rule can be obtained from (3-42b) if the factor $r_{j+1,1}$ in the last term is substituted by r_{j1} because the resulting expression is then the perfect square $\left(r_{j1}+r_{j2}\right)^2 = r_j^2$ of (3-9). Since r_{j1} and $r_{j+1,1}$ are independent rv's (they belong to different random chips) regardless of the true epoch value, it follows that such a substitution would increase the mean of the decision statistic Λ' under H_1 and slightly reduce the variance--the effect of which is a net improvement in performance for the synchronous detector. We will now take a closer look at the performance of (3-42b).

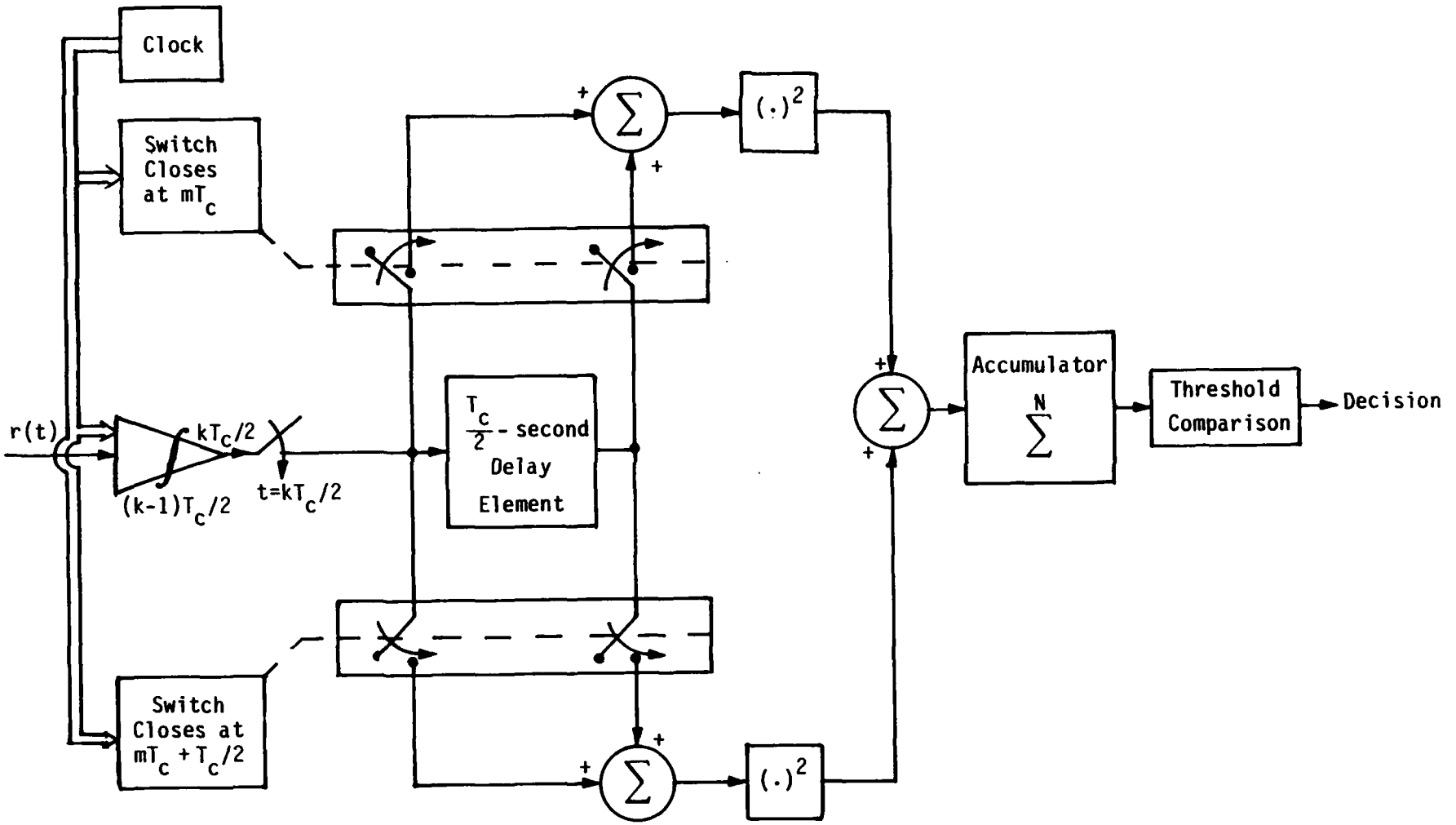

Figure 3.7. A Nonsynchronous, Two-Level Epoch Quantization Suboptimal Coherent Detector

Without any loss in generality, we can assume that the true epoch is $\varepsilon = 0$. The symmetry of the problem suggests that the results to be derived under such conditioning also represent the unconditional (average) performance in this two-possible-value case. In order to pursue the familiar Gaussian type of analysis, one needs the means and variances of the rv's r_{j1} and r_{j2} as per (3-41). Those are readily calculated to be

$$\mathcal{E}\left\{r_{jm}^2 \middle| H_k\right\} = \frac{N_0 T_c}{4}\left[1 + \gamma_c\, \delta_{k1}\right] \quad ; m=1,2 \quad ; k=0,1$$

$$\text{var}\left\{r_{jm}^2 \middle| H_k\right\} = \frac{\left(N_0 T_c\right)^2}{4}\left[\frac{1}{2} + \gamma_c\, \delta_{k1}\right] \tag{3-43}$$

Furthermore, it is easily shown that (See Appendix E)

$$\mathcal{E}\left\{r_{j2}\, r_{j+1,1} \middle| H_k;\varepsilon=0\right\} = 0 \quad ; \quad \mathcal{E}\left\{r_{j1}\, r_{j2} \middle| H_k;\varepsilon=0\right\} = \frac{S T_c^2}{4}\,\delta_{k1} \tag{3-44}$$

for k=0,1. Combining (3-42b), (3-43) and (3-44), it follows that

$$\mathcal{E}\left\{\Lambda' \middle| H_k;\varepsilon=0\right\} = N\left(\frac{N_0 T_c}{2}\right)\left[1 + \left(\frac{3}{2}\right)\gamma_c\, \delta_{k1}\right] \tag{3-45}$$

A complete evaluation of system performance would require an additional calculation of the variance $\text{var}\left\{\Lambda' \middle| H_k\right\}$, as was done for the decision statistic (3-9). However, matters can be simplified considerably if we observe that the result for the asynchronous variance should be higher than, but close to, the synchronous variance of section 3.1, particularly for the low SNR range of interest. The main rationale supporting such an assessment is the comparison between the asynchronous rule (3-42 b) and the expanded synchronous rule

$$(3\text{-}9) \Longleftrightarrow \sum_{j=1}^{N} r_{j1}^2 + r_{j2}^2 + r_{j1}\, r_{j2} + r_{j1}\, r_{j2} \tag{3-9'}$$

which shows them differing in only one of four contributing terms. Thus, a variance equal to $N(N_0T_c)^2/2$ (see (3-10b)) is a good approximation for all cases.

It follows from the above discussion and the underlying Gaussian assumption that the primary measure of performance degradation due to asynchronism is the reduction in the difference (distance) between the means of the two distributions corresponding to the alternative hypotheses. So, if we rewrite the synchronous expression of (3-10a) as $\mathcal{E}\left\{\Lambda' | H_k\right\} = N(N_0T_c)\left[1 + 2\,\gamma_c\,\delta_{k1}\right]/2$ and compare it to (3-45), we induce a loss factor of 4/3, or 1.25 dB, as the SNR penalty associated with the aforementioned asynchronous detector.

The above estimated loss can also be viewed as a lower bound on the performance losses of the continous-epoch uncertainty detector. This is because the two-point-uncertainty coherent detector discussed so far assumes a random epoch that can take on only two values; thus, it faces less uncertainty than any other multipoint or continuous type of epoch randomness. Therefore, it is bound to outperform any other asynchronous detector, including the continuous-uncertainty one.

It is also of interest here to derive an upper bound on the performance losses of the continuous-uncertainty detector. This can be done by assuming a truly continuous-epoch uncertainty and viewing the two-point detector as a suboptimal quantized implementation of the optimal continuous-uncertainty one. The performance losses of the suboptimal detector under a worst-case choice of the unquantized epoch will then clearly upperbound the losses of any other, higher complexity, multipoint or continuous detector.

Some reflection could persuade us that the worst epoch for the two-point quantized detector is the one straddling between $\varepsilon = 0$ and $\varepsilon = 1/2$, namely, $\varepsilon = 1/4$ (or, equivalently, $\varepsilon = 3/4$, whose performance, however, is identical). This is because, under H_1, r_{j1} will then have the lowest possible mean (namely, zero) half of the time while r_{j2} remains unaffected. Any other offset will yield a higher overall average for r_{j1}, thus improving performance.

It is shown in Appendix F that, under the worst epoch $\varepsilon = 1/4$, the joint statistics of r_{j1} and r_{j2} become

$$\mathcal{E}\left\{r_{j1}^2 \middle| H_k;\varepsilon=1/4\right\} = \left(\frac{N_0T_c}{4}\right)\left[1 + \frac{1}{2}\,\gamma_c\delta_{k1}\right]$$

$$\mathcal{E}\left\{r_{j2}^2 \middle| H_k;\varepsilon=1/4\right\} = \left(\frac{N_0T_c}{4}\right)\left[1 + \gamma_c\delta_{k1}\right]$$

$$\mathcal{E}\left\{r_{j2}r_{j1} \middle| H_k;\varepsilon=1/4\right\} = \mathcal{E}\left\{r_{j2}r_{j+1,1} \middle| H_k;\varepsilon=1/4\right\} = \left(\frac{N_0T_c}{4}\right)\left(\frac{\gamma_c}{2}\right)\delta_{k1} \quad (3\text{-}46)$$

which, when substituted in (3-42b), yields

$$\mathcal{E}\left\{\Lambda \middle| H_k;\varepsilon=1/4\right\} = N\left(\frac{N_0T_c}{2}\right)\left[1 + \left(\frac{5}{4}\right)\gamma_c\,\delta_{k1}\right] \quad (3\text{-}47)$$

A comparison of (3-47) with (3-10a) reveals a loss factor of 8/5, or 2 dB, with respect to the synchronous structure.

In conclusion, the lack of synchronism in the coherent detector costs anywhere from 1.25 dB (lower bound) to 2 dB (upper bound). Tighter bounds can be obtained by reiterating the above arguments for epoch-quantized detectors with more than two quantization points. As the number of points increases, one asymptotically converges to the actual performance of the continuous-epoch detector. In any case, a rough figure of an average 1.5-dB loss due to asynchronism should not be far from exact. Similar conclusions can be drawn for the noncoherent detectors of the previous sections.

3.4 Energy Detector (Radiometer)

The most commonly used energy measuring device, the "energy detector" or "radiometer", will now be analyzed as a potential candidate LPI detector. In the battle for implementational savings and hardware reduction, the radiometer is an easy winner: it is simply the cascade of a wide bandpass filter, followed by a square-law device, a zonal LPF (possibly excluded), an integrator* and, finally, a threshold comparator which produces the decision, as shown in Figure 3.8. The bandwidth of the BP filter should approximately cover the null-to-null bandwidth of the DS spread signal to be detected; thus, approximate knowledge of the chip rate is an implicit necessity.

Clearly, the hypothesis discriminating power of the radiometer is based on simple energy considerations: signal plus noise (under H_1) should possess more energy than noise alone (under H_0). Thus, by properly adjusting the decision threshold, a correct decision will, hopefully, be made. It goes without saying that performance, as measured by the pair (P_D, P_{FA}), increases monotonically with increasing SNR γ_c and observation time $T=NT_c$. On the other hand, selection of the RF bandwidth W_{BP} in the filter is subject to optimization and is discussed more thoroughly in the following.

It has long been known that the precise analysis of systems containing linear plus nonlinear elements, as in Figure 3.8 for arbitrary filter shapes and bandwidths, is generally unwieldy [11]. If the envelope detector of Figure 3.8 is assimilated to (or approximated by) an inphase-and-quadrature (I-Q) type of envelope detector, it can then be claimed that the output statistic Λ has a chi-squared distribution (central or noncentral, depending on whether a signal is absent or present, respectively), with $2NW_{BP}T_c$ degrees of freedom. The probabilities P_{FA} and P_D can then be calculated by a numerical integration of the corresponding densities, from the threshold Λ_0 to infinity, since those integrals cannot be found in closed form. This procedure can be very laborious. Fortunately, when the time-bandwidth product $W_{BP}(NT_c)$ is large (which is the case here, since N is large), one can very accurately approximate the probability densities of Λ under both hypotheses by Gaussian ones, by virtue of a central-limit-type argument. Then calculation of the overall performance becomes fairly straightforward.

---

*Since the integrator itself acts as a lowpass filter, the zonal LPF preceding it is typically eliminated; it is included here as a conceptual aid.

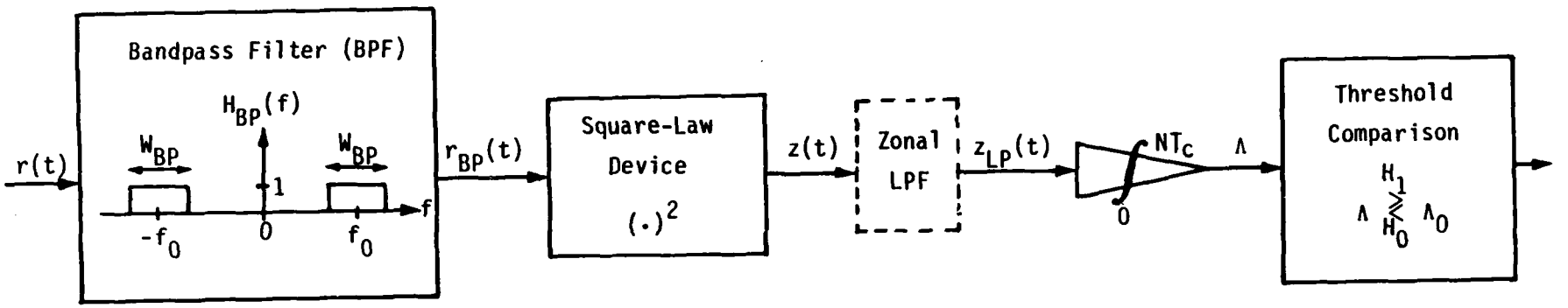

Figure 3.8. Energy Detector (Radiometer)

The received waveform r(t) is described by (3-2). The BPF is assumed to be rectangular with bandwidth W_{BP}. The output of the BPF in Figure 3.8 is

$$r_{BP}(t) = \sqrt{2S}\,\bar{c}(t)\cos(\omega_0 t + \phi) + n_{BP}(t) \qquad (3\text{-}48)$$

where $n_{BP}(t)$ is filtered AGN with the typical BP representation

$$n_{BP}(t) = \sqrt{2}\left[n_I(t)\cos\omega_0 t + n_Q(t)\sin\omega_0 t\right] \qquad (3\text{-}49)$$

In (3-49), $n_I(t)$ and $n_Q(t)$ are approximately independent, zero-mean, jointly Gaussian, lowpass noise processes, each with a PSD of N_0 W/Hz (one-sided) and bandwidth of $W_{BP}/2$ Hz (one-sided). The code signal, filtered by the BPF, is designated $\bar{c}(t)$ in (3-48). The zonal LPF (shown for analytical purposes only) rejects the $2f_0$ components of the square-law output z(t) and has an output given by

$$z_{LP}(t) = S\left(\bar{c}(t)\right)^2 + n_I^2(t) + n_Q^2(t) + 2\sqrt{S}\,\bar{c}(t)\,n_I(t) \qquad (3\text{-}50)$$

In order to maintain analytical tractability, we approximate and model $\bar{c}(t)$ as an attenuated, <u>but undistorted</u>, version of c(t), namely,

$$\bar{c}(t) \triangleq \alpha c(t) \qquad (3\text{-}51)$$

where the "<u>attenuation factor</u>" α^2 measures the (normalized) power reduction due to filtering:

$$\alpha^2 \triangleq \frac{\int_{-\infty}^{\infty} |H_L(f)|^2 S_c(f)df}{\int_{-\infty}^{\infty} S_c(f)df} = \left(\frac{2}{\pi}\right)\int_0^{\pi W_{BP}T_c/2}\left(\frac{\sin x}{x}\right)^2 dx \qquad (3.52)$$

since, for a ±1-valued code, the denominator of (3-52) equals $c^2(t) = 1$. In the previous expression, $S_c(f)$ is the PSD of the random code signal c(t) and $H_L(f)$ is the lowpass equivalent of the BPF $H_{BP}(t)$, i.e.,

$$H_L(f) = \begin{cases} 1 & |f| \leq W_{BP}/2 \\ 0 & \text{, otherwise} \end{cases}$$

By suitably adjusting $H_L(f)$, (3-52) can be generalized to filters other than the perfectly rectangular one considered above.

From the above definitions, it follows that $(\tilde{c}(t))^2 = \alpha^2$. Thus,

$$z_{LP}(t) = \alpha^2 S + n_I^2(t) + n_Q(t) + 2\sqrt{S}\,\alpha c(t)\, n_I(t) \qquad (3\text{-}53)$$

under H_1. Under the alternative H_0, $z_{LP}(t)$ is given by the above expression with $S = 0$. It follows that

$$\mathcal{E}\{z_{LP}(t)|H_k\} = \alpha^2 S\, \delta_{k1} + N_0 W_{BP}; \quad k=0,1 \qquad (3\text{-}54)$$

with δ_{k1} as per (3-10c). Thus, the expected value $\mathcal{E}\{\Lambda|H_k\}$ of test statistic Λ at the output of the integrator in Figure 3.8 can be calculated under either hypothesis H_k;k=0,1, as

$$\mathcal{E}\{\Lambda|H_k\} = \int_0^{NT_c} \mathcal{E}\{z_{LP}(t)|H_k\}dt = NT_c\left[N_0 W_{BP} + \alpha^2 S\delta_{k1}\right]; \; k=0,1 \quad (3\text{-}55)$$

The next step is to obtain the second-order statistics of $z_{LP}(t)$ and Λ. The typical approach, based on the assumption $W_{BP}NT_c \gg 1$, is to model $z_{LP}(t)$ as a very wideband ("delta-correlated") process with respect to the approximate bandwidth $(NT_c)^{-1}$ of the integrator. Thus, one needs to evaluate only the PSD of $z_{LP}(t)$ at the origin $f = 0$, distinguishing between the average (constant) contribution and the random contribution. Using the fact that $n_I(t)$ and $n_Q(t)$ are Gaussian, the autocorrelation function of $z_{LP}(t)$ can be obtained directly; from that, its PSD under H_1 is given by

$$S_{z_{LP}}(f) = \left(\alpha^2 S + N_0 W_{BP}\right)^2 \delta(f) + 4S_{n_I}(f) \circledast S_{n_Q}(f) + 4\alpha^2 S S_c(f) \circledast S_{n_I}(f) \qquad (3\text{-}56)$$

where $\circledast$ means "convolved with." The coefficient of the Dirac delta function $\delta(f)$ agrees with the first-order statistics of $z_{LP}(t)$ obtained directly in (3-54). The two-sided PSD of $z_{LP}(t)$ at $f = 0$ measures its random contribution

and is obtained by evaluating the last two terms of $S_{z_{LP}}(f)$ in (3-56) with f=0, resulting in

$$S_{z_{LP}}(f)\Big|_{f=0} = N_0^2 W_{BP} + 2\alpha^4 SN_0 \delta_{k1} \; ; \; k=0,1 \tag{3-57}$$

The delta-correlated random part of $z_{LP}(t)$ contributes to the variance of Λ as

$$\text{var}\left\{\Lambda \middle| H_k\right\} = (NT_c)S_{z_{LP}}(0) = (NT_c)\left(N_0^2 W_{BP} + 2\alpha^4 SN_0 \delta_{k1}\right) \tag{3-58}$$

The mean and variance of Λ in (3-55) and (3-58) suffice to characterize performance under the Gaussian assumption which hinges on the fact that $W_{NP}NT_c \approx N \gg 1$. The result is (3-11) with

$$\boxed{a = \sqrt{\frac{\alpha^4}{W_{BP}T_c}} \; ; \; b = 2a^2} \tag{3-59}$$

Clearly, the choice of W_{BP} has an impact on a through (3-59) and α^2 in (3-52). The quantity

$$a = \frac{\alpha^2}{\sqrt{W_{BP}T_c}} = \frac{\left(\frac{2}{\pi}\right)\int_0^{\pi W_{BP}T_c/2}\left(\frac{\sin x}{x}\right)^2 dx}{\sqrt{W_{BP}T_c}} \tag{3-60}$$

has been plotted in Figure 3.9 as a function of the product $W_{BP}T_c$. The maximum $a_{max} \approx 0.77$ is attained at $W_{BP}T_c \approx 1$. This corresponds to a minimum SNR loss of 1.1 dB with respect to the chip noncoherent detector (3-24). Since the above conclusions are based strictly on energy considerations and the interchip interference effects due to filtering have not been taken into account, the actual losses are somewhat higher. In the following comparisons, we select a nominal loss figure of -1.5 dB. We note that the above losses pertain to a

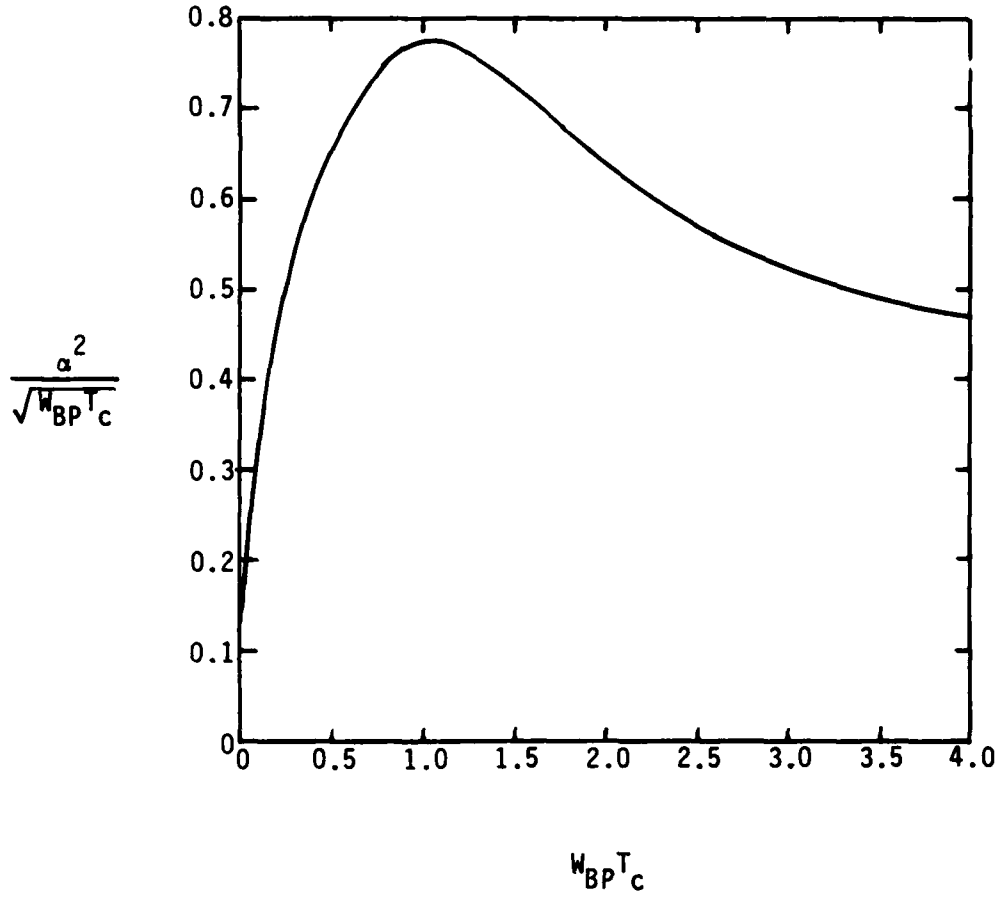

Figure 3.9. SNR Attenuation Due to the Choice of W_{BP} in the Radiometer

rectangular BPF; other filter shapes will result in different loss figures, typically of the same order. For example, [10] can be consulted for the effect of filtering on a baseband rectangular pulse in terms of output SNR losses, compared to a matched filter.

3.5 Comparisons and Discussion

All the previous theory was developed under the cardinal assumption that the received waveform r(t), on which the decision is based, is of the form (3-2). Excluding the fact that the spreading is done via DS methods (alternatives such as frequency and time hopping will be studied in the sequel), three key restrictions in the system modeling were applied: (a) under H_1, the whole observation interval (0,T) is occupied by the spread waveform, (b) there is only one version of signal plus noise available, and (c) the additive disturbance is white Gaussian noise. Let us now comment on each of these restrictions.

Assumption (a) is not as restrictive as it might seem at first. Admittedly, if the starting signal transmission time is unknown, the intercepting receiver will be forced to look at T-second observation intervals that are randomly placed with respect to the actual transmission time. One could develop a theory along lines similar to those presented herein, whereby the performance losses due to such realistic randomness are taken into account. Although the performance of each individual suggested system will certainly be altered, their relative ranking in terms of effectiveness is expected to remain the same. Thus, the conclusions and comparisons which we shall soon undertake should carry over more or less intact. In order to be definite, however, one should take a closer look in the future*.

Assumption (b) is more substantial in nature. In fact, it will now be shown that performance improvement can be gained by utilizing two receptions which cover the same geographical area (hence, contain the same useful signal), but possess independent RF circuits (hence, independent thermal noise components). In order to briefly illustrate the idea, let us consider a synchronous coherent system.

Let

$$\begin{aligned} r_1(t) &= \sqrt{S}\, c(t)\, \delta_{k1} + n_1(t) \\ r_2(t) &= \sqrt{S}\, c(t)\, \delta_{k1} + n_2(t) \end{aligned} \qquad \begin{pmatrix} 0 \leq t \leq T \\ k=0,1 \end{pmatrix} \qquad (3\text{-}61)$$

represent the two receptions. Here the two noise processes $n_m(t);m=1,2$ are Gaussian and independent, while the signal component c(t) is the same in both

*One could create a multitude of possible solutions, such as overlapping versus nonoverlapping observation intervals, etc.

waveforms. We should point out that, when implementing the cross-correlation which we are about to discuss, maximum care must be exercised to ensure that the two code signal components are indeed in phase since timing offsets of more than a code chip will result in involuntary signal spreading and total loss of detection capability.

The decision rule adopted here is a simple correlation (see Figure 3.10)

$$\Lambda' = \int_0^{NT_c} r_1(t)\, r_2(t)dt = \sum_{j=1}^{N} r_j^{(1)}\, r_j^{(2)} \underset{H_0}{\overset{H_1}{\gtrless}} \Lambda'_0 \qquad (3\text{-}62a)$$

where

$$r_j^{(m)} = \int_{(j-1)}^{jT_c} r_m(t)\, dt \qquad (3\text{-}62b)$$

We note that (3-62) is analogous to (3-9) once r_j^2 is substituted by $r_j^{(1)} r_j^{(2)}$. Clearly, in the absence of thermal noise, both (3-9) and (3-62) produce the same quantity, NST_c^2; however, performance is different in noise. Indeed, from (3-26), it easily follows that (see Appendix G):

$$\mathcal{E}\{\Lambda' | H_k\} = N(N_0 T_c)\, \gamma_c\, \delta_{k1} \qquad (3\text{-}63a)$$

and

$$\mathrm{var}\{\Lambda' | H_k\} = N(N_0 T_c)^2 \left[\frac{1}{4} + \gamma_c\, \delta_{k1}\right] \qquad (3\text{-}63b)$$

The resulting performance is again described by (3-11), where now

$$\boxed{a = 2\ ;\ b = 4} \qquad \text{(Two independent receptions)} \qquad (3\text{-}64)$$

Thus, a comparison with the corresponding performance parameters (3-12a) for the (one-reception) synchronous coherent radiometer reveals a gain factor of $\sqrt{2}$, or 1.5 dB in SNR for the present system. However, we would again like to emphasize that this gain is attained at the cost of higher complexity.

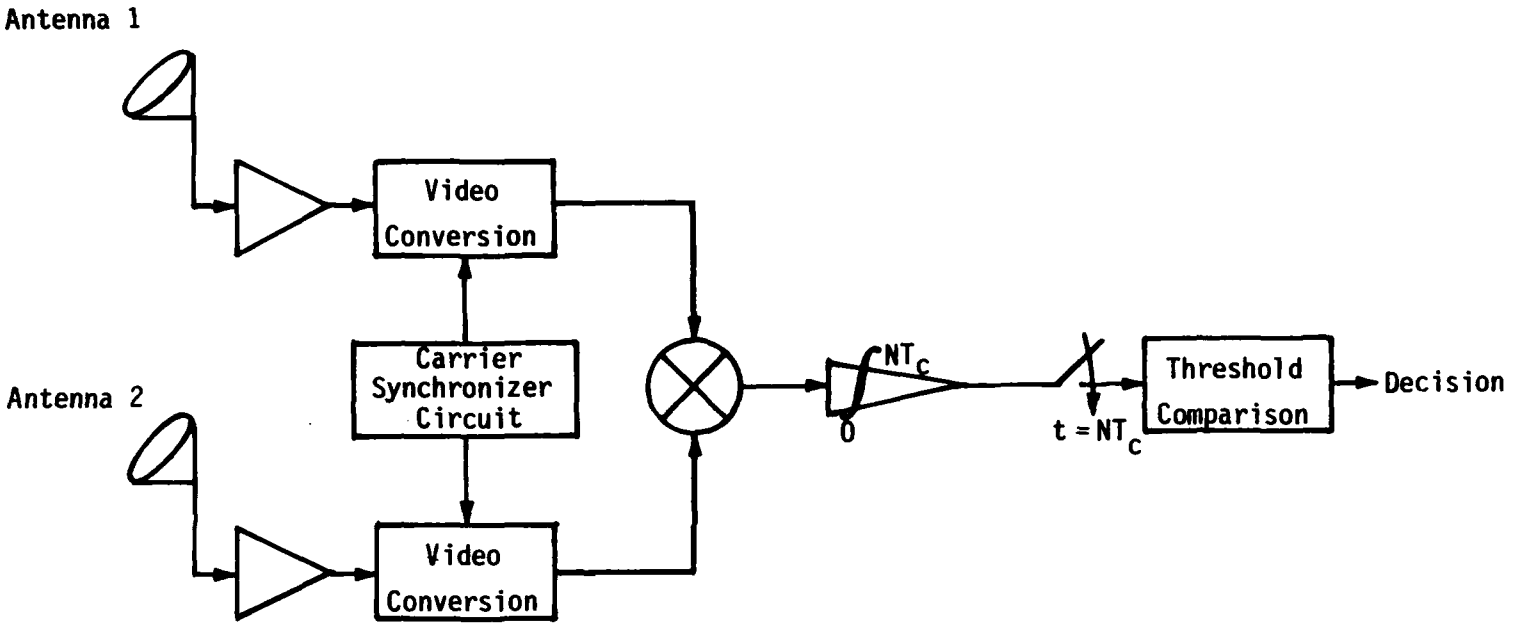

Figure 3.10. A Hypothetical, Two-Reception, Synchronous-Coherent Detector

Before commenting on the third assumption (c), let us attempt an evaluation of the relative merits of all the previous detector structures. The conclusions have been summarized in Figure 3.11 for the exemplary case of $P_{FA} = 10^{-2}$ and N = 1000 chips. Clearly, the ultimate upper bound in performance corresponds to the ideal (but unrealistic, from the LPI viewpoint) case of a totally known signal (under H_1), i.e., a code-matched receiver. Since it is an unachievable upper bound, it has been included merely to serve as a comparative yardstick. It is represented by curve ① , whose analytical description is via the distance d_{UB} (as per (2-2)):

$$d_{UB} = \sqrt{2N\gamma_c} \qquad (3\text{-}65)$$

where a coherent system has been assumed. Comparing (3-65) with (3-12b) implies that there is a loss factor of $\sqrt{\gamma_c}$ associated with the lack of code knowledge, and this factor is significant at low SNR's. On the other hand, all performances are lower bounded by that of the radiometer, which was derived in the previous subsection (see (3-59)) and is represented by curve ⑤ in Figure 3.11. The remaining curves ② , ③ and ④ pertain to alternate receivers which were considered herein: ② corresponds to a detector utilizing two independent, synchronous, coherent receptions, ③ to one synchronous, coherent detector, and ④ to a synchronous, chip-noncoherent detector. The difference between ② and ③ is roughly 1.5 dB which is also the difference between ③ and ④ , as well as ④ and ⑤ . It follows that, under fairly ideal conditions, i.e., two independent synchronous coherent receptions, one could utilize up to 4.5 or 5 dB gain above the radiometer; each of the added features (i.e., two receptions, synchronism and coherency) can be thought of as contributing 1.5 dB to the gain. We note that, in arriving at these gain figures, system imperfections and noncalibrated parameters such as doppler frequency offset have not been accounted for.

In conclusion, it is seen that certain gains are plausible with respect to the radiometer if careful designs are employed, but they are certainly not overwhelming--at least in the SNR range of interest. This is because a high-rate DS waveform is not very distinguishable from the background thermal AWG noise in which it is detected and, as is well known, the radiometer then becomes an asymptotically optimal detector. This is also in accordance with Krasner's approximate result regarding biorthogonal waveforms ([6, eq. (29)).

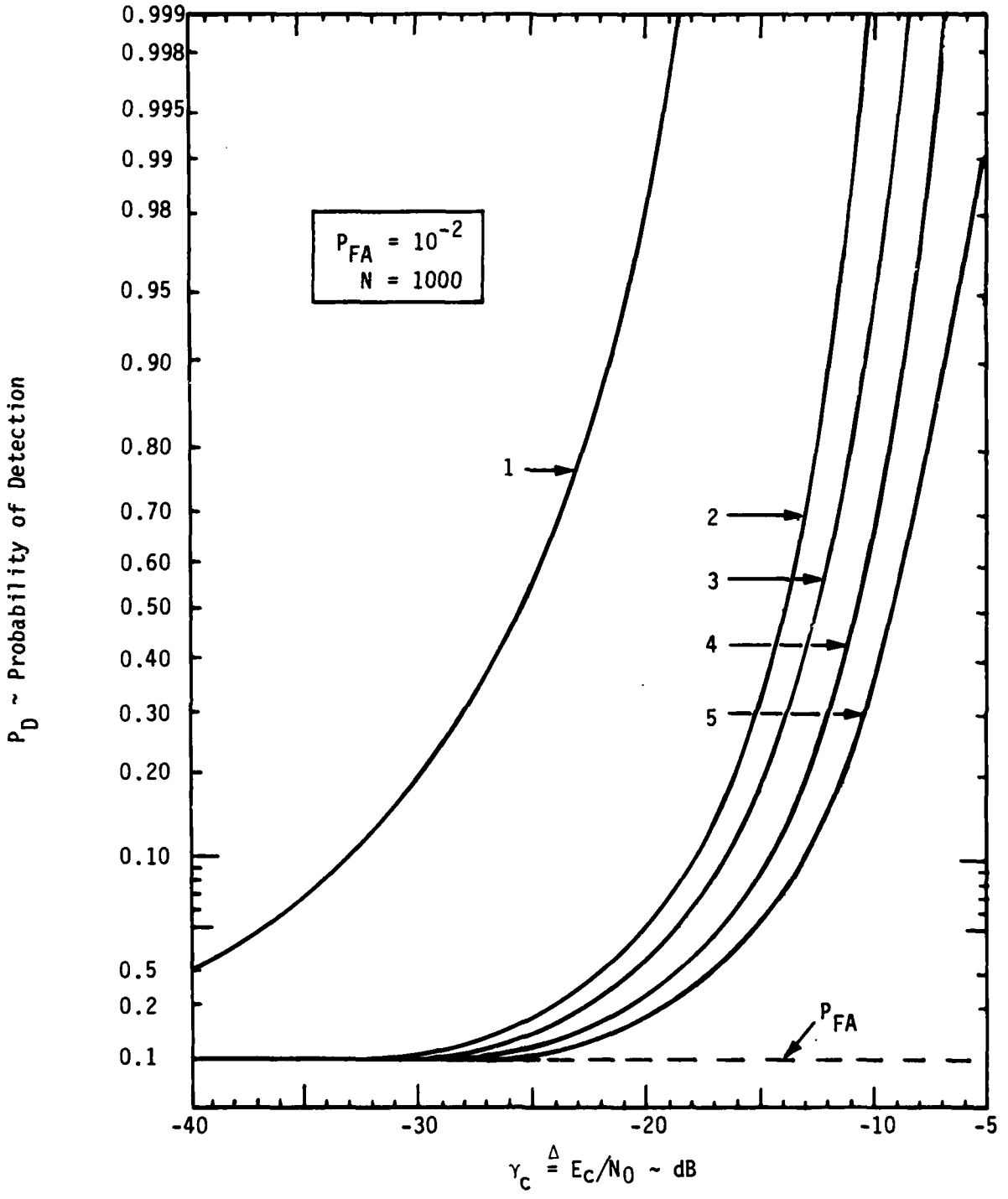

1. Completely known waveform
2. Two independent receptions, synchronous coherent detector
3. Synchronous coherent energy detector
4. Synchronous chip-noncoherent energy detector
5. Radiometer

Figure 3.11. Performance Comparisons for the Detection of DS Waveforms

However, if one removes the biorthogonality of the signal set and/or the AWG nature of the noise, the results can differ substantially. One illustration of the former case can be found in the following section regarding time hopping. Furthermore, if one removes assumption (c) about the white Gaussian nature of the noise, i.e., if some colored interference is superimposed on the thermal background noise, a whole new class of (mostly) open problems is generated. Tackling such problems from a theoretically optimal standpoint would be a much more complicated task in general than that which has been performed up to now for AWGN; nonetheless, the benefits derived from applying certain suboptimal solutions (which are, however, more sophisticated than the radiometer) could be signficant. One particular case of detecting DS waveforms in random-tone interference--and in the absence of thermal noise--is treated in section 5.2, wherein* it is shown that the application of real-time autocorrelation techniques can bring about impressive gains with respect to the radiometer. Although this is a rather ad-hoc technique and the hypothesized scenario is not the most general one, it still serves as a good motivating example of how benefical an extra degree of sophistication can be when the problem formulation and conditions vary.

*Although the development there formally pertains to a FH/DS hybrid system, it essentially addresses DS waveforms since it is concerned with the signal processing on a per-band (single hopping slot) basis.

4.0 DETECTION OF TIME-HOPPING WAVEFORMS

We now focus on the wideband detection of TH waveforms, where the code dictating the hopping is again assumed random. We shall consider only synchronous detectors (i.e., the timing or epoch of the hopping slot will be assumed known); asynchronism can be treated with methods similar to those used in section 3.3. Furthermore, both carrier-coherent and carrier-noncoherent systems will be examined. In particular, the former will assume a known carrier phase combined with a pulse-position-modulation (PPM) format while, for the latter, any modulation that randomizes the phase from frame to frame (e.g., BPSK) is well suited. We term such cases "pulse noncoherent." Clearly, one could hypothesize a noncoherent PPM system with an unknown constant carrier phase and derive the optimal detection rule. However, the resulting receiver and pertinent analysis are much too complicated (for a similar situation, refer to section 3.2 for DS); therefore, only pulse-noncoherent systems will be discussed here. Again, the lower-bounding performance of the radiometer will indicate that very little is lost by using this simplification.

For our purposes, the received waveforms (TH signal plus noise) can be written as

$$r(t) = \sqrt{2S} \sum_{k=-\infty}^{\infty} p\left(t - kT_F - \rho_k T_H\right)\cos\left(\omega_0 t + \theta_k\right) + n(t) \qquad (4\text{-}1)$$

where T_F is the frame length, T_H is the hop length (width of each time slot), and ρ_k, θ_k are random variables that are independent from frame to frame* and of each other, denoting the slot location and carrier phase, respectively, during the $\underline{k}$th frame. Here, ρ_k can take on any one of the equiprobable values $\rho_k = 0, \ldots, N_F - 1$, where $N_F \triangleq T_F/T_H$ is the total number of slots per frame and θ_k summarizes both the unmodulated carrier phase ϕ plus any superimposed PSK modulation. For coherent systems, θ_k is assumed known for every k. Finally, p(t) is a unit pulse of duration T_H seconds, while n(t) is the usual bandpass AWGN. A noiseless sample waveform (realization) of the T_H signal is shown in Figure 4.1. We shall assume that the total observation interval consists of Q frames, i.e., $T = QT_F = QN_F T_H$.

*The independence of θ_k is within the aforementioned spirit of a "pulse-noncoherent" system.

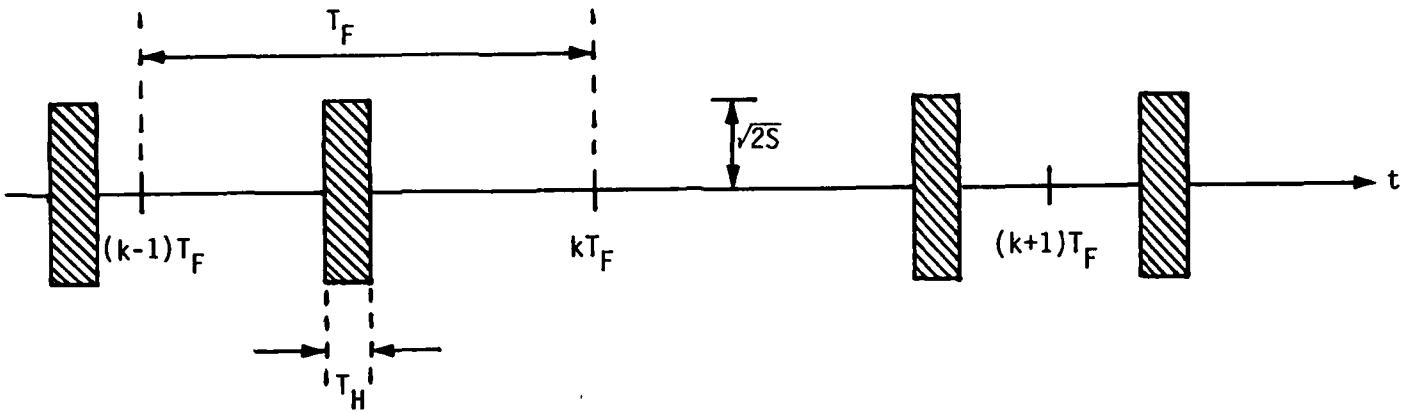

Figure 4.1. A Time-Hopping Signal with N_F = 10 and Random RF Phase from Frame to Frame

4.1 Synchronous Coherent Detectors

Under the coherent assumption, "1" is substituted for $\sqrt{2}\cos(\omega_0 t+\theta_k)$ in (4-1). Then a straightforward application of the generalized likelihoood ratio yields

$$\Lambda(r(t)) = \prod_{m=1}^{Q}\left\{\frac{\exp\{-\gamma_H\}}{N_F}\sum_{k=1}^{N_F}\exp\left\{\frac{2\sqrt{S}}{N_0}\,r_{km}\right\}\right\} \underset{H_0}{\overset{H_1}{\gtrless}} \Lambda_0 \qquad (4\text{-}2)$$

where

$$\gamma_H \triangleq \frac{ST_H}{N_0} \qquad (4\text{-}3)$$

is the SNR per time hop (slot) and

$$r_{km} = \int_{(m-1)T_F+(k-1)T_H}^{(m-1)T_F+kT_H} r(t)\,p(t-kT_H)dt \qquad (4\text{-}4)$$

is the integral of r(t) in the kth slot of the mth frame. If γ_H is a small number, so that $\exp\{x\} \approx 1+x$, (4-2) can be simplified to the approximate

$$\Lambda'(r(t)) \approx \int_0^T r(t)dt \underset{H_0}{\overset{H_1}{\gtrless}} \Lambda'_0 \qquad (4\text{-}5)$$

i.e., just the coherent integral of r(t). However, since γ_H is typically above 0 dB (much larger than γ_c), such approximations are not as successful as in the DS case--a fact to which the comparisons in section 4.3 will attest.

The distance d_{coh} for the coherent rule (4-2) can be derived based on (2-3) and the following steps, as in [3]:

$$d^2_{coh} = \ell n\, \mathcal{E}\{\Lambda^2 | H_0\} = Q\, \ell n\, \mathcal{E}\{\Lambda_F^2 | H_0\} \qquad (4\text{-}6)$$

where Λ_F is the likelihood ratio per frame. But,

$$\ell n\, \mathcal{E}\left\{\Lambda_F^2 \middle| H_0\right\} = \ell n\left[1 + \mathrm{var}_{H_0}\left\{\frac{\exp\{-\gamma_H\}}{N_F} \sum_{k=0}^{N_F-1} \exp\left\{\frac{2\sqrt{S}}{N_0} r_{km}\right\}\right\}\right]$$

$$= \ell n\left[1 + \frac{\exp\{-2\gamma_H\}}{N_F} \mathrm{var}_{H_0}\left\{\exp\left\{\frac{2\sqrt{S}}{N_0} r_{km}\right\}\right\}\right]$$

$$= \ell n\left[1 + \frac{\exp\{-2\gamma_H\}}{N_F}\left(\exp\{4\gamma_H\} - \exp\{2\gamma_H\}\right)\right] \qquad (4\text{-}7)$$

since r_{km} is a zero-mean Gaussian random variable (rv) under H_0. Combining (4-6) and (4-7) results in

$$d_{coh} = \sqrt{Q\, \ell n\left[1 + \frac{1}{N_F}\left(e^{2\gamma_H} - 1\right)\right]} \qquad (4\text{-}8)$$

The distance $d_{coh,appr}$ for the approximate rule (4-5) is derived much easier since

$$\mathcal{E}\left\{\Lambda' \middle| H_k\right\} = \sqrt{S}\, Q\, T_H\, \delta_{k1} \;;\; k = 0,1 \qquad (4\text{-}9a)$$

and

$$\mathrm{var}\left\{\Lambda' \middle| H_0\right\} = \left(N_F Q T_H\right) \frac{N_0}{2} \qquad (4\text{-}9b)$$

Therefore,

$$d_{coh,appr} = \frac{\mathcal{E}\left\{\Lambda' \middle| H_1\right\} - \mathcal{E}\left\{\Lambda' \middle| H_0\right\}}{\left(\mathrm{var}\left\{\Lambda' \middle| H_0\right\}\right)^{1/2}} = \sqrt{2\left(\frac{Q}{N_F}\right)\gamma_H} \qquad (4\text{-}10)$$

It is clear from (4-8) and (4-10) that d_{coh} asymptotically approaches $d_{coh,appr}$ as $\gamma_H \to 0$, an expected result. Furthermore, we can compare the approximate coherent rules (3-9) for DS versus (4-5) for TH and note that the first involves a nonlinear operation on the data prior to integration, while the second does not. This has a reflection on their corresponding distances as (3-12b) is directly proportional to γ_c, while (4-10) is proportional to $\sqrt{\gamma_H}$. Thus, for the very low SNR case, the latter would outperform the former; therefore, TH is a more detectable waveform than DS.

4.2 Synchronous-Noncoherent Detectors

Starting from (4-1) and invoking the independent phase assumption results in the decision rule

$$\Lambda = \prod_{m=1}^{Q} \left\{ \frac{\exp\{-\gamma_H\}}{N_F} \sum_{k=1}^{N_F} I_0\left(\frac{2\sqrt{S}}{N_0} R_{km}\right) \right\} \underset{H_0}{\overset{H_1}{\gtrless}} \Lambda_0 \tag{4-11}$$

where R_{km} is the kth slot, mth frame envelope

$$R_{km} = \sqrt{e_{I,km}^2 + e_{Q,km}^2} \tag{4-12a}$$

and

$$\begin{bmatrix} e_{I,km} \\ e_{Q,km} \end{bmatrix} = 2 \int_{(m-1)T_F+(k-1)T_H}^{(m-1)T_F+kT_H} r(t) \begin{bmatrix} \cos \omega_0 t \\ \sin \omega_0 t \end{bmatrix} dt \tag{4-12b}$$

$$k=1,\ldots,N_F \quad ; \quad m=1,\ldots,Q$$

The distance d_{noncoh} associated with (4-11) is derived by steps identical to (4-7) as

$$d_{noncoh} = \sqrt{Q \, \ell n\left[1 + \frac{1}{N_F}\left(I_0(2\gamma_H) - 1\right)\right]} \tag{4-13}$$

Since $I_0(x) < \exp\{x\}$ for every $x > 0$, it follows from the comparison of (4-8) and (4-13) that $d_{coh} > d_{noncoh}$ for every γ_H, as expected.

Instead of analyzing the noncoherent rule which approximates (4-11) for low SNR, let us consider only the performance of the radiometer that operates on the time-hopped waveform (4-1) for T_H seconds. Following the steps outlined in section 3.4, it can be shown that

$$d_{rad} \approx \sqrt{K_{rad}\left(\frac{Q}{N_F}\right)\gamma_H} \tag{4-14}$$

where the constant $K_{rad} \triangleq \alpha^4/W_{BP} T_H$ again measures the loss due to filtering.

As in section 3.4, K_{rad} can be set at its optimal value $K_{rad} = (0.77)^2 \approx 0.6$. We should note here that (4-14) is actually an optimistic prediction (i.e., an upper bound) of the radiometer's performance since it is based on the assumption that the variance of the test statistic under H_1 is approximately the same as under H_0. For medium-to-high γ_H, this is not true (unlike the DS case where it is justified by the low values of γ_C). Although a more meaningful performance description can easily be derived*, we shall be content with (4-14) for comparison purposes.

*It will consist of a pair of equations similar to (3-11) and (3-59) under an appropriate interpretation of the parameters involved.

4.3 Comparisons and Discussion

First, we are interested in comparing the relative loss of the approximate coherent rule (4-5) versus the exact (4-2) since the former can be implemented trivially (a simple integrator) in contrast to the significant complexity of the latter. The comparison is in terms of the relative SNR values γ_H (in dB) required by each in order to achieve the same performance level (d^2) for the same fixed values of Q and N_F. It is based on (4-8) and (4-10) and is shown in Figure 4.2 ($N_F = 10$). As expected, the difference diminishes at low SNR, but is rather pronounced at medium-to-high SNR. So, $\gamma_H^{coh} = 0$ dB corresponds to $\gamma_H^{coh,appr} = 3.9$ dB--a gap that increases rapidly as γ_H^{coh} increases.

Second, we look at the gains brought about by the coherent assumption versus the noncoherent by comparing the "exact" distances in (4-8) and (4-13). The result, again in terms of the required SNR's for the same performance level, is shown in Figure 4.3. The difference here diminishes as SNR increases, while it can be substantial at low SNR. The final comparison is between the noncoherent "exact" performance (4-13) (or its equivalent log-likelihood sum) versus the radiometer performance estimate (4-14). It is shown in Figure 4.4 for $K_{rad} = 0.6$ and $N_F = 10$. The irreducible distance of 1.1 dB as the SNR goes to zero is due to the $\sqrt{K_{rad}}$ factor*. Again, we should keep in mind that the actual SNR losses of the radiometer are higher than those shown in Figure 4.4 by an amount that increases with SNR due to previously discussed reasons. Furthermore, a common trend is evident from Figures 4.2 and 4.4, namely, that the simplifying deviations from the optimal decision rules incur comparative losses that increase fairly rapidly with the available hop SNR for values of γ_H above 2 - 3 dB. Since this is the dominant range of importance in TH applications, optimal devices (albeit complex) should attract due attention.

*However, this margin will probably disappear if the loss due to asynchronism is accounted for in an asynchronous, noncoherent, optimal detector.

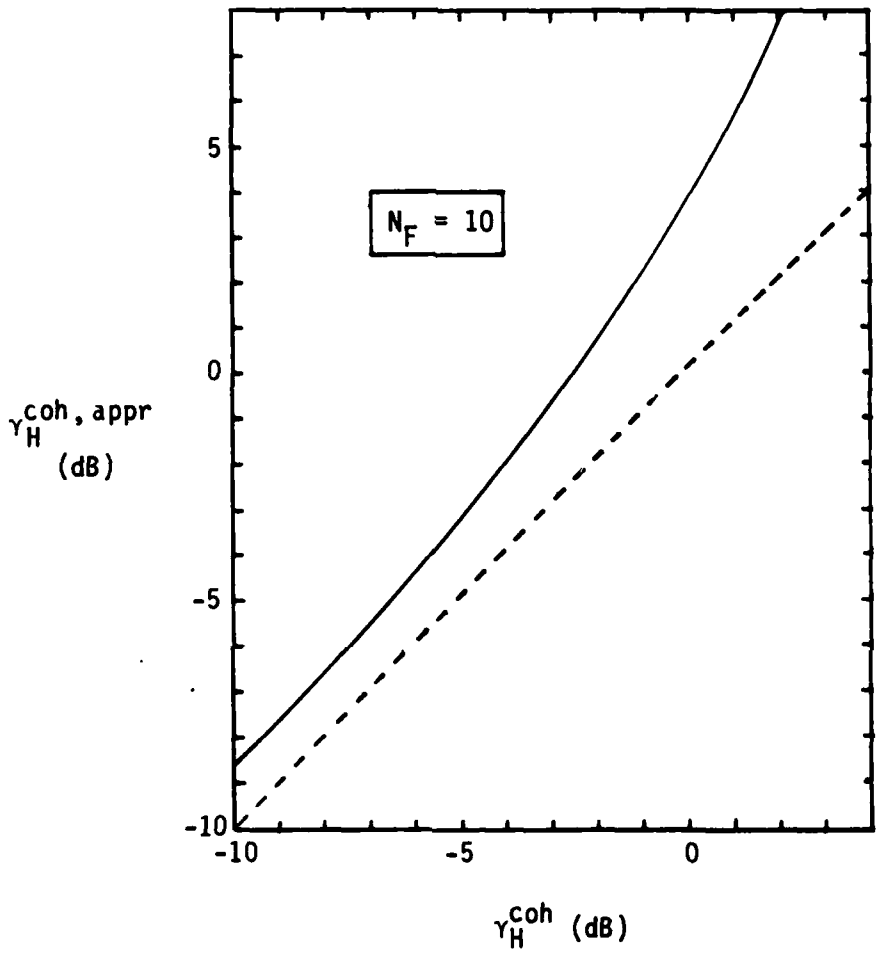

Figure 4.2. Comparison of the Exact (4-2) versus the Approximate (4-5) Coherent Time-Hopping Rules in Terms of Slot SNR's

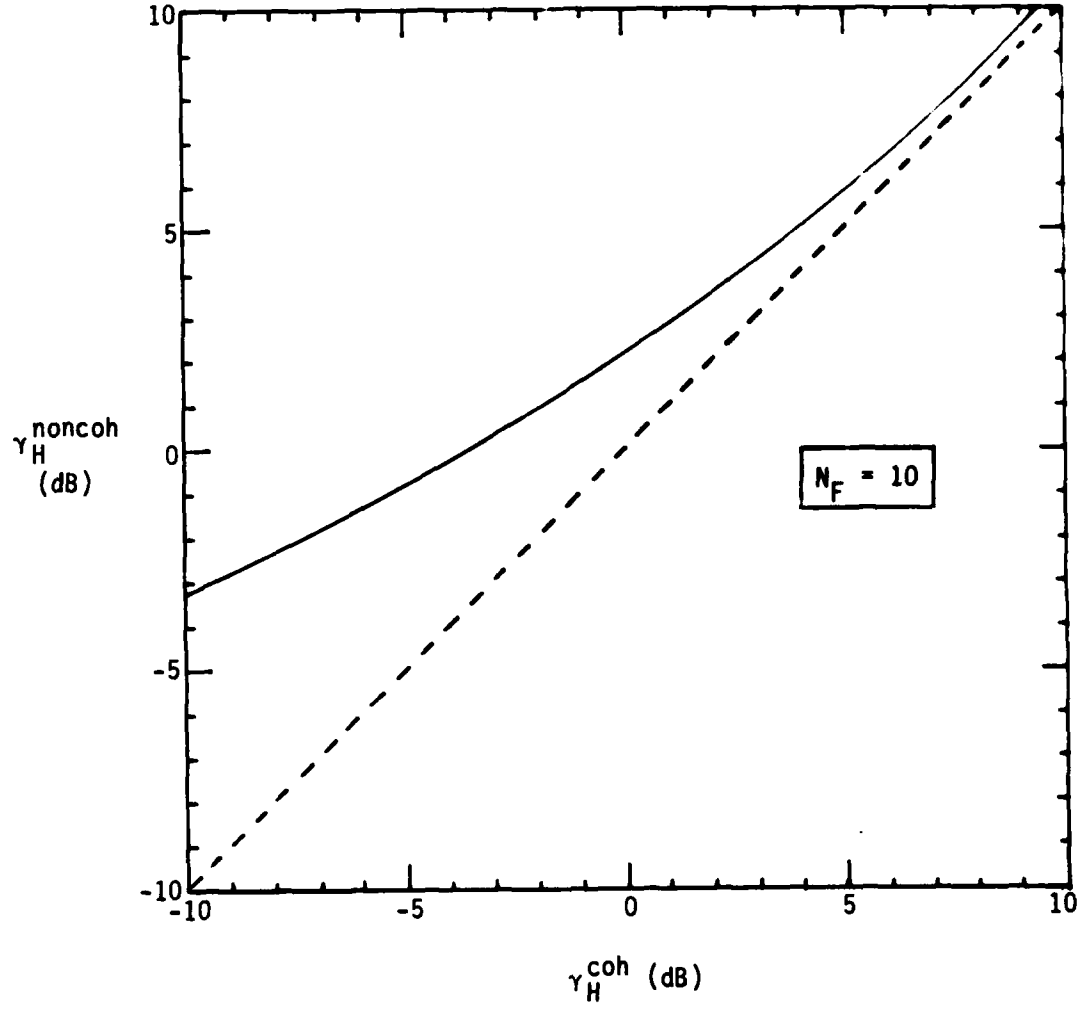

Figure 4.3. Comparison of the Coherent (4-2) versus the Noncoherent (4-11) Time-Hopping Rules in Terms of Slot SNR's

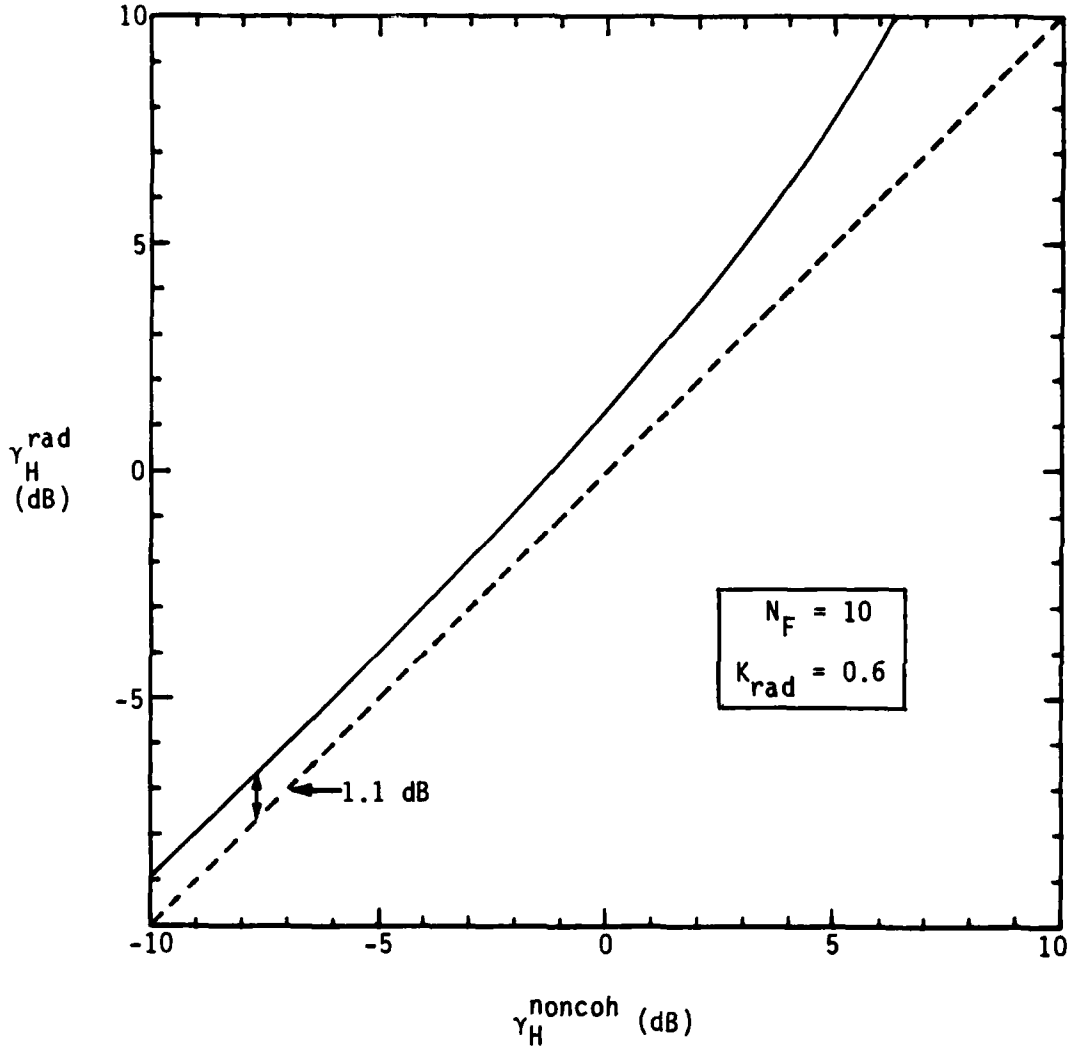

Figure 4.4. Comparison of the Noncoherent Rule (4-11) versus the Radiometer

5.0 DETECTION OF FREQUENCY-HOPPING SIGNALS USING AUTOCORRELATION TECHNIQUES

We shall now focus on the detection of FH or FH/DS waveforms embedded in different forms of additive interference. The two particular cases of interest are: (1) FH signals in AWGN (section 5.1) and, (2) FH/DS signals in random-tone interference (section 5.2). Although optimal detectors can be derived--at least for case (1)--following the guidelines of Sections 3 and 4, those will not receive any in-depth treatment here because their exact implementation is usually hampered by excessive complexity. Instead, we shall deal with improved suboptimal wideband detection procedures, such as real-time autocorrelation-domain algorithms. Our approach has been motivated by recent advances in the technology of real-time autocorrelation and convolution devices with large time-bandwidth products [12, 13]. The rationale for introducing such techniques in the context of wideband detection is explained herein.

Let $s(t)$ be the frequency-hopped signal to be detected (under H_1) in AWGN within a total spread bandwidth of W_s Hz. If $R_H \triangleq T_H^{-1}$ is the hopping rate and the hopping frequencies are contiguous and equispaced by the minimum noncoherent orthogonal separation $\Delta f = R_H$, it follows that the total number M of possible hopping locations is $M = W_s/R_H = W_s T_H$--typically, a very large number. If the total observation time T is for N_T hops, i.e., $T = N_T T_H$, it can then be shown under suitable assumptions that the log likelihood ratio reduces to

$$\sum_{n=1}^{N_T} \ell n \left(\sum_{m=1}^{M} I_0 \left(\frac{2\sqrt{S}}{N_0} R_{nm} \right) \right) \underset{H_0}{\overset{H_1}{\gtrless}} \Lambda'_0 \tag{5-1}$$

where R_{nm} is the envelope output, at the end of the nth hopping interval, of the matched filter centered around the mth hopping frequency (spectral slot), $I_0(\cdot)$ is the zeroth-order Bessel function, and S, N_0 are the signal power and one-sided noise power spectral density (PSD), respectively. Equation (5-1) is the dual to (4-11) for the TH case; it thus follows that performance is quantified by the "exact" distance

$$d_{ex} = \sqrt{N_T \ell n \left[1 + \frac{1}{M} \left(I_0(2\gamma_H) - 1 \right) \right]} \tag{5-2}$$

where γ_H is the hop SNR

$$\gamma_H = \frac{ST_H}{N_0} \tag{5-3}$$

analogous to (4-13).

The most inconvenient aspect of the optimal rule (5-1) is perhaps its complexity: whether implemented as a bank of matched channels or via an FFT (which would simultaneously provide all the spectral estimates R_{nm},m=1, ...,M for each hopping time), the resulting complexity, measured by the number of required filters, can be enormous. One way of alleviating the problem is shown in Figure 5.1: the total bandwidth W_s is subdivided into large contiguous segments of B Hz, each being much larger than the optimal bandwidth of R_H Hz. Appropriate processing produces a per-band decision which is then fed into an overall accumulator (e.g., a majority-logic combiner) for a final decision (H_1 versus H_0). Let us note that alternate reduced configurations have also appeared in the literature [4,5], such as the partial-band filter-bank combiner. There, only a fraction of the total number M of the hopping slots is being observed, but the observation bandwidth per slot is optimal ($B = R_H$). A comparison between alternatives has not yet been performed.

The focus of this section is the waveform-processing (WP) aspect on a per-band basis. Clearly, algorithms improving performance on that level will also increase the overall system performance. We shall assume throughout this development that the time-bandwidth product

$$G \triangleq B\,T_H = B/R_H \gg 1 \tag{5-4}$$

is very large, i.e., of the order of hundreds. The factor G also measures the order of the reduction in complexity when implementing the suboptimal structure of Figure 5.1 instead of the optimal. As a consequence, the input SNR per band, γ_{in}, defined as

$$\gamma_{in} \triangleq \frac{S}{N_0 B} \tag{5-5}$$

is typically very small compared to unity ($\gamma_{in} \ll 1$).

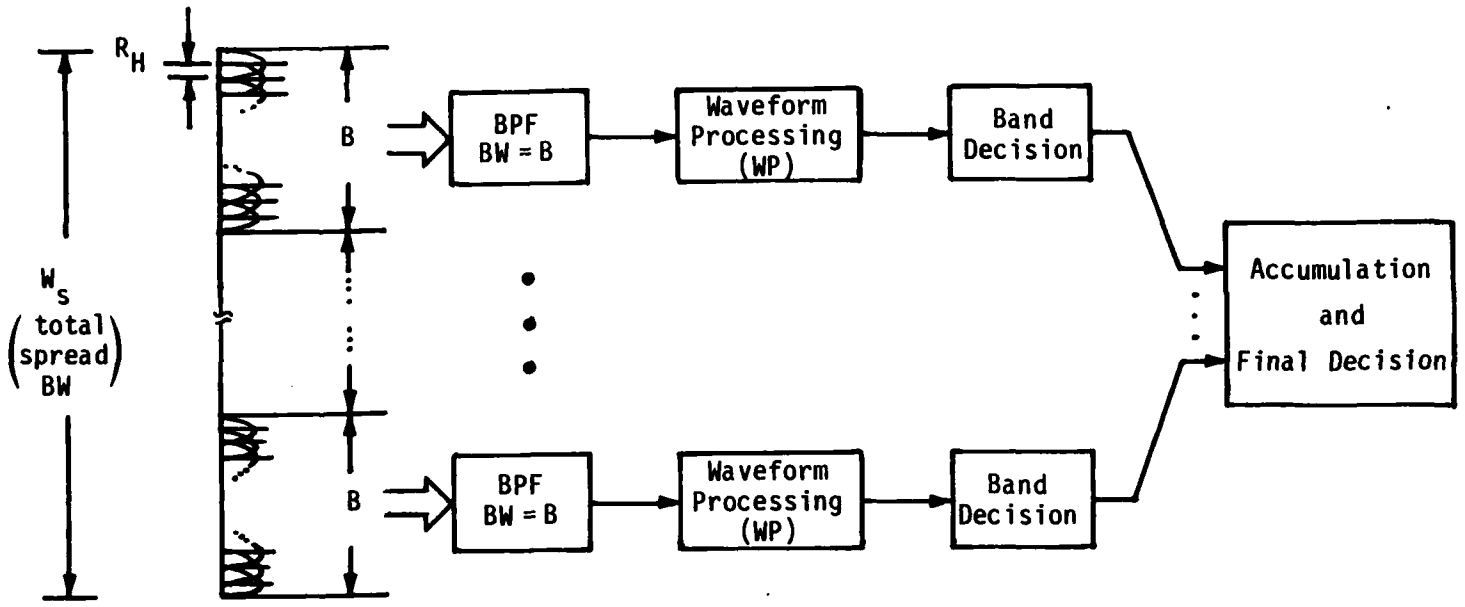

Figure 5.1. Suboptimal Processing: Segmenting W_s into B-Hz Bands ($B \gg R_H$)

Two questions arise immediately:

(1) Into how many bands should the spectrum be divided?

(2) What kinds of WP alternatives are available or could be used?

With respect to (1), it is intuitively clear that one should use as many bands as the number of devices which can be afforded since, by decreasing B and thus increasing γ_{in} from (5-5), more reliable decisions on a per-band basis can be achieved; an elaborate cost-versus-payoff study is of significant interest in this area, but will not be pursued here. As for the second question, we note that the device which immediately comes to mind is the familiar radiometer, designed to measure energy in the band of B Hz, as shown in Figure 5.2. Under the Gaussian assumption for the output decision statistic Y (which is well justified for very large G via a central-limit-type argument), its performance is easily derived to be

$$d_{rad} = Q^{-1}[P_{FA}] - Q^{-1}[P_D] = \sqrt{SNR_{out}} \qquad (5\text{-}6a)$$

where

$$SNR_{out} = SNR_{out}^{rad} = G \cdot \gamma_{in}^2 = G^{-1} \cdot \gamma_H^2 \qquad (5\text{-}6b)$$

Note that the second equality in (5-6b) signifies the small signal suppression effect of square-law detectors [11, page 267]. Again, it should be emphasized that (P_D, P_{FA}) pertain to the per-band decision--not the overall decision scheme.

The autocorrelation-domain methods to be elaborated upon in the following sections can be viewed as a step towards higher sophistication and, therefore, efficiency, of the WP component. In essence, a real-time correlator performs a transformation of the detection problem from the time domain (with parameter t) to a new one, namely, the correlation domain (with parameter τ), in the hope that the new "data", i.e., the correlation function $y(\tau)$, can provide enhanced feature separation between the signal and interference. The merit of such techniques will always be judged against the radiometer which, by nature, takes no account of any signaling details.

We note that the two scenarios to be examined involve the two most different types of interference from a spectral viewpoint, namely, totally flat (AWGN) and totally peaked (tones). Furthermore, they are designed such that

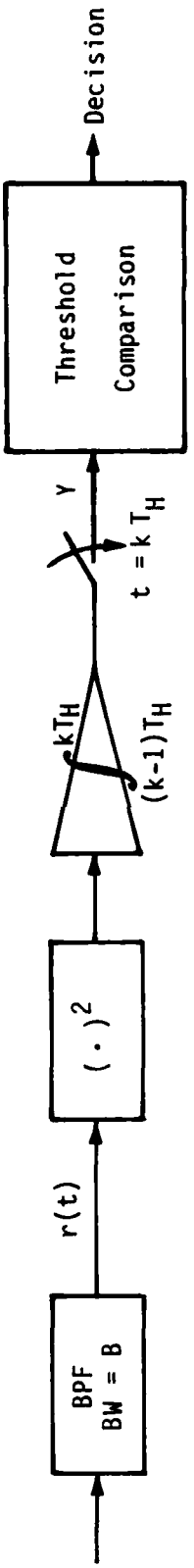

Figure 5.2. The Radiometer Used for the Wideband FH Case

the structural differences between the signal and interference can indeed be exploited to the fullest. As a result, significant gains can be extracted from the correlation domain with respect to the radiometer. At the other extreme, no intelligent algorithm could distinguish, for instance, a random hopping tone from unrelated extraneous random-tone interference, in the absence of additional information. But even then, correlation algorithms would perform no worse than the radiometer. In conclusion, it can be stated that the algorithms to be analyzed herein offer the potential of performance improvement over the common energy detector, which can range from none to impressive, depending on the scenario. The structure and performance of decision rules which will bring about those gains in the presence of mixed types of interference, will be the topic of future research.

5.1 Wideband Detection of FH in AWGN

5.1.1 System Model and Proposed Algorithm

Henceforth, the term "wideband" will be used to indicate detection on a per-band basis under the cardinal restriction (5-4). One mathematical representation of a real-time autocorrelator whose actual implementation is discussed in [12] is shown in Figure 5.3. Let us note that the offset τ, which is the domain parameter for the output autocorrelation function $y(\tau)$, varies linearly with the actual time t of the incoming waveform as a result of the real-time nature of the correlating device. Therefore, the actual integration time is from τ to T_H. Since the radiometer output is only $y(0)$, i.e., just a data point in the new domain, improved performance due to the new scheme is naturally expected.

The decision rule adopted here is as follows: The output $y(\tau)$ is power sampled at multiples of B^{-1}, where B is the input BPF bandwidth and the resulting samples are linearly combined and compared to a threshold, whereupon a decision is reached (H_1 versus H_0 for the corresponding spectral band). Notationally,

$$Y = \sum_{k=1}^{G-1} a_k W_k \underset{H_0}{\overset{H_1}{\gtrless}} \text{Threshold} \qquad (5\text{-}7a)$$

where Y is the decision statistic, $\tau_k \triangleq k \cdot B^{-1}, k=1,2,\ldots,G-1$ is the kth sampling point in the τ domain, and

$$W_k = y^2(\tau_k)\Big|_{\text{Lowpass}} \qquad (5\text{-}7b)$$

is the power measurement around the τ_k point. The set of coefficients $\{a_k\}_1^{G-1}$ can be chosen according to any particular philosophy and is subject to optimization. It can be argued that, under a low-SNR assumption, setting all coefficients equal to a constant $a_k=1$ is a near-optimal choice. This, however, is not a well-founded conclusion as it involves a number of approximations. Fortunately, simulation has indicated (see section 5.1.3) that performance of the summation (5-7a) is very insensitive to the exact value of a_k and a number of reasonable choices would work as long as the upper limit of the summation is properly

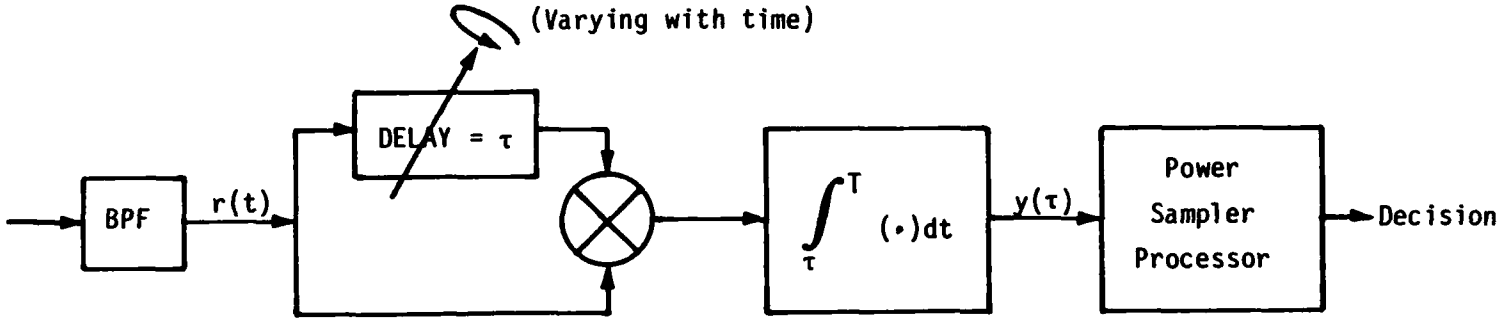

Figure 5.3. Mathematical Model of a Real-Time Autocorrelation Detector

truncated at a level of λG, which is less than G (i.e., $\lambda < 1$). This is because the last samples possess such an increased variance that their inclusion in the summation is detrimental. Analytically, this is equivalent to letting $a_k = 0$ for $\lambda G+1,\ldots,G$ in (5-7a). Thus, a proper choice of λ is rather crucial, while that of $\{a_k\}_{k=1}^{\lambda G}$ is not. For reasons that will soon be clear, it will be mathematically convenient to let

$$a_k = \begin{cases} \left(T_H - \tau_k\right)^{-2} & ; \; k=1,\ldots,\lambda G \\ 0 & ; \; k=\lambda G+1,\ldots,G \end{cases} \tag{5-8}$$

in the following calculations.

5.1.2 Performance Analysis

Here we shall attempt a performance evaluation of the decision rule (5-7) when the interference consists of bandpass AWGN n(t). Thus, during one hop interval $0 \leq t \leq T_H$, under H_1, the input r(t) to the autocorrelator of Figure 5.3 consists of a tone at some radian frequency ω_0 within the observed band plus noise, i.e.,

$$r(t) = \sqrt{2S} \cos \omega_0 t + n(t) \tag{5-9a}$$

where n(t) assumes the typical bandpass representation*

$$n(t) = \sqrt{2}\left[n_I(t) \cos \omega_0 t - n_Q(t) \sin \omega_0 t\right] \tag{5-9b}$$

In (5-9b), $N_I(t)$ and $N_Q(t)$ are the inphase and quadrature lowpass noise processes, respectively, which are approximately independent and identically distributed, with zero mean, flat two-sided PSD of $N_0/2$ W/Hz, and two-sided bandwidth of B Hz each. Since double frequencies are filtered out by the integrator, the autocorrelator output $y(\tau)$ around the signal frequency is

$$y(\tau) = \int_t^{T_H} r(t)r(t-\tau)dt = y_{SS}(\tau) + y_{SN}(\tau) + y_{NS}(\tau) + y_{NN}(\tau) \tag{5-10}$$

with

$$y_{SS}(\tau) = S\left(T_H - \tau\right) \cos \omega_0 \tau \tag{5-11a}$$

$$y_{SN}(\tau) = \sqrt{S}\left(N_I^d(\tau) \cos \omega_0 \tau + N_Q^d(\tau) \sin \omega_0 \tau\right) \tag{5-11b}$$

$$y_{NS}(\tau) = \sqrt{S}\left(N_I(\tau) \cos \omega_0 \tau - N_Q(\tau) \sin \omega_0 \tau\right) \tag{5-11c}$$

$$y_{NN}(\tau) = \left(N_{II}(\tau) + N_{QQ}(\tau)\right) \cos \omega_0 \tau + \left(N_{IQ}(\tau) - N_{QI}(\tau)\right) \sin \omega_0 \tau \tag{5-11d}$$

*Since we shall be concerned with noncoherent detection, an arbitrary phase θ can be inserted in the bandpass description of the noise without altering the results.

where the correlation-domain noise processes have been introduced, i.e.,

$$N_{\begin{bmatrix} I \\ Q \end{bmatrix}}^{d}(\tau) = \int_{\tau}^{T_H} n_{\begin{bmatrix} I \\ Q \end{bmatrix}}(t-\tau)dt \qquad (5\text{-}12a)$$

$$N_{\begin{bmatrix} I \\ Q \end{bmatrix}}(\tau) = \int_{\tau}^{T_H} n_{\begin{bmatrix} I \\ Q \end{bmatrix}}(t)dt \qquad (5\text{-}12b)$$

$$N_{II}(\tau) = \int_{\tau}^{T_H} n_I(t)\, n_I(t-\tau)dt \qquad (5\text{-}12c)$$

$$N_{QQ}(\tau) = \int_{\tau}^{T_H} n_Q(t)\, n_Q(t-\tau)dt \qquad (5\text{-}12d)$$

$$N_{IQ}(\tau) = \int_{\tau}^{T_H} n_I(t)\, n_Q(t-\tau)dt \qquad (5\text{-}12e)$$

$$N_{QI}(\tau) = \int_{\tau}^{T_H} n_Q(t)\, n_I(t-\tau)dt \qquad (5\text{-}12f)$$

Much of the following theory deals with the statistical characterization of the above noise processes. For instance, it is clear that the first four processes in (5-12a) and (5-12b) are zero mean and Gaussian, while the remaining are not Gaussian. However, they will be approximately treated as such in the analysis, particularly for $0 < \tau \ll T_H$, by virtue of a central-limit type argument, as follows: The bandwidth B of $n_I(t)$ and $n_Q(t)$ is much larger than T_H^{-1}; thus, each integral in (5-12c) through (5-12f) can be approximated by a large sum of noise-product samples, each sample taken B^{-1} seconds apart. Since we shall be interested in values of τ that are multiples of B^{-1}, it can be shown that those samples are mutually uncorrelated. Although this does not imply statistical independence (which is a prerequisite for a rigorous application of the central-limit theorem), it nonetheless reinforces the validity of the approximation. This will permit us to calculate higher moments using Gaussian identities whose exact evaluation would otherwise be unwieldy. We furthermore note that simulation has confirmed the accuracy of the approximation to a pleasantly surprising degree (see section 5.1.3).

The first point of interest is the mean value of $y(\tau)$ in (5-10). We shall assume that the input BP filter in Figure 5.3 has a perfectly rectangular transfer function ("brick wall"), which implies that the autocorrelation function $R_{nn}(\tau)$ for both $n_I(t)$ and $n_Q(t)$ is given by

$$R_{nn}(\tau) \triangleq \mathcal{E}\{n_I(t)n_I(t-\tau)\} = \mathcal{E}\{n_Q(t)n_Q(t-\tau)\} = \left(\frac{N_0B}{2}\right)\mathrm{Sa}(\pi B\tau) \qquad (5\text{-}13)$$

where $\mathrm{Sa}(x) \triangleq (\sin x)/x$. Using the fact that

$$\mathcal{E}\{N_I\} = \mathcal{E}\{N_I^d\} = \mathcal{E}\{N_Q\} = \mathcal{E}\{N_Q^d\} = \mathcal{E}\{N_{IQ}\} = \mathcal{E}\{N_{QI}\} = 0 \qquad (5\text{-}14a)$$

and

$$\mathcal{E}\{N_{II}(\tau)\} = \mathcal{E}\{N_{QQ}(\tau)\} = (T_H - \tau)\, R_{nn}(\tau) \qquad (5\text{-}14b)$$

we conclude from (5-10) through (5-14) that

$$\mathcal{E}\{y(\tau)\} = \left[S + (N_0B)\ \mathrm{Sa}(\pi B\tau)\right](T_H - \tau)\cos\omega_0\tau \qquad (5\text{-}15)$$

Certain interesting observations can be made on (5-15). First, although the quadrature component $(\sin\omega_0\tau)$ has been eliminated, the mean $\mathcal{E}\{y(\tau)\}$ still includes an oscillation of unknown frequency*. That is why noncoherent (power) sampling must be performed at the signal-processing unit. Second, we note that the mean value at zero offset $\mathcal{E}\{y(0)\} = (S + N_0B)T_H$ is just the average energy measured by the radiometer at the end of T_H seconds, as it should be. Since we have assumed that $\gamma_{in} \ll 1$, implying that $S \ll N_0B$, it follows that the radiometer output is dominated by the noise contribution--definitely not a helpful situation. Third, and most important, it follows from (5-15) that, if the output $y(\tau)$ is power sampled at multiples of B^{-1}, i.e., $\tau_k = kB^{-1}$; k an integer, the contribution of the mean noise will be eliminated due to the nulls of the Sa(x) function. This fact will be exploited in the following.

*The only thing known about $f_0 = \omega_0/2\pi$ is that it belongs in the frequency band observed, but it is otherwise unspecified.

Let us return to (5-10) for a moment. Since we shall be interested in the low-SNR case, we make the simplifying assumption that the signal times noise terms $y_{SN}(\tau)$ and $y_{NS}(\tau)$ are negligible compared to the noise times noise term $y_{NN}(\tau)$. For γ_{in} below -15 dB or so, such a simplification is quite justified, as also indicated by the simulation. When γ_{in} is higher, the neglected terms increase the variance of the output statistic under H_1 (they clearly are not present under H_0), with a resulting deterioration in overall performance. At this stage, however, we shall derive a performance estimate for low SNR, leaving more refined (and much more cumbersome) calculations for later. Within this formulation, $y(\tau)$ can be rewritten as

$$y(\tau) = C(\tau) \cos \omega_0\tau + N_I^{eq}(\tau) \cos \omega_0\tau + N_Q^{eq}(\tau) \sin \omega_0\tau \tag{5-16}$$

where

$$C(\tau) = \begin{cases} S(T_H-\tau) & (H_1) \\ 0 & (H_0) \end{cases} \tag{5-17a}$$

and the equivalent noises

$$N_I^{eq}(\tau) \triangleq N_{II}(\tau) + N_{QQ}(\tau) \tag{5-17b}$$

and

$$N_Q^{eq}(\tau) \triangleq N_{IQ}(\tau) - N_{QI}(\tau) \tag{5-17c}$$

As mentioned, $y(\tau)$ will be power sampled at $\tau_k = kB^{-1}$; at which points,

$$\mathcal{E}\left\{N_I^{eq}(\tau_k)\right\} = \mathcal{E}\left\{N_Q^{eq}(\tau_k)\right\} = 0 \tag{5-18}$$

According to our previous discussion, N_I^{eq} and N_Q^{eq} will be treated as Gaussian noises. Furthermore, it is shown in Appendix H that $N_I^{eq}(\tau_k)$ and $N_Q^{eq}(\tau_j)$ are uncorrelated for every k,j=1,2,3...,G; similarly, the pairs $\left(N_I^{eq}(\tau_{k_1}), N_I^{eq}(\tau_{k_2})\right)$ and $\left(N_Q^{eq}(\tau_{k_1}), N_Q^{eq}(\tau_{k_2})\right)$ are uncorrelated as long as $\tau_{k_1} \neq \tau_{k_2}$. Coupling this result with the approximate Gaussian assumption, it follows that the sequences

of noise samples $\left\{N_I^{eq}(\tau_k)\right\}_{k=1}^{G}$ and $\left\{N_Q^{eq}(\tau_k)\right\}_{k=1}^{G}$ contain 2G Gaussian rv's which are zero mean and approximately independent. Thus, to complete their statistical description, the second moments (or variances, for this case) are required. Those are obtained in Appendix H, wherein it is shown that

$$\mathcal{E}\left\{\left(N_I^{eq}(\tau_k)\right)^2\right\} = \left(N_0B\right)^2\left(T_H-\tau_k\right)^2\left(F_1(k) + F_2(k)\right) \tag{5-19a}$$

and

$$\mathcal{E}\left\{\left(N_Q^{eq}(\tau_k)\right)^2\right\} = \left(N_0B\right)^2\left(T_H-\tau_k\right)^2\left(F_1(k) - F_2(k)\right) \tag{5-19b}$$

where

$$F_1(k) = \int_0^1 (1-\rho')\, Sa^2\left[\pi G(1 - \zeta_k)\rho'\right] d\rho' \tag{5-20a}$$

and

$$F_2(k) = \int_0^1 (1-\rho')Sa\left[\pi G\left((1 - \zeta_k)\rho' + \zeta_k\right)\right] Sa\left[\pi G\left((1-\zeta_k)\rho' - \zeta_k\right)\right] d\rho' \tag{5-20b}$$

and the normalized parameter ζ_k is defined as

$$\zeta_k \triangleq \frac{\tau_k}{T_H} = \frac{k}{BT_H} = \frac{k}{G}\ ;\ k=1,\ldots,G-1 \tag{5-20c}$$

so that $0 < \zeta_k < 1$. Some meditation on the functional form of $F_2(k)$ reveals that it has a negligible contribution compared to $F_1(k)$, so it will be dropped henceforth. From (5-19), we then have that

$$\sigma_N^2(k) \triangleq \mathcal{E}\left\{\left(N_I^{eq}(\tau_k)\right)^2\right\} \approx \mathcal{E}\left\{\left(N_Q^{eq}(\tau_k)\right)^2\right\}$$

$$\approx \left(N_0B\right)^2\left(T_H-\tau_k\right)^2 F_1(k) = \left(N_0BT_H\right)^2(1 - \zeta_k)^2\, F_1(k) \tag{5-21}$$

which is a fairly simple expression, but also fundamental for the following.

Let us now return to (5-16). As mentioned, the lack of knowledge regarding ω_0 forces us to noncoherent sampling. Let $W_k \triangleq y^2(\tau_k)\big|_{\text{Lowpass}}$ denote such a sample, which is also defined in (5-7b). We note that this kind of sampling can be implemented via a square-law device, followed by a wideband lowpass integrating filter; its bandwidth should be several times larger than the input bandwidth B, but still much narrower than twice the carrier frequency. Then (5-16) and (5-17a) imply that, under H_1,

$$W_k = (ST_H)^2 (1 - \zeta_k)^2 + \left(N_I^{eq}(\tau_k)\right)^2 + \left(N_Q^{eq}(\tau_k)\right)^2 ; \; k=1,\ldots,G-1 \qquad (5\text{-}22)$$

By virtue of the approximate statistical independence of the second and third noise terms in (5-22), $\{W_k\}_{k=1}^{G-1}$ is a sequence of approximately independent noisy samples, upon which the decision is based. As mentioned, this valuable property of independence gradually diminishes as $k \to G-1$ because the fundamental assumption in assessing it (i.e., Gaussian equivalent noise) weakens toward the end. This is also why those latest samples should be ignored. Nonetheless, such a property is the key ingredient in the anticipated superiority of the correlator versus the radiometer--namely, the fact that additional information can be exploited by incorporating all those new samples in the decision. Their approximate independence keeps these samples from being statistically useless.

In order to proceed with the evaluation of rule (5-7), we need the mean and variance of the W_k's. From (5-19) and (5-22), we have that the difference of the means of W_k under the two hypotheses, $\Delta\mathcal{E}\{W_k\}$, is given by

$$\Delta\mathcal{E}\{W_k\} \triangleq \mathcal{E}\{W_k|H_1\} - \mathcal{E}\{W_k|H_0\} = (ST_H)^2 (1 - \zeta_k)^2 \qquad (5\text{-}23)$$

Furthermore, using the independence between $N_I^{eq}(\tau_k)$ and $N_Q^{eq}(\tau_k)$ along with the Gaussian assumption yields the variance as

$$\begin{aligned} \text{var}\{W_k\} &= 2\text{var}\left\{\left(N_I^{eq}(\tau_k)\right)^2\right\} = 2\left[\mathcal{E}\left\{\left(N_I^{eq}(\tau_k)\right)^4\right\} - \mathcal{E}^2\left\{\left(N_I^{eq}(\tau_k)\right)^2\right\}\right] \\ &= 2\left[3\sigma_N^4(k) - \sigma_N^4(k)\right] = \left(2\sigma_N^2(k)\right)^2 \end{aligned} \qquad (5\text{-}24)$$

with σ_N^2 as per (5-21).

As seen in (5-23), (5-24) and (5-21), the quantities of interest for W_k include a multiplicative factor $(1 - \tau_k)^2$, a reflection of the fact that the integration time reduces proportionally to τ_k as $\tau_k \to T_H$. The insertion of the coefficients a_k in (5-8) purported to remove this factor without essentially altering the results. Thus, if we define

$$W_k' \triangleq \frac{W_k}{(T_H - \tau_k)^2} = \frac{W_k}{T_H^2(1 - \tau_k)^2} \tag{5-25}$$

it follows from (5-23) and (5-24) that

$$\Delta\mathcal{E}\{W_k'\} = S^2 \tag{5-26a}$$

and

$$\mathrm{var}\{W_k'\} = 4(N_0B)^4 F_1^2(k) \tag{5-26b}$$

while the decision rule (5-7a) reads:

$$Y = \sum_{k=1}^{\lambda G} W_k' \tag{5-27}$$

We shall now define performance for the correlator in a manner that is analogous to the radiometer as manifested by (5-6). In other words, within the Gaussian assumption for Y, performance is quantified by (5-6a), where the output SNR for the correlator is now

$$\mathrm{SNR}_{\mathrm{out}}^{\mathrm{corr}} = \frac{\left(\mathcal{E}\{Y|H_1\} - \mathcal{E}\{Y|H_0\}\right)^2}{\mathrm{var}\{Y|H_0\}} \tag{5-28}$$

We wish to emphasize again that (5-28) is meaningful only when Y possesses a distribution that is sufficiently close to Gaussian and the variance under either hypothesis is the same. The latter assumption is justified for very low-input SNR, while the former can be validated only though simulation. For

somewhat higher SNR, the proper measure of performance and comparison is the pair (P_D, P_{FA}); in which case, $\text{var}\{Y|H_1\}$ is larger than $\text{var}\{Y|H_0\}$ by a significant factor. More discussion on this topic can be found in the following section.

Based on (5-26), (5-27) and the uncorrelatedness of W_k's, it follows from (5-28) that

$$SNR_{out}^{corr} = \frac{(\lambda G S^2)^2}{4(N_0 B)^4 \sum_{k=1}^{\lambda G} F_1^2(k)} = \frac{\lambda^2 G^2}{4 \sum_{k=1}^{\lambda G} F_1^2(k)} \cdot \gamma_{in}^4$$

or, using the fact that $\gamma_H = G \cdot \gamma_{in}$,

$$SNR_{corr}^{out} = A(\lambda, G)\, G^{-1} \cdot \gamma_H^4 \tag{5-29}$$

where the coefficient $A(\lambda, G)$ is defined as

$$A(\lambda, G) \triangleq \frac{\lambda^2}{4G \sum_{k=1}^{\lambda G} F_1^2(k)} \tag{5-30}$$

and will be called the "correlator processing gain" or, for brevity, CPG. The terminology is easily understood if we combine (5-6b) and (5-29) into a ratio:

$$\frac{SNR_{out}^{corr}}{SNR_{out}^{rad}} = A(\lambda, G) \cdot \gamma_H^2 \tag{5-31}$$

The interpretation of (5-31) is that, within the framework of performance established herein, the correlator will outperform the radiometer if the product $A(\lambda, G) \cdot \gamma_H^2$ is above unity and vice versa. We note that this product signifies some kind of utility factor and is separated into two components: (1) $A(\lambda, G)$, depends on features of the device used (G) and the signal-processing algorithm employed (λ), and (2) $\gamma_H = ST_H/N_0$, depends on scenario parameters (signal and noise strength, hopping duration). Thus, the acronym CPG is naturally attached

to the component (gain), depending on the signal-processing aspects of the detector. Let us briefly focus on it in the following.

Exact evaluation of $A(\lambda,G)$ unfortunately requires numerical integration by computer, which somewhat destroys any anticipated insight. However, a bounding argument can be developed which, in essence, warrantees a minimum value for $A(\lambda,G)$, namely, $A_{min}(\lambda,G)$. This minimum value (or lower bound) can be used in conjunction with (5-31) to warrantee a minimum gain for the correlator versus the radiometer and is, in fact, very tight to the exact result for low values of λ. The argument is based on the observation that the quantity $F_1(k)$ in (5-20a) is a monotonically increasing function of the argument ζ_k; thus,

$$F_1(k) \leq F_1(\lambda G) = \int_0^1 (1-\rho')Sa^2\left[\pi G(1-\lambda)\rho'\right]d\rho' \; ; \; k=1,\ldots,\lambda G \tag{5-32}$$

since $\zeta_{\lambda G} = \lambda$ from (5-20c). The inequality in (5-32) can be strengthened by the following steps:

$$\begin{aligned}
&\int_0^1 (1-\rho')Sa^2\left[\pi G(1-\lambda)\rho'\right]d\rho' \\
&< \int_0^1 Sa^2\left[\pi G(1-\lambda)\rho'\right]d\rho' = G^{-1}(1-\lambda)^{-1}\int_0^{G(1-\lambda)} Sa^2[\pi x]dx \\
&< G^{-1}(1-\lambda)^{-1}\int_0^{\infty} Sa^2[\pi x]dx \\
&= G^{-1}(1-\lambda)^{-1}(1/2)
\end{aligned} \tag{5-33}$$

Thus, from (5-32) and (5-33),

$$\sum_{k=1}^{\lambda G} F_1^2(k) < \lambda G\, F_1^2(\lambda G) < \frac{\lambda}{4G(1-\lambda)^2}$$

which, when combined with (5-30), yields

$$A(\lambda,G) > A_{min}(\lambda,G) = A_{min}(\lambda) = \lambda(1-\lambda)^2 \tag{5-34}$$

We note that the lower bound A_{min} depends on λ only, while the exact gain $A(\lambda,G)$ also depends on G. This is just a fortunate coincidence, and indicates that A_{min} can be used for every G, as long as $G \gg 1$. Thus, we arrive at the following bound:

$$\frac{SNR_{out}^{corr}}{SNR_{out}^{rad}} > \lambda(1-\lambda)^2 \gamma_H^2 \qquad (5\text{-}35)$$

which, as mentioned, should be tight for small λ.

In addition to this general bound, we can create a good approximate formula for the above ratio when $G(1-\lambda) \gg 1$, as follows: since the steps used to derive (5-33) are, in fact, tight successive approximations, we conclude that $F_1(k) \approx G^{-1}\left(1-kG^{-1}\right)^{-1}(1/2)$, which leads to

$$\sum_{k=1}^{\lambda G} F_1^2(k) \approx \frac{1}{4} \sum_{k=1}^{\lambda G} \frac{1}{(G-k)^2} \cong \frac{1}{4} \sum_{m=G(1-\lambda)}^{G} \frac{1}{m^2}$$

The last summation can be well approximated by the integral

$$\sum_{m=G(1-\lambda)}^{G} \frac{1}{m^2} \approx \int_{G(1-\lambda)}^{G} \frac{dx}{x^2} = \frac{1}{G}\left[\frac{1}{1-\lambda} - 1\right] = \frac{\lambda}{G(1-\lambda)}$$

provided that $G(1-\lambda) \gg 1$. Substitution into (5-30) leads to

$$\boxed{\frac{SNR_{out}^{corr}}{SNR_{out}^{rad}} \approx \lambda(1-\lambda) \gamma_H^2} \qquad (5\text{-}36)$$

which differs from the bound (5-35) in the exponent of $(1-\lambda)$. For low λ, (5-35) and (5-36) agree closely. In any case, (5-35) and (5-36) indicate that the relative merit of the correlator increases proportionally to the square of the hop SNR and could therefore reach significant levels, depending on the application (coded or uncoded systems, slow or fast hopping, etc.).

5.1.3 Simulation Results and Discussion

The proposed correlation algorithm plus the radiometer were simulated by computer; a detailed description of this simulation can be found in Appendix I. Here, we shall summarize the findings and discuss them.

First, the tightness of the predicted bound (5-35) was examined. The following parameters were chosen so that the theoretical assumptions involved in the analysis would be well justified: (1) large time-bandwidth product (G= 1000 or 30 dB), (2) small input SNR $\left(\gamma_{in} \leq -10 \text{ dB}\right)$, (3) small λ ($\lambda = 0.1$) and, (4) large number of trials (200), so as to assume statistical confidence. Since those numbers were in accordance with the assumptions made, any deviations of the simulation from the theory would indicate an error in the modeling process (Gaussianness, etc.). Fortunately, that was not the case, as evidenced by the closeness of the theoretical and simulation results, as shown in Table 5.1, which lists the output SNR difference ΔSNR (in dB) between $\left(\text{SNR}_{\text{out}}^{\text{corr}}\right)_{\text{dB}}$ and $\left(\text{SNR}_{\text{out}}^{\text{rad}}\right)_{\text{dB}}$, both from theory (5-35) and the simulation. In other words, the theoretical lower bound from (5-35) is

$$\left[\left(\Delta\text{SNR}\right)_{\text{dB}}\right]_{\text{LB}} \triangleq \left[\left(\text{SNR}_{\text{out}}^{\text{corr}}\right)_{\text{dB}} - \left(\text{SNR}_{\text{out}}^{\text{rad}}\right)_{\text{dB}}\right]_{\text{LB}} = \left[\lambda(1-\lambda)^2\right]_{\text{dB}} + 2\left(\gamma_H\right)_{\text{dB}} \quad (5\text{-}37)$$

For λ=0.1, the first term on the right-hand side of (5-37) is equal to -11 dB while, for $G=10^3$, $\left(\gamma_H\right)_{\text{dB}} = 30 \text{ dB} + \left(\gamma_{in}\right)_{\text{dB}}$. We note that the simulation result in Table 5.1 is slightly below its theoretical counterpart (lower bound) for the first two columns, while it exceeds the latter in the last column. This can be attributed to both the many analytical approximations involved and the possibility that γ_{in}, in the first two columns, is insufficiently small. For $\gamma_{in} < -20$ dB, the simulation seems to agree perfectly with the theory. In any case, the gains depicted in Table 5.1 for the correlator range from 9 dB to 29 dB--definitely a major improvement over the radiometer.

Next, we look at the sensitivity of the decision rule (5-27) with respect to the choice of λ. This is illustrated in Figure 5.4, where the detection probability P_D is plotted versus $\lambda (0 < \lambda \leq 1)$ for various values of γ_{in} and P_{FA}, while G = 100 is constant. For each set of three curves associated with a single value of γ_{in}, the corresponding values of P_{FA} are 10^{-1}, 10^{-4} and 10^{-6},

Table 5.1. Theoretical and Simulation Values For $(\Delta SNR)_{dB} = \left(SNR_{out}^{corr}\right)_{dB}$, For Various Values of γ_{in} (dB)

$G = 10^3$, $\lambda = 0.1$			
γ_{in} (dB)	-10	-15	-20
ΔSNR (dB) theoretical (lower bound)	29	19	9
ΔSNR (dB) Simulation	28	18.5	10

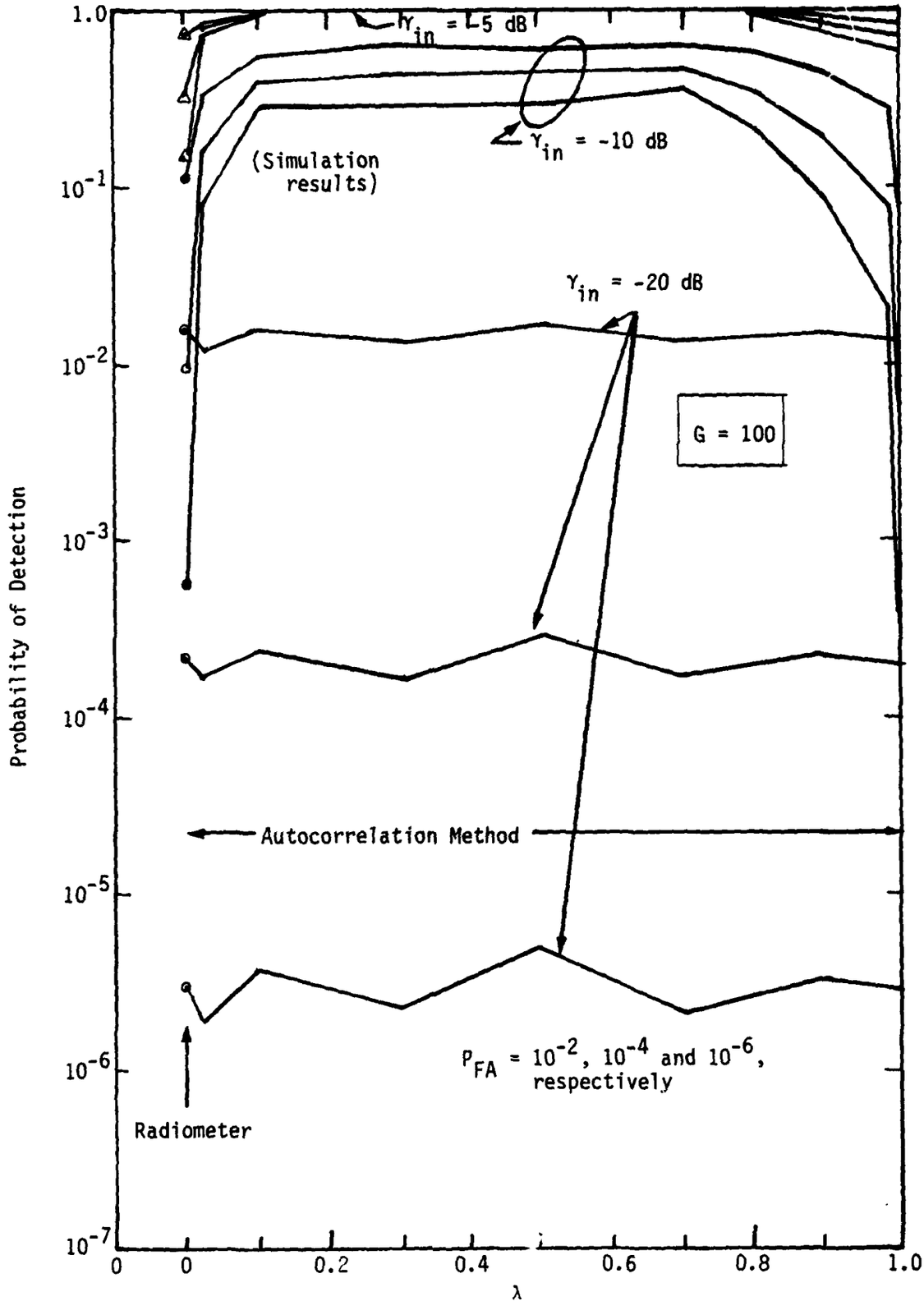

Figure 5.4. P_D Versus λ For Various γ_{in} and P_{FA}

from top to bottom, respectively. In all cases examined, the trend is clear: performance is insensitive to changes of λ over a very wide range as long as λ is neither too small nor too large. So, any λ in the range (0.1,0.8) would be a suitable choice. Although the curves shown in Figure 5.4 are for a particular choice of a_k's (the ones in (5-8)), an identical kind of behavior was also found for other choices. This is a rather convenient conclusion since one does not have to worry about optimizing λ whenever the constants are changed. Furthermore, it was found as a more general conclusion that the overall performance (P_D, P_{FA}) was insensitive to the particular choice of a_k's. Thus, one can set $a_k=1$, $k=1,\ldots,\lambda G$, which would simplify the decision rule to a mere accumulation (summation) of the power samples W_k and a threshold comparison.

A set of simulated design curves for both the radiometer and the correlator are provided in Figure 5.5, parts (a) and (b), respectively. There, P_D is plotted as a function of γ_{in} (dB), for various values of P_{FA} in the range of 10^{-1} to 10^{-6}. For comparison purposes, the $P_{FA}=10^{-1}$ and 10^{-4} curves for both have been redrawn in Figure 5.6 so that the relative gains of the correlator versus the radiometer in input SNR can be assessed easier. We reiterate that direct invocation of (5-36) or (5-31) would not be meaningful in this case, where G is relatively low and γ_{in} is relatively high, because the variance of the decision statistic under H_1 is many times greater than under H_0. Thus, any gains in SNR should be directly read off the operating curves. An alternative comparison is offered in Figure 5.7, which depicts the familiar "receiver operating characteristic" (ROC) curves for both systems, parameterized by γ_{in}. The parameter G was set at $G=10^2$. Clearly, for $\gamma_{in} > -20$ dB, the correlator will outperform the radiometer by an amount which increases with γ_{in}.

Finally, let us note that attention should be given to implementing the almost instantaneous power measurement W_k; this can be accomplished using a square-law device, followed by a fairly wide lowpass filter whose bandwidth is many times that of the observation bandwidth B (i.e., its response time is a small fraction of B^{-1}). Still, that filter should be narrow compared to the IF frequency in order to avoid undesirable power measurement errors.

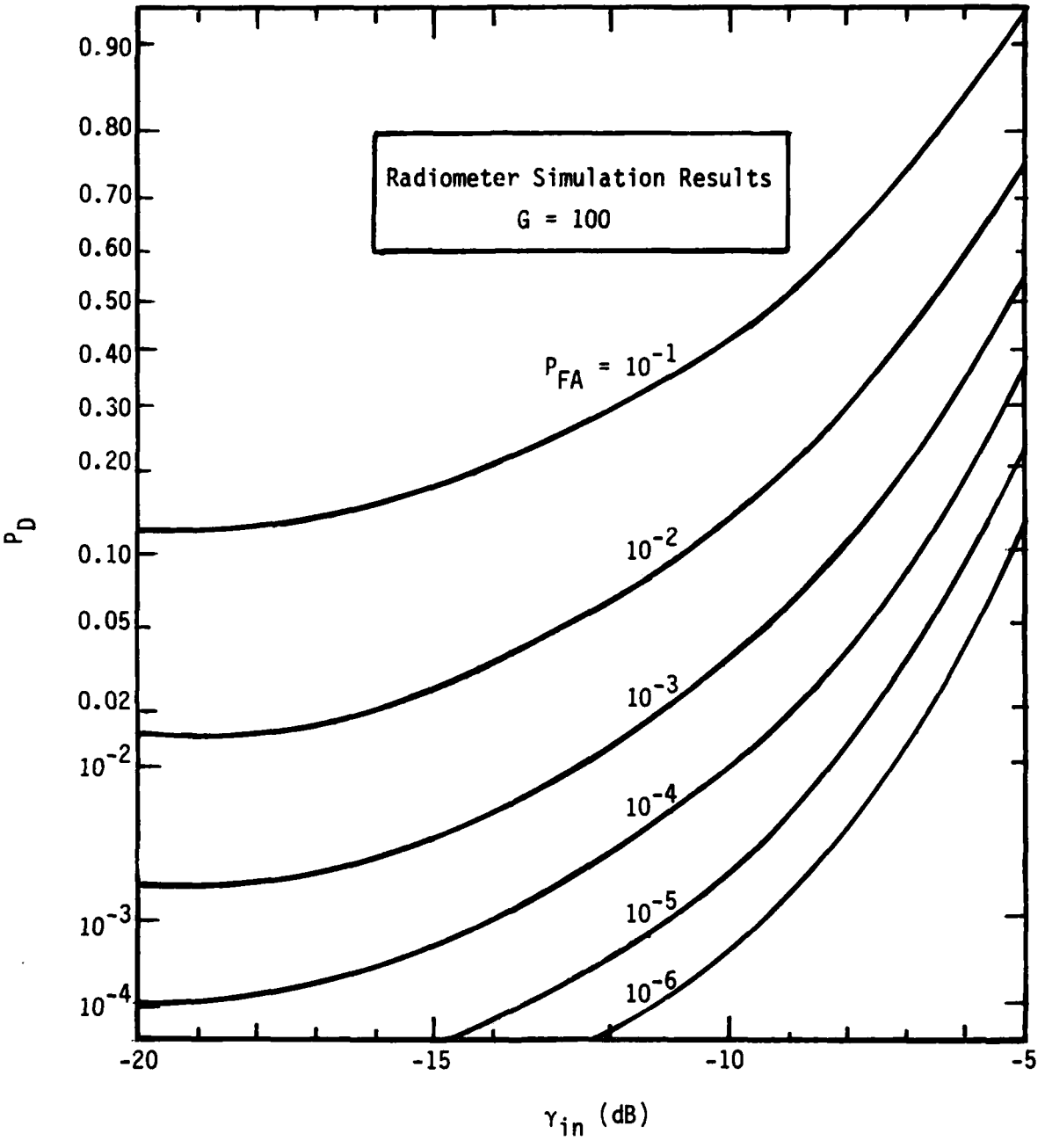

Figure 5.5(a). Simulated Plot of P_D Versus γ_{in} for the Radiometer, Parameterized by P_{FA}

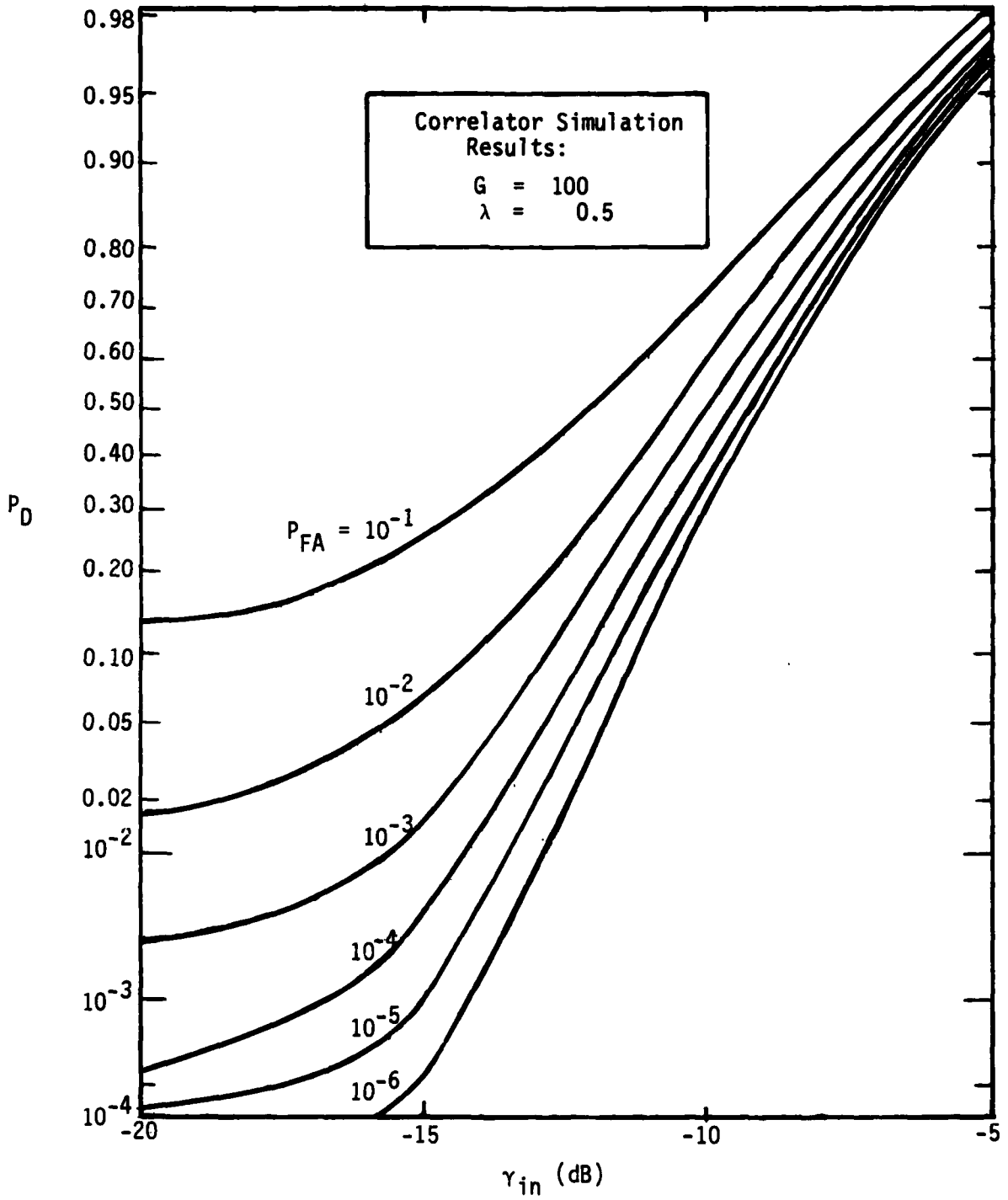

Figure 5.5(b). Simulated Plot of P_D Versus γ_{in} for the Correlator, Parameterized by P_{FA}

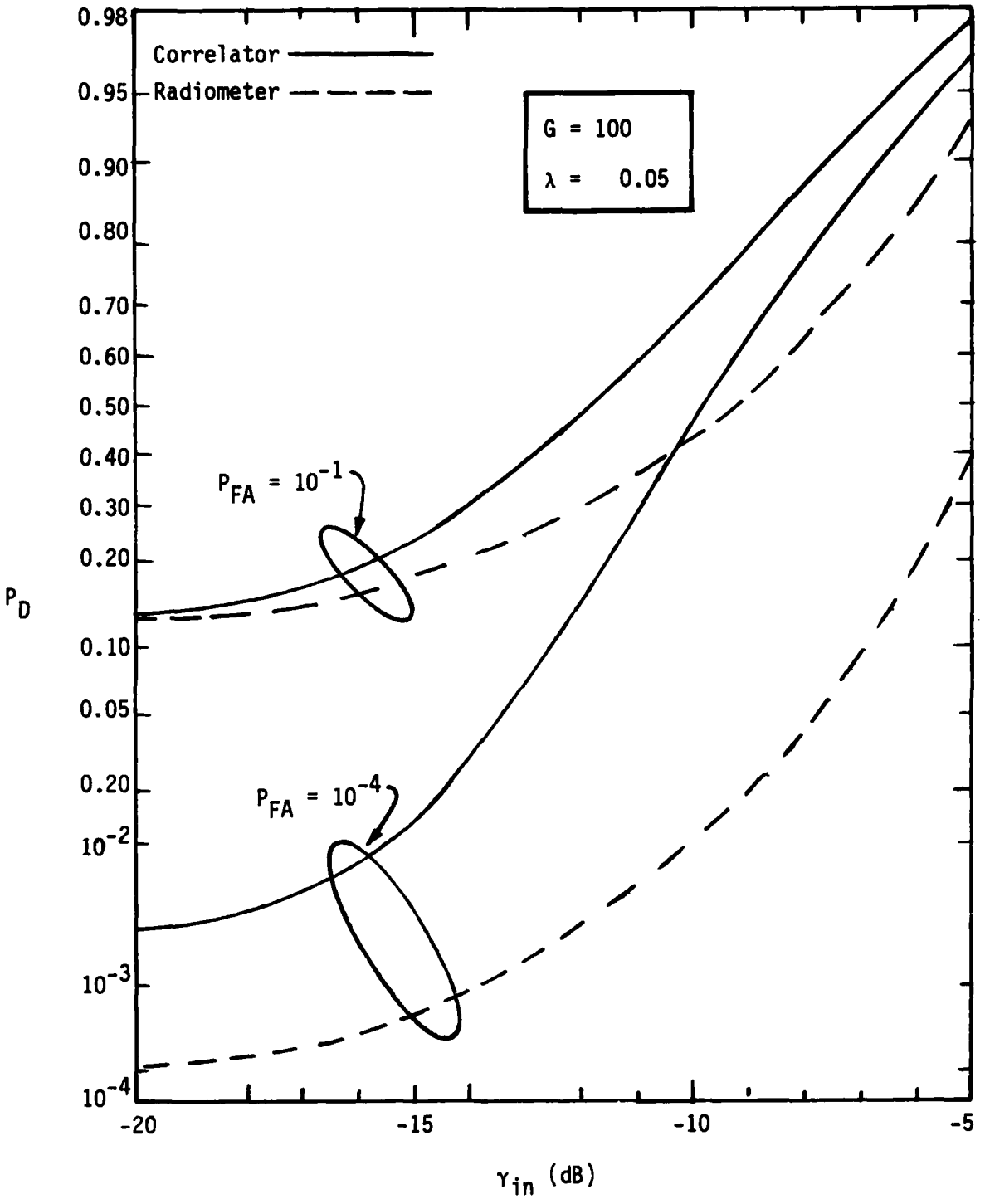

Figure 5.6. Comparison Between the Correlator and Radiometer in Terms of the (P_D, γ_{in}) Pair

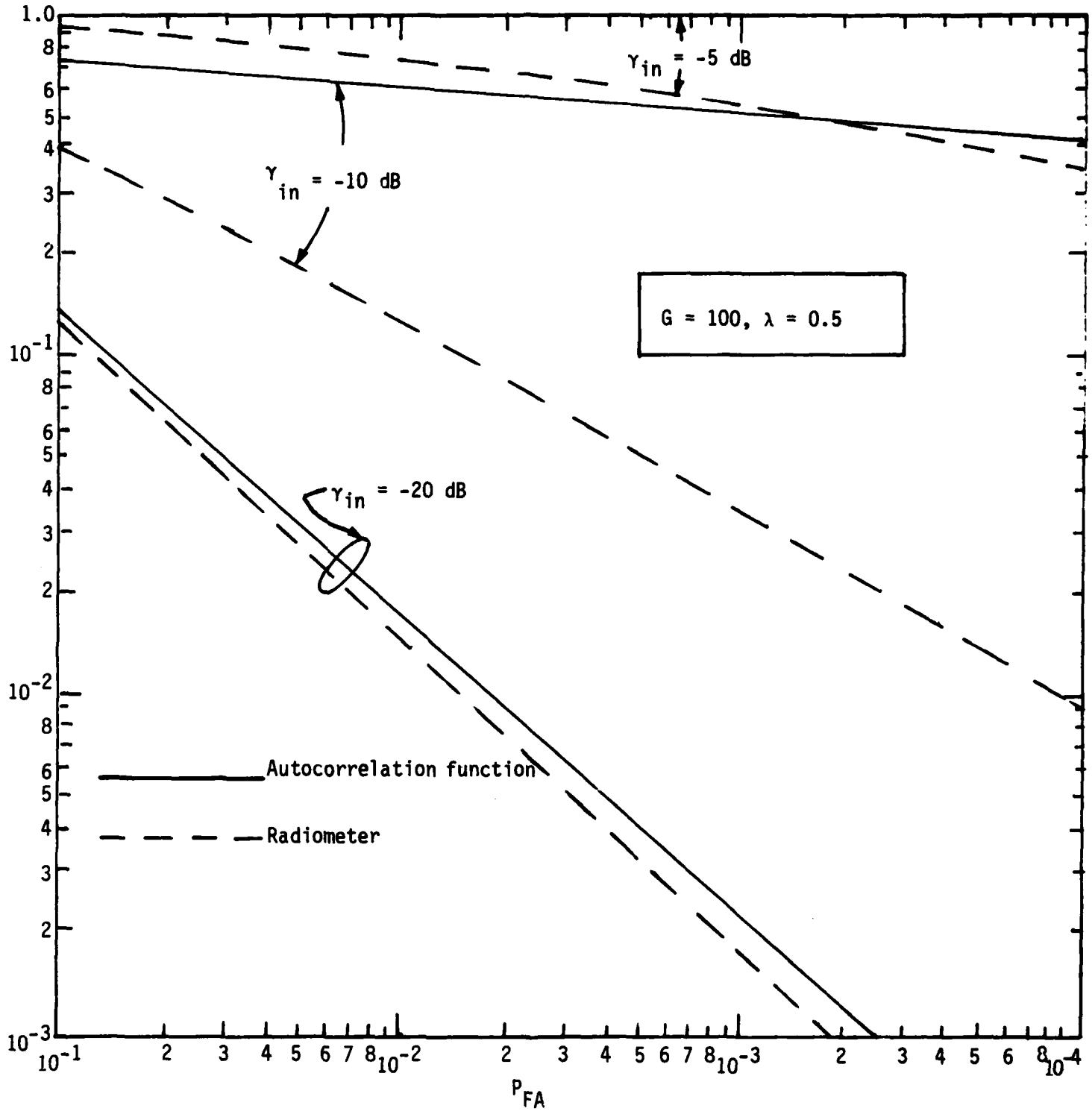

Figure 5.7. Receiver Operating Characteristic Curves (P_D, P_{FA}) For Both The Correlator and Radiometer, Parameterized by γ_{in}

5.2 Wideband Detection of FH/DS in Random Tone Interference

In section 5.1, a scheme was proposed for improving the detection of frequency-hopping (FH) waveforms in wideband additive Gaussian noise (AWGN) using samples from the autocorrelation domain. It was shown there that, under fairly general operational assumptions, an approximate gain of $\pi(\lambda,G)\gamma_H^2$ in decision SNR can be achieved over the energy discriminator (radiometer), where γ_H is the hop SNR. This gain--being defined on a per-band basis--has a direct positive impact on the overall system detection capability. The proposed algorithm, albeit inferior to the optimal likelihood ratio test, had the advantage of greatly reduced (hence, manageable) complexity.

The overall approach has been motivated by the recent implementational feasibility of large time-bandwidth-product/real-time correlators such as SAW devices. The purpose of this section is to show that, depending on the specific scenario at hand, the use of such devices can bring about impressive gains in detector performance, especially when compared to simpler alternatives such as the radiometer. In particular, we shall consider the case of detecting a frequency-hopping/direct-sequence (FH/DS) hybrid waveform when the dominant component of the observation "noise" is random tone interference, arbitrarily located within the hopping bandwidth. In addition, it will be assumed that the total power of this tone interference is much greater than that of the background thermal noise, so the latter can be ignored. It will then be shown that, for observation data with a large time-bandwidth-product G (defined by (5-4)), a very simple algorithm operating on the output of a real-time autocorrelation device can achieve almost perfect performance--in stark contrast with the poor performance of the radiometer.

Hybrid schemes have become increasingly popular spread-spectrum communication choices due to the enhanced antijam margin which they offer. Adding DS modulation to FH also improves the anti-intercept capability because the "noiselike" appearance of DS makes detection more difficult. On the other hand, multiple tones constitute a common model of nonwhite interference and can emerge in a number of scenarios, i.e., it can be intentional (jamming of the band) or unintentional (multiple users in a broadcast environment, adjacent radar sources, etc.). It is also conceivable that the tone interference has been deliberately inserted by the communicator in a pseudorandom manner so as to impede the interceptor's task, while it can be pseudorandomly avoided by the intended receiver.

In all of the cases previously cited, the tone interference could be filtered out (notch filtering) and various techniques for doing so effectively have recently been presented [14]. The key provision of these techniques is, however, that each tone stays at the notched frequency long enough for the filter to adapt; in the context of LPI detection, then, fast FH or low-duty-cycle pulsed interference could present a severe challenge for such systems. It is also clear that, as the number of interfering tones increases, the required complexity (number of filters) would soon surpass acceptable limits.

Here we address exactly those severe cases wherein the number of tones per observation interval is both large and arbitrary (random), with unknown frequencies, durations and phases. It will soon be seen that, in such environments, the radiometer is doomed to fail as a detector. It therefore comes as a pleasant surprise to conclude that the autocorrelation-domain algorithm proposed here can provide excellent performance independent of all those interference parameters. The section is structured as follows: Section 5.2.1 presents the system model and proposed algorithm, while section 5.2.2 proceeds with the analysis of its performance; that of the radiometer is also outlined here. Section 5.2.3 provides the simulation results and concludes with a brief discussion.

5.2.1 System Model and Proposed Algorithm

The overall system structure is similar to that described previously. Therefore, we shall illuminate only those aspects which are unique to the present scenario. Again, our concern is the decision rule performance on a per-band basis, as defined below. The autocorrelation domain will be employed to produce a decision statistic since an optimal rule similar to (5.1), would, in this case, be hard to establish and too complicated to implement.

Let the FH/DS hybrid signal to be detected be represented by $s(t) = \sqrt{2S}\, c(t) \cos \omega_0 t$, where ω_0 is an unknown frequency within the observed spectral band, $c(t)$ is the DS code of rate $R_c = T_c^{-1}$ and S is the signal power. The unknown interference consists of M tones (M is a random variable in each observation interval, which is equal to the hop time $T_H = R_H^{-1}$), with I_k, ω_k and ϕ_k denoting, respectively, the power, radian frequency and phase of the kth tone. The total received signal in $(0,T_H)$, under hypothesis H_1 (signal present), is given by

$$r(t) = \sqrt{2S}\, c(t) \cos \omega_0 t + \sum_{k=1}^{M} \sqrt{2I_k} \cos(\omega_k t + \phi_k) \qquad (5\text{-}38)$$

Note the absence of thermal noise in (5-38), as previously discussed. The code $c(t)$ can be modeled as either a random sequence of independent, identically distributed ± 1's with $Pr[c(t) = 1] = 0.5$, or a PN code with a full period equal to T_H. As per the ratio $N \triangleq T_H/T_c = R_c/R_H$ increases (N denotes the number of code chips per hop), the performance difference becomes insignificant, a fact also verified by simulation.

Let B denote the input observation bandwidth. The presence of the DS code implies that B should be at least equal to R_c or higher, but definitely much larger than R_H. Equivalently, the time-bandwidth product $G \triangleq BT_H \gg 1$. Furthermore, for simplicity, we shall assume that all tones have equal power $I_k = I/M, k=1,\ldots,M$, where I is the total interference power, and they are equi-spaced within the bandwidth B. In other words, the frequency separation $|f_k - f_{k+1}|$ between adjacent tones equals $B/(M+1)$, which is much greater than T_H^{-1}, i.e., $|f_k - f_{k+1}| \gg T_H^{-1}$. None of the above assumptions is critical in the forthcoming conclusions; they simply ease the analytical burden.

The real-time autocorrelation operation produces the output

$$y(\tau) = \int_{\tau}^{T_H} r(t)\, r(t-\tau)dt \quad ; \quad 0 \leq \tau \leq T_H \qquad (5\text{-}39)$$

Substituting (5-38) into (5-39) and rearranging redefines $y(\tau)$ as

$$y(\tau) = Sy_c(\tau) \cos \omega_0 \tau + \left(\frac{I}{M}\right)(T_H - \tau) \sum_{m=1}^{M} \cos \omega_m \tau + \sqrt{\frac{SI}{M}} \left(\sum_{k=1}^{M} n_k^{\alpha}(\tau) + n_0^{\beta}(\tau) \right) \qquad (5\text{-}40)$$

where $y_c(\tau)$ is the code partial-correlation function (a random variable)

$$y_c(\tau) = \int_{\tau}^{T_H} c(t)\, c(t-\tau)dt \qquad (5\text{-}41)$$

and $n_0^{\beta}(\tau), n_k^{\alpha}; k=1,2,\ldots,M$, are approximately Gaussian (via a central-limit-theorem-type argument), bandpass processes (signal x interference terms) defined by

$$n_k^{\alpha}(\tau) = \alpha_k^I(\tau) \cos \omega_k \tau - \alpha_k^Q(\tau) \sin \omega_k \tau \qquad (5\text{-}42a)$$

and

$$n_0^{\beta}(\tau) = \left(\sum_{k=1}^{M} \beta_k^I(\tau) \right) \cos \omega_0 \tau + \left(\sum_{k=1}^{M} \beta_k^Q(\tau) \right) \sin \omega_0 \tau \qquad (5\text{-}42b)$$

where

$$\alpha_k^I(\tau) = \int_{\tau}^{T_H} c(t) \cos\left[(\omega_0 - \omega_k)t - \phi_k\right] dt \quad , \qquad (5\text{-}43a)$$

$$\alpha_k^Q(\tau) = \int_{\tau}^{T_H} c(t) \sin\left[(\omega_0 - \omega_k)t - \phi_k\right] dt \quad , \qquad (5\text{-}43b)$$

$$\beta_k^I(\tau) = \int_{\tau}^{T_H} c(t-\tau) \cos\left[(\omega_0 - \omega_k)t - \phi_k\right] dt \quad , \qquad (5\text{-}43c)$$

and

$$\beta_k^Q(\tau) = \int_{\tau}^{T_H} c(t-\tau) \sin\left[(\omega_0 - \omega_k)t - \phi_k\right] dt \qquad (5\text{-}43d)$$

Before discussing the statistical characterization of the above noise processes (section 5.2.2), let us examine the noiseless (mean) part of $y(\tau)$ in (5-40), as shown in Figure 5.8. Of particular interest here are the envelopes of the useful signal (small shaded triangle) and the interference (large triangle), respectively, since the actual components, e.g., the first two terms in (5-40), are modulated by the unknown frequencies. The structural difference between the two correlations is evident: the DS code superimposed on each hop creates

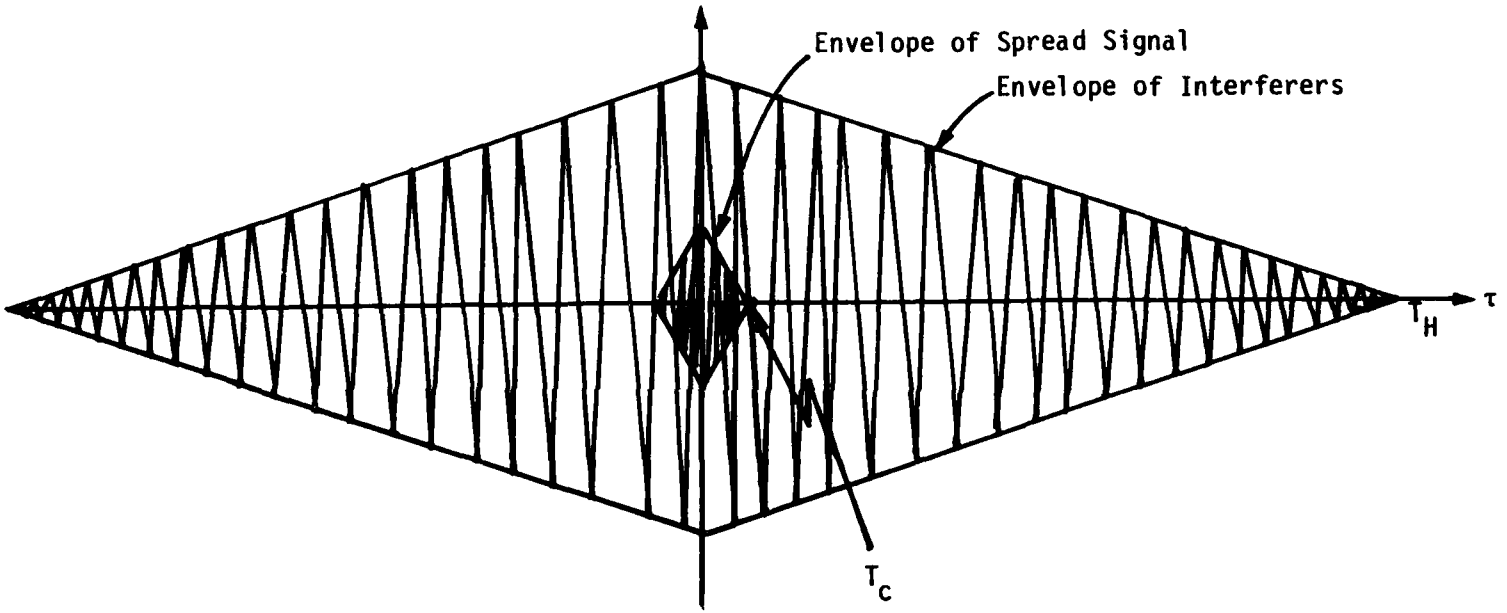

Figure 5.8. Mean of Output $y(\tau)$: The Signal and Interference Additive Components

a narrow mean-autocorrelation function for $|\tau| \geq T_c$ since the expected value of the function $y_c(\tau)$ in (5-41) is zero. Contrary to that, the interfering tones correlate for the whole interval $[0,T_H]$. Clearly, then, a power (noncoherent) sample at $\tau_1 = T_c$ would measure interference only*; this sample could be subtracted from the corresponding one at $\tau_0 = 0$ so that, under H_1, contains the full signal power plus interference. This subtraction would approximately cancel the interference contribution at $\tau_0 = 0$ so that, under H_1, only the signal would emerge while, under H_0, the statistic would be almost zero. Thus, the adopted decision rule is (see Figure 5.9)

$$\Delta = y^2(0)\Big|_{LP} - y^2(T_c)\Big|_{LP} \underset{H_0}{\overset{H_1}{\gtrless}} \Delta_0 \qquad (5\text{-}44)$$

where Δ_0 is a fixed threshold. In the absence of thermal noise, Δ_0 can be set at a very small (positive) level in order to maximize the detection probability. The next section shows that the performance resulting from (5-44) is excellent.

5.2.2 Performance Analysis

We focus here on the statistics of $n_k^{\alpha}(\tau)$ and $n_0^{\beta}(\tau)$, defined in (5-42) and (5-43). Let $\mathcal{E}\{\cdot\}$ and $\mathrm{var}\{\cdot\}$ indicate the mean and variance, respectively. It is then easily shown that

$$\mathcal{E}\left\{\alpha_k^j(\tau)\right\} = \mathcal{E}\left\{\beta_k^j(\tau)\right\} = 0 \quad ; \quad j=I,Q \qquad (5\text{-}45)$$

and that

$$\mathrm{var}\left\{\alpha_k^j(\tau)\right\} = \mathrm{var}\left\{\beta_k^j(\tau)\right\} = \mathcal{E}\left\{\left(\alpha_k^I(\tau)\right)^2\right\} \qquad (5\text{-}46)$$

In the following, we shall concentrate on offsets $\tau = mT_c$; $m=0,1,2,\ldots,N$. In fact, only $\tau = 0$ and $\tau = T_c$ are of interest (see (5-44)). Then lengthy manipulations can establish the following facts (for proof, see Appendix J):

---

*Any $\tau_1 > T_c$ would also do, especially in the face of some uncertainty about T_c.

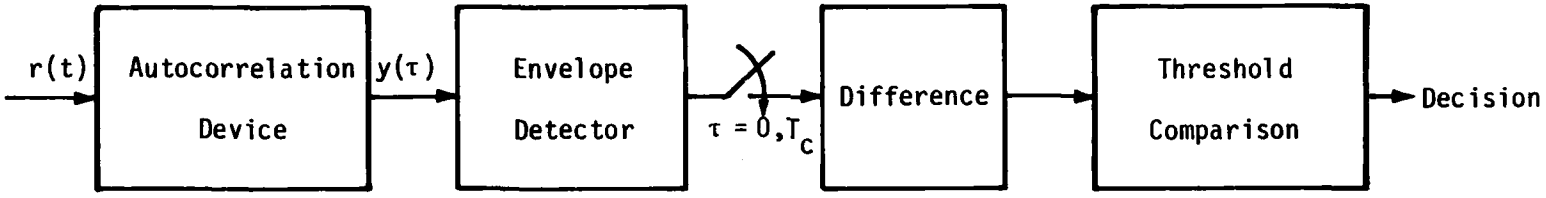

Figure 5.9. Block Diagram of the Decision Rule in the Autocorrelation Domain

(a) The variance in (5-46) is given by

$$\mathcal{E}\left\{\left(\alpha_k^I(mT_c)\right)^2\right\} = \frac{(N-m)T_c^2}{2}\,Sa^2\left[\pi(f_0 - f_k)T_c\right] \qquad (5\text{-}47)$$

where $Sa(x) \triangleq \sin x/x$ is the sampling function.

(b) Each noise process has mutually uncorrelated inphase and quadrature components (therefore, by the Gaussian assumption, independent).

(c) Noises corresponding to different frequencies (e.g., $n_k^\alpha(\tau)$ and $n_\ell^\alpha(\tau)$ with $k \neq \ell$) are uncorrelated.

(d) Processes $n_k^\alpha(\tau)$ and $n_0^\beta(\tau)$, however, have different properties, i.e., $n_k^\alpha(\tau)$ is a highly correlated process (as a function of τ), while $n_0^\beta(\tau)$ generally is not; in fact, samples of $n_0^\beta(\tau)$ taken T_c apart could be uncorrelated.

Of the above conclusions, (d) is probably the most interesting from a performance viewpoint: If the noise $n_0^\beta(\tau)$ had been as highly correlated as $n_k^\alpha(\tau)$, the decision rule performance (5-44) would have been perfect since the same* random-noise sample would be obtained at $\tau = 0$ and $\tau = T_c$; thus, they would cancel out. This not being true, a slight degradation in performance is expected, as was also observed in the simulation. Nonetheless, since the mean part of the interference ((second term in (5-40)) does cancel out, the performance of this scheme is far superior to that of the radiometer, which is oblivious to that term. In fact, the radiometer output is merely the value $y(0)$, which is dominated by the power of the random interference (see Figure 5.8). Without further assistance, it is impossible to determine if there is any signal in the total observed power since the interference contribution is random and, hence, unknown.

As mentioned above, the high correlation of $\alpha_k(\tau)$ implies that $\alpha_k^j(0) \approx \alpha_k^j(T_c)$; j=I,Q. On the other hand, the degree of correlation between $\beta_k(0)$ and $\beta_k(T_c)$ varies with the frequency difference $\Delta f_k = f_0 - f_k$. For the special case wherein one of the interfering frequencies f_{k_0} coincides with f_0, it is easily seen that $\beta_{k_0}^j(0) \approx \beta_{k_0}^j(T_c)$; j=I,Q. Those facts are used in the subsequent analysis.

---

*Same within a totally insignificant change.

We can now return to the decision rule (5-44): upon squaring, taking the difference, lowpass filtering (e.g., rejecting double-frequency terms), assuming that $f_{k_0} = f_0$ for one frequency and using the above conclusions, it follows that

$$\Delta = \frac{S^2}{2}\left(T_H^2 - y_c^2(T_c)\right) + \left(\frac{SI}{M}\right)\left(n^2(0) - n^2(T_c)\right)\Big|_{LP}$$

$$+ S\sqrt{\frac{SI}{M}}\left[\left(\alpha_{k_0}^I(0) + \sum_{k=1}^{M}\beta_k^I(0)\right)T_H - \left(\alpha_k^I(T_c) + \sum_{k=1}^{M}\beta_k^I(T_c)\right)y_c(T_c)\right]$$

$$+ \left(\frac{I}{M}\right)T_H\sqrt{\frac{SI}{M}}\left[\sum_{k=1}^{M}\left(\beta_k^I(0) - \beta_k^I(T_c)\right)\right] + ST_H\left(\frac{I}{M}\right)\left(T_H - y_c(T_c)\right) \qquad (5\text{-}48)$$

where

$$n(\tau) = \sum_{k=1}^{M} n_k^{\alpha}(\tau) + n_0^{\beta}(\tau) \qquad (5\text{-}49)$$

is the total BP equivalent noise. Let us note that, at least for the case of a full PN code period per hop, $y_c(T_c)$ is approximately zero, which considerably simplifies (5-48). Furthermore, even for the random-code model, a comparison between analysis and simulation for the one-tone case (see next section) has indicated that the impact of the rv $y_c(T_c)$ is unnoticeable; hence, setting $y_c(T_c) = 0$ seems to be a reasonable approximation for the general case. Still, a full analysis of (5-48) without further simplifying assumptions is extremely complicated. In order to gain some insight here, we shall focus on the one-tone random interference ($M = 1$), with the reasonable conjecture that the multi-tone case should provide analogous conclusions.

Since, in this case, $\beta_1^I(T_c) \approx \beta_1^I(0) = \alpha_1^I(0) \approx \alpha_1^I(T_c) \triangleq a_1$ and $n^2(0) = n^2(T_c)$, it follows from (5-48) that

$$\Delta = \frac{(ST_H)^2}{2}\left[1 + 2\gamma_I^{-1}\left(1 + 2\sqrt{\gamma_I}\ a_1, \text{norm}\right)\right] \qquad (5\text{-}50)$$

where we have defined the signal-to-interference ratio $\gamma_I \triangleq S/I$ and the normalized random variable

$$a_{1,\text{norm}} \triangleq \frac{a_1}{T_H} = \left(\frac{T_c}{T_H}\right) \cos \phi_1 \sum_{n=1}^{N} c_n \tag{5-51}$$

In (5-51), $c_n; n=1,\ldots,N$ are the code chips and ϕ_1 is the random phase of the interference. Clearly, under H_0, $\Delta = 0$ with probability 1. Under H_1, it is shown in Appendix K that

$$\mathcal{E}\{\Delta | H_1\} = \frac{(ST_H)^2}{2}\left(1 + 2\gamma_I^{-1}\right) \tag{5-52a}$$

and

$$\text{var}\{\Delta | H_1\} = 2(ST_H)^4(N\gamma_I)^{-1} \tag{5-52b}$$

Based on (5-52) and the Gaussian assumption about Δ, the performance of this decision scheme is predicted by the detection probability

$$P_D^{\text{corr}} = 1 - Q\left[\sqrt{\frac{N\gamma_I}{2}}\left(\frac{1}{2} + \gamma_I^{-1} - \Delta_0^*\right)\right] \tag{5-53}$$

where $\Delta_0^* = \Delta_0/(ST_H)^2$ is a normalized threshold and $Q(x)$ is the Gaussian integral function. In the absence of thermal noise, Δ_0^* can be set arbitrarily close to zero; thus, it always yields the zero false-alarm rate $P_{FA} = 0$. In practice, Δ_0^* would be set according to the thermal-noise level and the degree of uncertainty about the power S of the detected signal†.

The performance predicted by (5-53) is indeed excellent. We note that increasing the interference power (hence, increasing γ_I^{-1}) actually helps detection instead of deterring it, while it has no effect on false alarm. For instance, it can be shown that, if $N > 60$, then $P_D^{\text{corr}} > 99\%$, independently of

†Alternatively, this can be expressed in terms of the uncertainty regarding the transmitter/intercept receiver's true distance.

γ_I, as long as $\Delta_0^* \leq 0.4$, i.e., one can tolerate 40% uncertainty about the signal power and still expect excellent detection capabilities, regardless of the interference power. The above conclusion is rather insensitive to N in that, for N = 10, the corresponding minimum P_D^{corr} is 90%.

The radiometer performance (shown in Figure 5.2) is easier to analyze for an arbitrary M and is based on the fact that its output $Y_{rad} = y(0)$ can be written as

$$Y_{rad} = ST_H + IT_H + 2\sqrt{S\frac{I}{M}}\left(\sum_{k=1}^{M} a_k^I(0)\right) \tag{5-54}$$

Let M_{max} be the maximum number of tones which can be expected in any hop. Here, for simplicity, we consider only the case $M_{max} = 1$, where Prob[one interfering tone] = Pr[no interfering tone] = 1/2 for each hop. Assuming that the threshold Y_0 is set at $Y_0 = I_1 T_H$, so that† $P_{FA} = 0$, it can then be shown that (see Appendix L)

$$P_D^{rad} = \begin{cases} 1 - \frac{1}{2} Q\left[\sqrt{\frac{N\gamma_I}{2}}\right], & \text{if } \gamma_I > 1 \\ \frac{1}{2}\left(1 - Q\left[\sqrt{\frac{N\gamma_I}{2}}\right]\right), & \text{if } \gamma_I \leq 1 \end{cases} \tag{5-55}$$

Thus, the obtainable performance decreases with decreasing signal-to-interference ratio γ_I and in the limit

$$\lim_{\gamma_I \to 0} P_D^{rad} = \frac{1}{4} \quad (M_{max} = 1, \tag{5-56}$$

which is certainly poor compared to P_D^{corr}. It has also been shown that the radiometer performance is a decreasing function of M_{max} so that the above results constitute an upper bound for the general case. Finally, we note that the

†This is selected so as to match the zero P_{FA} of the correlator; another choice of Y_0 would lead to $P_{FA} = 0.5$.

question of threshold setting is much more crucial for the radiometer than the correlator since the performance of the latter is effectively independent of the jamming power.

5.2.3 Simulation Results and Discussion

The correlator with one tone interference was simulated by computer; the results shown in Figure 5.10 are based on 10,000 independent trials. (For simulation details, consult Appendix M.) Also shown in this figure are the analytical predictions (dotted lines) whose agreement with the simulation is quite striking, even for such low values of N as N = 3 and N = 10. Since detection probability is monotonically increasing with N (see (5-53)), those values represent worst-case designs which nonetheless yield excellent performance results. It was somewhat surprising to find that the Gaussian model provides such an accurate analytical prediction, even for N = 3; furthermore, setting $y_c(T_c)$ equal to zero proved to be a well-justified simplification. Note that no false alarm was observed ($P_{FA} = 0$) and that performance is practically insensitive to the amount of interference inserted. In contrast, the radiometer performance (as evidence by (5-55)) deteriorates rapidly with decreasing S/I, as expected. Finally, let us mention that the performance shown in Figure 5.10 is for a nonoptimized (arbitrarily chosen) threshold $\Delta_0^* = S^2T_H^2/N$. In the absence of thermal noise, further improvement can be attained for the correlator by decreasing Δ_0^* to a very small (but positive) value.

Although analysis and simulation are not yet available for the multitone case, it is anticipated that the gap between the radiometer and the correlator performances will increase as the interference-to-noise ratio increases, independently of M_{max}. That again is due to the relative insensitivity of the correlator to the interference nuisance parameters.

Comments pertaining to the power measurement of (5-44) are the same as those in section 5.1.3. Furthermore, we note that, if the carrier frequency f_0 of the signal sought is known, narrow bandpass filtering of the output $y(\tau)$ in (5-40) prior to the power measurement will further enhance performance.

As mentioned, the theory of this section does not include thermal noise. The determination, analytical evaluation and simulation of algorithms which operate satisfactorily in a mixed environment (i.e., both thermal noise and random interference) will be the topic of future research.

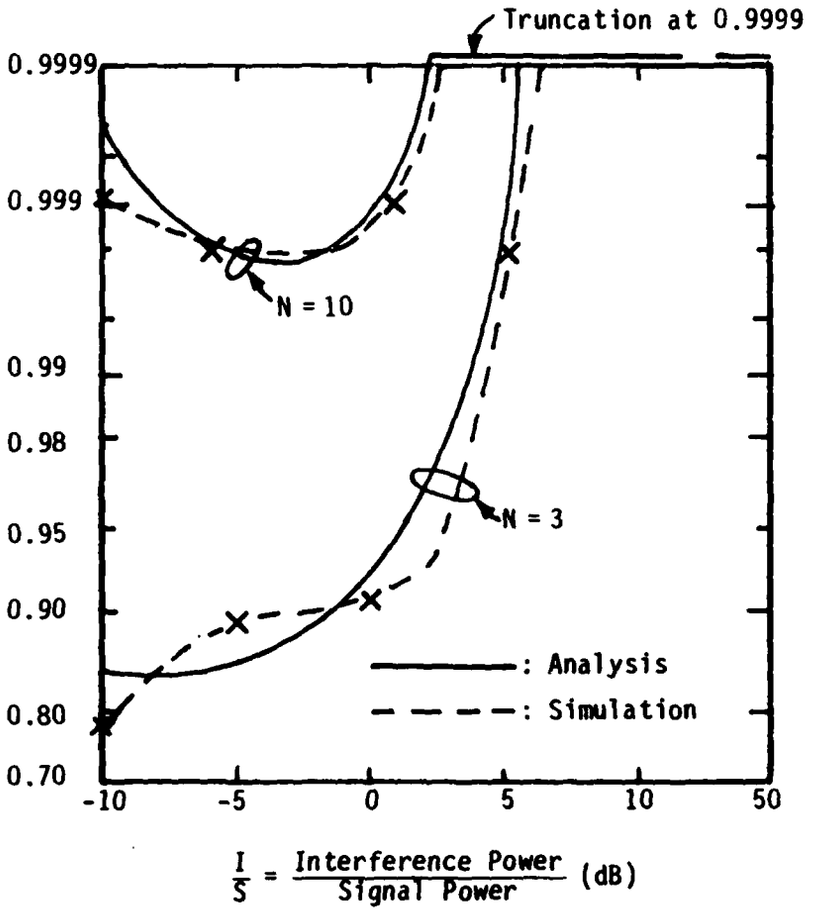

Figure 5.10. P_D Versus I/S for the Real-Time Autocorrelator (Nonoptimized Threshold)

REFERENCES

1. H. Urkowitz, "Energy Detection of Unknown Deterministic Signals," Proc. IEEE, Vol. 55, April 1967, pp. 523-531.

2. R. A. Dillard, "Detectability of Spread Spectrum Signals," IEEE Trans. Aerosp. Electron. Sys., Vol. AES-15, July 1979, pp. 526-537.

3. W. W. Peterson, T. G. Birdsall and W. C. Fox, "The Theory of Signal Detectability," IRE Trans., PGIT-1954.

4. J. D. Edell, "Wideband, Noncoherent, Frequency-Hopped Waveforms and Their Hybrids in Low-Probability-of-Intercept Communications, NRL Report, Code 8025, November 1976.

5. D. Woodring and J. Edell, "Detectability Calculation Techniques," NRL Report, Code 5480, September 1977.

6. N. F. Krasner, "Optimal Detection of Digitally Modulated Signals," IEEE Trans. on Comm., Vol. COM-30, No. 5, May 1982, pp. 885-895.

7. A. Polydoros and C. L. Weber, "Optimal Detection Considerations for Low Probability of Intercept," MILCOM'82 Proceedings, October 1982, pp. 2.1.1 to 2.1.5.

8. N. F. Krasner, "Maximum Likelihood Parameter Estimation for LPI Signals," MILCOM'82 Proceedings, October 1982, pp. 2.3-1 to 2.3-4.

9. A. Polydoros and J. K. Holmes, "Autocorrelation Techniques for Wideband Detection of FH/DS Waveforms in Random Tone Interference," MILCOM'83 Proceedings, October 1983.

10. M. Schwartz, Information Transmission, Modulation and Noise," McGraw-Hill, Second Edition, 1970.

11. W. B. Davenport, Jr., and W. L. Root, An Introduction to the Theory of Random Signals in Noise, McGraw-Hill, 1958.

12. G. S. Kino et al, "Signal Processing by Parametric Interactions in Delay-Line Devices," IEEE Transactions on Microwave Theory and Techniques, Vol. MTT-21, April 1973, pp. 244-248.

13. L. B. Milstein and P. K. Das, "Spread Spectrum Receiver Using Surface Acoustic-Wave Technology," IEEE Trans. on Comm., Vol. COM-25, No. 8 August 1977, pp. 841-847.

14. Special Issue on Spread Spectrum Communications, IEEE Trans. on Comm., May 1982.

15. A. Papoulis, Probability, Random Variables and Stochastic Processes, McGraw-Hill, 1965.

APPENDIX A

PROOF OF EQUATION (3-8)

Let us start from (3-5), i.e.,

$$\Lambda\left(\underline{r}(t)\right) = \frac{\exp\left\{-N\gamma_c\right\}}{2^N} \sum_{i=1}^{2^N} \exp\left\{\frac{2\sqrt{S}}{N_0} \sum_{j=1}^{N} r_j c_{ij}\right\} \underset{H_0}{\overset{H_1}{\gtrless}} \Lambda_0 \qquad \text{(A-1)}$$

with γ_c as per (3-6), c_{ij} denoting the jth chip of the ith code pattern and r_j as per (3-7). Consider the N-dimensional linear space consisting of all binary patterns $\underline{c}_i; i=1,\ldots,2^N$ of length N. Now observe that this space can be divided into two disjoint complementary subsets, each of cardinality 2^{N-1}, by the rule that, for each possible vector $\underline{c}_i$ belonging to one of the subsets, $-\underline{c}_i$ belongs to the other subset. Exactly which vectors $\underline{c}_i$ are included in which subset is immaterial as long as the above rule holds. We can now perform the summation in (A-1) over one of the two complementary subsets instead of the whole linear space, with the equivalent rule.

$$\sum_{\substack{i=1 \\ i\in\mathcal{S}}}^{2^{N-1}} \cosh\left[\left(\frac{2\sqrt{S}}{N_0}\right) \underline{r}\cdot\underline{c}_i\right] \underset{H_0}{\overset{H_1}{\gtrless}} \Lambda_0' \qquad \text{(A-2)}$$

where $\underline{r} \triangleq (r_1,\ldots,r_N)$, $\mathcal{S}$ is one of the aforementioned disjoint subsets and any resulting scale factors are absorbed into the threshold Λ_0'. In (A-2), cosh(x) is the hyperbolic cosine function

$$\cosh(x) = \frac{e^x + e^{-x}}{2} \qquad \text{(A-3)}$$

Since cosh(x) is an even function of x, the summation in (A-2) can be extended over the whole linear space

$$\sum_{i=1}^{2^N} \cosh\left(\frac{2\sqrt{S}}{N_0}\,\underline{r}\cdot\underline{c}_i\right) \underset{H_0}{\overset{H_1}{\gtrless}} \Lambda_0 \tag{A-4}$$

In order to proceed, we first need to introduce the superscripts $\underline{r}^{(N)}$ and $\underline{c}_i^{(N)}$, which will indicate the length of the corresponding vectors, and then prove the following:

Lemma A. It is true that:

$$\sum_{i=1}^{2^N} \cosh\left(\underline{r}^{(N)}\cdot\underline{c}^{(N)}\right) = 2^N \prod_{i=j}^{N} \cosh(r_j) \tag{A-5}$$

Proof: The proof is by induction. First, let N=1. Then,

$$\sum_{i=1}^{2} \cosh\left(\underline{r}^{(1)}\cdot\underline{c}^{(1)}\right) = \cosh(r_1) + \cosh(-r_1) = 2\cosh(r_1) \tag{A-6}$$

since cosh(x) is even function. Thus, (A-5) is satisfied for N=1. Next, assume that it is true for N=k, i.e.,

$$\sum_{i=1}^{2^k} \cosh\left(\underline{r}^{(k)}\cdot\underline{c}_i^{(k)}\right) = 2^k \prod_{j=1}^{k} \cosh(r_j) \tag{A-7}$$

and prove it for N=k+1. Indeed,

$$\sum_{i=1}^{2^{k+1}} \cosh\left(\underline{r}^{(k+1)}\cdot\underline{c}_i^{(k+1)}\right) = \sum_{i=1}^{2^k} \left[\cosh\left(\underline{r}^{(k)}\cdot\underline{c}^{(k)} + r_{k+1}\right) + \cosh\left(\underline{r}^{(k)}\cdot\underline{c}^{(k)} - r_{k+1}\right)\right] \tag{A-8}$$

But,

$$\cosh(a+b)+\cosh(a-b) = \frac{e^{a+b}+e^{-a-b}+e^{a-b}+e^{-a+b}}{2}$$

$$= e^{a}\left(\frac{e^{b}+e^{-b}}{2}\right) + e^{-a}\left(\frac{e^{n}+e^{-b}}{2}\right) = \left(e^{a}+e^{-a}\right)\left(\frac{e^{b}+e^{-b}}{2}\right)$$

$$= 2\cosh(a)\cosh(b)$$

which, upon substitution in (A-8), yields

$$\sum_{i=1}^{2^{k+1}} \cosh\left(\underline{r}^{(k+1)}\cdot\underline{c}_i^{(k+1)}\right) = \sum_{k=1}^{2^k} 2\cosh\left(\underline{r}^{(k)}\cdot\underline{c}_i^{(k)}\right)\cosh\left(r_{k+1}\right)$$

$$= 2\cosh\left(r_{k+1}\right)\sum_{i=1}^{2^k}\cosh\left(\underline{r}^{(k)}\cdot\underline{c}_i^{(k)}\right)$$

$$= 2\cosh\left(r_{k+1}\right)2^{k}\prod_{j=1}^{k}\cosh\left(r_j\right) = 2^{k+1}\prod_{j=1}^{k+1}\cosh\left(r_{j+1}\right) \quad \text{(A-10)}$$

where the truth of (A-8) has been used. Equation (A-10) completes the proof of Lemma A.

If Lemma A is applied to (A-4), it renders it equivalent to

$$2^{N}\prod_{j=1}^{N}\cosh\left(\frac{2\sqrt{5}}{N_0}r_i\right)\gtrless_{H_0}^{H_1}\Lambda'_0 \quad \text{(A-11)}$$

which is (3-8).

APPENDIX B

PROOF OF EQUATION (3-10)

Let us rewrite the decision rule (3-9) as

$$\Lambda' = \sum_{j=1}^{N} y_j \underset{H_0}{\overset{H_1}{\gtrless}} \Lambda'_0 \tag{B-1}$$

where the independent, identically distributed random variables (iid rv's) $y_j \triangleq r_j^2$ assume the form

$$y_j = \begin{cases} n_j^2 & \text{under } H_0 \\ \left(\sqrt{S}\, T_c\, c_j + n_j\right)^2 & \text{under } H_1 \end{cases} \tag{B-2}$$

In (3-14), n_j represents the Gaussian rv

$$n_j = \int_{(j-1)T_c}^{jT_c} n_I(t)\, dt \tag{B-3}$$

whose statistics are independent of j.

A precise analysis should account for the exact distribution of y_j under either hypothesis. So, for instance, under H_0, y_j is chi-squared rv with N degrees of freedom. For large N (of the order of hundreds or more, that is the practical case), very satisfactory approximate results can be obtained which circumvent the difficulties of an exact, but enormously complicated, analysis. This is done by invoking a central-limit-type argument: The decision statistic Λ', being the sum of a large number of iid rv's y_j, is approximately Gaussian distributed, with mean

$$\mathcal{E}\{\Lambda' | H_k\} = N\mathcal{E}\{y_j | H_k\} \; ; \quad k=0,1 \tag{B-4a}$$

and variance

$$\text{var}\{\Lambda|H_k\} = N\,\text{var}\{y_j|H_k\}\;; \quad k=0,1 \tag{B-4b}$$

under either hypothesis. Thus, having the second-order statistics of the individual rv's y_j and, subsequently, of Λ' from (B-1) enables us to determine performance immediately.

Let

$$m = \sqrt{S}\,T_c\,c_j\,\delta_{k1} \tag{B-5}$$

so that

$$y_j = (m + n_j)^2 = m^2 + n_j^2 + 2mn_j \tag{B-6}$$

Furthermore, the Gaussian rv n_j has zero mean and variance

$$\sigma_n^2 = \mathcal{E}\{n_j^2\} = \frac{N_0 T_c}{2} \tag{B-7}$$

Thus, from (B-6),

$$\mathcal{E}\{y_j\} = m^2 + \sigma_n^2 = ST_c^2\,\delta_{k1} + \frac{N_0\,T_c}{2}$$

$$= (N_0\,T_c)\left(\frac{1}{2} + \frac{ST_c}{N_0}\,\delta_{k1}\right) = (N_0\,T_c)\left(\frac{1}{2} + \gamma_c\delta_{k1}\right) \tag{B-8}$$

Finally,

$$\text{var}\{y_j\} = \text{var}\{m^2 + n_j^2 + 2mn_j\} = \text{var}\{n_j^2 + 2mn_j\} = \text{var}\{n_j^2\} + 4m^2\,\text{var}\{n_j\} \tag{B-9}$$

since the random variables n_j^2 and n_j are uncorrelated $\left(\mathcal{E}\{n_j^3\} = 0\right)$. Thus, from (B-7) and (B-9),

$$\text{var}\{y_j\} = \left(3\sigma_n^4 - \sigma_n^4\right) + 4m^2\sigma_n^2 = 2\sigma_n^2\left[\sigma_n^2 + 2m^2\right] = (N_0T_c)^2\left[\frac{1}{2} + 2\gamma_c\delta_{k1}\right] \tag{B-10}$$

Equation (3-10) results from combining (B-8) and (B-10) with (B-4).

APPENDIX C

PROOF OF EQUATION (3-20)

Let the received waveform be

$$r(t) = \begin{cases} \sqrt{2S} \sum_{j=-\infty}^{\infty} c_j \, p(t - jT_c) \cos(\omega_0 t + \phi_j) + n(t) & (H_1) \\ n(t) & (H_0) \end{cases} \qquad 0 \leq t \leq T_H \quad \text{(C-1)}$$

where $\{\phi_j\}$ is a sequence of independent phases and the synchronous model ($\epsilon = 0$) is used. Let $\underline{c} = [c_1, c_2, \ldots, c_N]$ and $\underline{\phi} = [\phi_1, \phi_2, \ldots, \phi_N]$ denote the random vectors whose components are the successive random chip and phase values, respectively. Then, by virtue of the assumed independence, the generalized likelihood ratio reduces to

$$\Lambda r(t) = \mathcal{E}_{\underline{c}} \, \mathcal{E}_{\underline{\phi}} \left\{ \frac{f\left(r(t) \middle| H_1, \underline{c}, \underline{\phi} \; ; \; 0 \leq t \leq T\right)}{f\left(r(t) \middle| H_0\right)} \right\}$$

$$= \prod_{j=1}^{N} \mathcal{E}_{c_j} \, \mathcal{E}_{\underline{\phi}} \left\{ \frac{f\left(r(t) \middle| H_1, c_j, \underline{\phi}; \; (j-1)T_c \leq t \leq jT_c\right)}{f\left(r(t) \middle| H_0\right)} \right\}$$

$$= \prod_{j=1}^{N} \mathcal{E}_{c_j} \, \mathcal{E}_{\phi_j} \left\{ \frac{f\left(r(t) \middle| H_1, c_j; \phi_j; \; (j-1)T_c \leq t \leq jT_c\right)}{f\left(r(t) \middle| H_0\right)} \right\}$$

$$= \prod_{j=1}^{N} \left[\mathcal{E}_{c_j} \left\{ I_0\left(\frac{2\sqrt{S}}{N_0} r_j\right) \right\} \exp\{-\gamma_c\} \right] \underset{H_0}{\overset{H_1}{\gtrless}} \Lambda_0 \qquad \text{(C-2)}$$

where the jth chip-interval envelope r_j is given by

$$r_j = \sqrt{r_{I_j}^2 + r_{Q_j}^2} \tag{C-3}$$

and r_{I_j}, r_{Q_j} have been defined in (3-18). Furthermore, we note that, although r_{I_j} and r_{Q_j} depend on $c_j = \pm 1$ through the combination of (3-18) and (C-1), their squares do not (simply because $c_j^2 = 1$). Thus, r_j of (C-3) is independent of c_j, which means that

$$\mathcal{E}_{c_j}\left\{I_0\left(\frac{2\sqrt{S}}{N_0} r_j\right)\right\} = I_0\left(\frac{2\sqrt{S}}{N_0} r_j\right) \tag{C-4}$$

substituting (C-4) into (C-2) yields

$$\Lambda(r(t)) = \exp\{-N\gamma_c\} \prod_{j=1}^{N} I_0\left(\frac{2\sqrt{S}}{N_0} r_j\right) \underset{H_0}{\overset{H_1}{\gtrless}} \Lambda_0 \tag{C-5}$$

whose equivalent logarithmic version is (3-20).

APPENDIX D

PROOF OF EQUATION (3-23)

A Gaussian-approximation-based analysis of the low-SNR, chip-noncoherent detector, illustrated in Figure 3.3, can be performed following guidelines similar to those in Appendix B, as follows: Let the bandpass AWGN n(t) be represented by

$$n(t) = \sqrt{2}\left\{n_I(t)\cos\omega_0 t - n_Q(t)\sin\omega_0 t\right\} \tag{D-1}$$

where $n_I(t)$ and $n_Q(t)$ are baseband, independent, Gaussian processes with a flat one-sided PSD of N_0 W/Hz each. Conditioned on the unknown phase ϕ_j and the ± 1-chip c_j of the interval $(j-1)T_c \geq t \geq jT_c$, the inphase and quadrature variables r_{I_j} and r_{Q_j} of (3-18) are Gaussian with means

$$\begin{aligned} \mathcal{E}\left\{r_{I_j}\middle|\phi_j,c_j\right\} &= \sqrt{S}\,T_c\,c_j\,\delta_{k1}\cos\phi_j \\ \mathcal{E}\left\{r_{Q_j}\middle|\phi_j,c_j\right\} &= \sqrt{S}\,T_c\,c_j\,\delta_{k1}\sin\phi_j \end{aligned} \qquad \begin{matrix} j=1,2,\ldots,N \\ k=0,1 \end{matrix} \tag{D-2}$$

and common variance σ_n^2

$$\sigma_n^2 \triangleq \mathrm{var}\left\{r_{I_j}\right\} = \mathrm{var}\left\{r_{Q_j}\right\} = \frac{N_0 T_c}{2} \tag{D-3}$$

where δ_{k1} was defined in (3-10c). Thus, averaging the phase* ϕ_j, it follows that each of the independent envelope rv's r_j of (3-21) has, under H_1, a Rician distribution

*Again it is easily seen that the value of c_j becomes irrelevant due to the squaring.

Assuming that an instantaneous power measurement can be formed at time $\tau = 0$ and $\tau = T_c$, we have the decision rule:

$$\Delta = P(0) - \left(\frac{N}{N-1}\right)^2 P(T_c) \underset{H_0}{\overset{H_1}{\gtrless}} \Delta_0 \qquad \text{(M-11)}$$

with P(t) the power at time t and with

$$\Delta_0 = \frac{S^2 T_H^2}{N} \qquad \text{(M-12)}$$

The factor

$$\left(\frac{N}{N-1}\right)^2$$

is used to make $\Delta = 0$ under H_0. Each chip of c(t) is modeled as an independent random variable with values ±1, each with probability 0.5.

Figure 5.10 from the text presents the probability of detection (P_D) for various values of N at a false-alarm probability of zero. Each point used to determine the plot of P_D utilized 10,000 trial runs. Besides the code sequence, the phase ϕ_1 was randomized over 0 to 2π radians.

$$f(r_j|H_1) = \frac{r_j}{\sigma^2} \exp\left[-\frac{1}{2}\left(\frac{r_j^2}{\sigma^2} + 2\gamma_c\right)\right] I_0\left(\frac{r_j}{\sigma}\sqrt{2\gamma_c}\right) (r_j \geq 0) \quad j=1,2,\ldots,N \qquad \text{(D-4)}$$

where γ_c is the predetection SNR while, under H_0 (i.e., signal absent, $\gamma_c = 0$), (D-4) reduces to a Rayleigh distribution

$$f(r_j|H_0) = \frac{r_j}{\sigma^2} \exp\left[-\frac{r_j^2}{2\sigma^2}\right] (r_j \geq 0) \qquad \text{(D-5)}$$

Therefore, the statistics of the decision rv $\sqrt{\Lambda'}$ in (3-22), being the square root of the sum of N iid rv's, can be precisely found. For example, under H_0, it is a chi-squared rv with 2N degrees of freedom, resulting in a false-alarm probability

$$P_{FA} = \frac{1}{(N-1)!} \int_{x_0^2/2}^{\infty} x^{N-1} \exp[-x]\, dx = 1 - (\text{incomplete Gamma function}) \qquad \text{(D-6)}$$

while the corresponding detection probability is given in terms of the generalized Marcum Q function

$$P_D = Q_N(\psi, x_0) = \int_{x_0}^{\infty} x\left(\frac{x}{\psi}\right)^{N-1} \exp\left(-\frac{x^2+\psi^2}{2}\right) I_{N-1}(\psi x)\, dx \qquad \text{(D-7)}$$

In the above equations, x_0 is a normalized threshold

$$x_0 = \sqrt{\frac{\Lambda_0}{\sigma}} \qquad \text{(D-8a)}$$

while

$$\psi = \sqrt{\frac{2NE_c}{N_0}} = \sqrt{2N\gamma_c} \qquad \text{(D-8b)}$$

Although the above results are exact, they are cumbersome to use from a computational viewpoint, expecially for large N (N>100). Besides, the Gaussian approximation about Λ' becomes sufficiently tight in that region and thus emerges as an attractive and simple tool.

Let us start from the fact that

$$r_{I_j} = \sqrt{S}\, T_c\, c_j\, \delta_{kl} \cos\phi_j + n_{I_j} \tag{D-9a}$$

and

$$r_{Q_j} = \sqrt{S}\, T_c c_j \delta_{kl} \sin\phi_j + n_{Q_j} \tag{D-9b}$$

In (D-9), the Gaussian rv's n_{I_j} and n_{Q_j} are defined by

$$n_{I_j} = \int_{(j-1)T_c}^{jT_c} n_I(t)\, dt \tag{D-10a}$$

and

$$n_{Q_j} = \int_{(j-1)T_c}^{jT_c} n_Q(t)\, dt \tag{D-10b}$$

and are, therefore, mutually independent, each with zero mean and variance σ_n^2. Then, the squared envelope r_j^2 is

$$r_j^2 = r_{I_j}^2 + r_{Q_j}^2 = ST_c^2\, \delta_{kl} + n_{I_j}^2 + n_{Q_j}^2 + 2\sqrt{S}\, T_c\, c_j\, \delta_{kl}\left(n_{I_j}\, \phi_j + n_{Q_j} \sin\phi_j\right) \tag{D-11}$$

It immediately follows that

$$\mathcal{E}\left\{r_j^2\right\} = ST_c^2\, \delta_{kl} + 2\sigma_n^2 = ST_c^2\, \delta_{kl} + N_0T_c = \left(N_0T_c\right)\left(1 + \gamma_c\, \delta_{kl}\right) \tag{D-12}$$

which is (3-23a).

In order to calculate the variance of r_j^2 in (D-11), we note that the first term is a constant (thus, it can be neglected), while the second, third and fourth terms are pairwise uncorrelated. This is because: (a) $n_{I_j}^2$ and $n_{Q_j}^2$

are functions of independent rv's and, (b) the fourth term includes both c_j and ϕ_j, which are independent of the noise and zero mean. As a conclusion,

$$\text{var}\{r_j^2\} \triangleq \mathcal{E}\left\{\left(r_j^2 - \mathcal{E}\{r_j^2\}\right)^2\right\} = \text{var}\{n_{I_j}^2\} + \text{var}\{n_{Q_j}^2\}$$

$$+ 4ST_c^2\,\delta_{k1}\,\text{var}\{n_{I_j}\cos\phi_j + n_{Q_j}\sin\phi_j\}$$

$$= 4\sigma_n^4 + 4ST_c^2\,\sigma_n^2\,\delta_{k1} = (N_0T_c)^2 + 2ST_c^3N_0\,\delta_{k1}$$

$$= (N_0T_c)^2(1 + 2\gamma_c\delta_{k1}) \qquad \text{(D-13)}$$

since

$$\text{var}\{\cos\phi_j\} = \text{var}\{\sin\phi_j\} = \frac{1}{2}$$

Equation (D-13) is identical to equation (3-23b).

APPENDIX E

PROOF OF EQUATIONS (3-44) and (3-45)

First, let us note that, once T_c is substituted by $T_c/2$, (3-43) is derivable from equation (3-10), i.e.,

$$\mathcal{E}\left\{r_{jm}^2 \middle| H_k\right\} = \frac{N_0 T_c}{2}\left(\frac{1}{2} + \frac{ST_c}{2N_0}\delta_{k1}\right) = \frac{N_0 T_c}{4}\left(1 + \gamma_c \delta_{k1}\right)$$

and

$$\text{var}\left\{r_{jm}^2 \middle| H_k\right\} = \left(\frac{N_0 T_c}{2}\right)^2\left(\frac{1}{2} + \frac{ST_c}{N_0}\delta_{k1}\right) = \frac{\left(N_0 T_c\right)^2}{4}\left(\frac{1}{2} + \gamma_c \delta_{k1}\right)$$

as per (3-43). We shall now show that

$$\mathcal{E}\left\{r_{j2}\, r_{j+1,1} \middle| H_k ; \varepsilon=0\right\} = 0 \qquad \text{(E-1)}$$

and

$$\mathcal{E}\left\{r_{j1}\, r_{j2} \middle| H_k ; \varepsilon=0\right\} = \frac{ST_c^2}{4}\delta_{k1} \qquad \text{(E-2)}$$

Consider the situation in Figure E.1. From (3-41), it follows that

$$r_{j2} = \sqrt{S}\left(\frac{T_c}{2}\right) c_j\, \delta_{k1} + n_{j2} \qquad \text{(E-3)}$$

$$r_{j+1,1} = \sqrt{S}\left(\frac{T_c}{2}\right) c_{j+1}\, \delta_{k1} + n_{j+1,1} \qquad \text{(E-4)}$$

where noises n_{j2} and $n_{j+1,1}$ are mutually independent, as are c_j and c_{j+1}. Thus,

$$\mathcal{E}\left\{r_{j2}\, r_{j+1,1}\right\} = S\left(\frac{T_c}{2}\right)^2 \delta_{k1}\, \mathcal{E}\left\{c_j\, c_{j+1}\right\} + \mathcal{E}\left\{n_{j2}\, n_{j+1,1}\right\} = 0$$

In an analogous way,

$$r_{j1} = \sqrt{S}\left(\frac{T_c}{2}\right) c_j\, \delta_{k1} + n_{j1} \qquad \text{(E-5)}$$

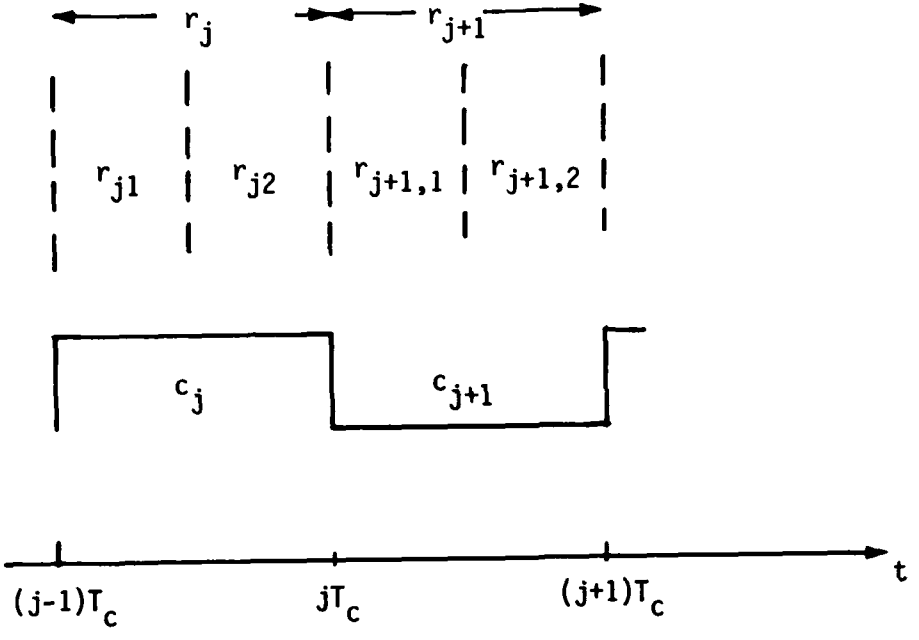

Figure E.1. Definition of rj's, Assuming H_1 (Signal Present) and $\varepsilon = 0$

which, combined with (E-3) yields

$$\mathcal{E}\{r_{j1}\, r_{j2}\} = \frac{ST_c^2}{4}\,\delta_{k1} + \mathcal{E}\{n_{j1}\, n_{j2}\} = \frac{ST_c^2}{4}\,\delta_{k1} \qquad \text{(E-6)}$$

by virtue of independence between n_{j1} and n_{j2}. Finally, substituting (3-43) and (3-44) into (3-42b) yields

$$\begin{aligned}
\mathcal{E}\{\Lambda\} &= N\left[2\,\mathcal{E}\{r_{j1}^2\} + \mathcal{E}\{r_{j1}\, r_{j2}\}\right] \\
&= N\left[\frac{(N_0T_c)}{2}\left(1 + \gamma_c\,\delta_{k1}\right) + \frac{ST_c^2}{4}\,\delta_{k1}\right] \\
&= N\left(\frac{N_0T_c}{2}\right)\left[1 + \gamma_c\,\delta_{k1} + \frac{\gamma_c}{2}\,\delta_{k1}\right] \\
&= N\left(\frac{N_0T_c}{2}\right)\left[1 + \left(\frac{3}{2}\right)\gamma_c\,\delta_{k1}\right] \qquad \text{(E-7)}
\end{aligned}$$

which is (3-45).

APPENDIX F

PROOF OF EQUATION (3-46)

We follow a procedure similar to Appendix E; however, the picture is changed to Figure F.1, under the assumption of a worst epoch $\varepsilon = 1/4$. Then, we can write that

$$r_{j2} = \sqrt{S}\left(\frac{T_c}{2}\right) c_j \, \delta_{k1} + n_{j2} \tag{F-1}$$

and

$$r_{j1} = \sqrt{S}\left(\frac{T_c}{4}\right) \left[c_{j-1} + c_j\right] + n_{j1} \tag{F-2}$$

Note that r_{j2} is identical to (E-3); thus, $\mathcal{E}\left\{r_{j2}^2 \middle| H_k ; \varepsilon=1/4\right\}$ is as per (3-43). Furthermore,

$$\mathcal{E}\left\{r_{j1}^2 \middle| H_k ; \varepsilon=1/4\right\} = \left(\frac{1}{2}\right) \left[\mathcal{E}\left\{r_{j1}^2 \middle| H_k ; \varepsilon=1/4 ; A_{same}\right\} + \mathcal{E}\left\{r_{j1}^2 \middle| H_k ; \varepsilon=1/4 ; A_{diff}\right\}\right] \tag{F-3}$$

where the conditioning events A_{same} and A_{diff} refer to c_{j-1} and c_j having the same or a different sign. Clearly,

$$P_r\left\{A_{same}\right\} = P_r\left\{A_{diff}\right\} = \frac{1}{2} \tag{F-4}$$

a fact used in (F-3). Let us now note that, under A_{diff}, the mean of r_{ji} is zero while, under A_{same}, it is equal to $\sqrt{S}\, T_c/2$. Thus,

$$\mathcal{E}\left\{r_{j1}^2 \middle| H_k ; \varepsilon=1/4\right\} = \left(\frac{1}{2}\right)\left[\left(\frac{N_0 T_c}{4}\right)\left(1 + \gamma_c \, \delta_{k1}\right) + \left(\frac{N_0 T_c}{4}\right)\right] = \left(\frac{N_0 T_c}{4}\right)\left[1 + \frac{1}{2}\, \gamma_c \, \delta_{k1}\right] \tag{F-5}$$

In exactly the same way,

$$\mathcal{E}\left\{r_{j1}\, r_{j2} \middle| H_k ; \varepsilon=1/4\right\} = S\left(\frac{T_c^2}{8}\right) \mathcal{E}\left\{c_j \left(c_{j-1} + c_j\right)\right\} \delta_{k1} + \mathcal{E}\left\{n_{j1}\, n_{j2}\right\}$$

$$= \left(\frac{S T_c}{N_0}\right)\left(\frac{N_0 T_c}{8}\right)\delta_{k1} = \left(\frac{N_0 T_c}{4}\right)\left(\frac{\gamma_c}{2}\right)\delta_{k1}$$

which completes the proof of (3-46).

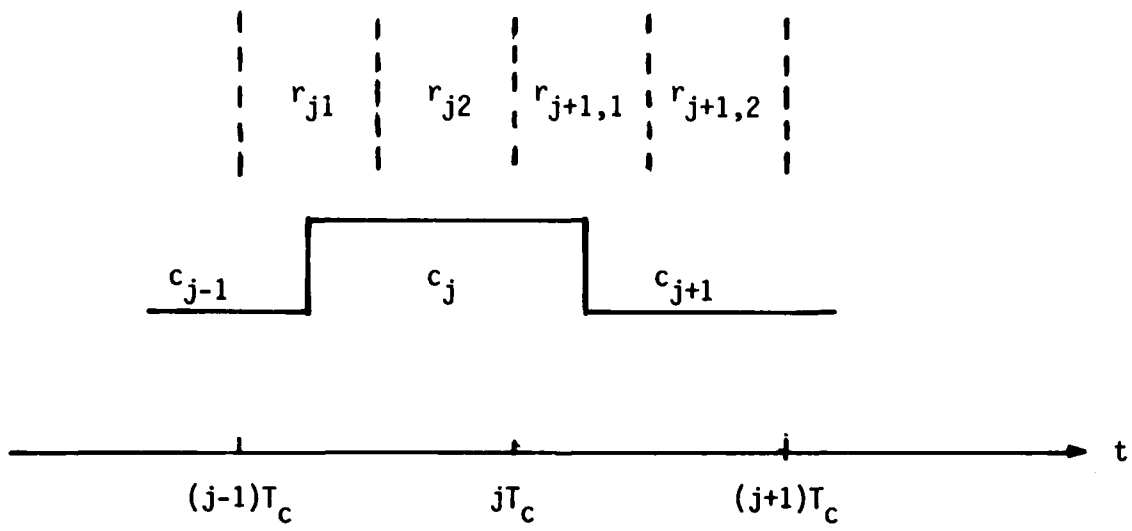

Figure F.1. Definition of r_j's, Assuming H_1 and $\varepsilon = 1/4$

APPENDIX G

PROOF OF EQUATION (3-63)

Let

$$\Lambda' = \sum_{j=1}^{N} y_j \underset{H_0}{\overset{H_1}{\gtrless}} \Lambda_0' \tag{G-1}$$

be the decision rule (3-62a), where

$$y_j = r_j^{(1)} r_j^{(2)} \tag{G-2}$$

and $r_j^{(i)}$;i=1,2 is given by (3-62b). Then,

$$r_j^{(i)} = \sqrt{S}\, T_c\, c_j\, \delta_{kl} + n_j^{(i)} \tag{G-3}$$

where $n_j^{(1)}$ and $n_j^{(2)}$ are zero mean, mutually independent Gaussian rv's with common variance $\sigma_n^2 = N_0 T_c/2$. From (G-2) and (G-3), it follows that

$$y_j = S\, T_c^2\, \delta_{kl} + \sqrt{S}\, T_c\, c_j\, \delta_{kl} \left(n_j^{(1)} + n_j^{(2)} \right) + n_j^{(1)}\, n_j^{(2)} \tag{G-4}$$

Thus,

$$\mathcal{E}\left\{ y_j \right\} = S\, T_c^2\, \delta_{kl} = \left(N_0 T_c \right) \gamma_c\, \delta_{kl} \tag{G-5}$$

which justifies (3-63a). Furthermore,

$$\mathrm{var}\left\{ y_j \right\} = S\, T_c^2\, \delta_{kl}\, \mathrm{var}\left\{ n_j^{(1)} + n_j^{(2)} \right\} + \mathrm{var}\left[n_j^{(1)}\, n_j^{(2)} \right]$$

$$= S\, T_c^2\, \delta_{kl}\, 2\sigma_n^2 + \sigma_n^4 = 4\sigma_n^4 \left[\left(\frac{1}{4} \right) + \frac{S T_c^2}{2\sigma_n^2}\, \delta_{kl} \right]$$

$$= \left(N_0 T_c \right)^2 \left[\frac{1}{4} + \gamma_c\, \delta_{kl} \right]$$

as per (3-63b).

APPENDIX H

STATISTICAL CHARACTERIZATION OF NOISE PROCESSES

$N_I^{eq}(\tau)$ AND $N_Q^{eq}(\tau)$

We define $N_I^{eq}(\tau)$ and $N_Q^{eq}(\tau)$ as per (5-17) and (5-12). It then follows from (5-13), (5-14) and (5-15) that $N_I^{eq}(\tau_k)$, $N_Q^{eq}(\tau_k)$; $\tau_k = kB^{-1}$ are zero-mean random variables, i.e., (5-18). Furthermore, by virtue of a central-limit-type argument (summations of a large number of rv's), they are assumed to be approximately Gaussian.

We shall first show that $N_I^{eq}(\tau_k)$ and $N_Q^{eq}(\tau_j)$ are uncorrelated for every k and j; in which case, they are also approximately independent (due to the Gaussian assumption). Indeed, from (5-17),

$$\mathcal{E}\left\{N_I^{eq}(\tau_k)\, N_Q^{eq}(\tau_j)\right\} = \mathcal{E}\left\{N_{II}(\tau_k)\, N_{IQ}(\tau_j)\right\} + \mathcal{E}\left\{N_{QQ}(\tau_k)\, N_{IQ}(\tau_j)\right\}$$

$$- \mathcal{E}\left\{N_{II}(\tau_k)\, N_{QI}(\tau_j)\right\} - \mathcal{E}\left\{N_{QQ}(\tau_k)\, N_{QI}(\tau_j)\right\} \qquad \text{(H-1)}$$

Let us consider the first term on the right-hand side of (H-1); a similar line of argument applies to the next three terms. By definition,

$$\mathcal{E}\left\{N_{II}(\tau_k)\, N_{IQ}(\tau_j)\right\} = \int_{\tau_k}^{T_H}\int_{\tau_k}^{T_H} \mathcal{E}\left\{n_I(t_1)n_I(t_1-\tau_k)n_I(t_2)n_Q(t_2-\tau_j)\right\}dt_1dt_2 \qquad \text{(H-2)}$$

However, $n_Q(t)$ is independent of $n_I(t)$, which implies that the integrand of (H-2) contains the factor $\mathcal{E}\left\{n_Q(t_2-\tau_j)\right\}$, which is zero. Thus,

$$\mathcal{E}\left\{N_{II}(\tau_k)\, N_{IQ}(\tau_j)\right\} = 0 \qquad \text{(H-3)}$$

Along with (H-1) and the above remarks, (H-3) establishes the uncorrelatedness of $N_I^{eq}(\tau_k)$ and $N_Q^{eq}(\tau_j)$.

Let us now consider $N_I^{eq}(\tau_{k_1})$ and $N_I^{eq}(\tau_{k_2})$ for $\tau_{k_1} \neq \tau_{k_2}$. We have that

$$\mathcal{E}\left\{N_I^{eq}(\tau_{k_1})N_I^{eq}(\tau_{k_2})\right\} = \mathcal{E}\left\{N_{II}(\tau_{k_1})N_{II}(\tau_{k_2})\right\} + \mathcal{E}\left\{N_{QQ}(\tau_{k_1})N_{QQ}(\tau_{k_2})\right\}$$

$$+ \mathcal{E}\left\{N_{II}(\tau_{k_1})N_{QQ}(\tau_{k_2})\right\} + \mathcal{E}\left\{N_{QQ}(\tau_{k_1})N_{II}(\tau_{k_2})\right\} \quad \text{(H-4)}$$

But,

$$\mathcal{E}\left\{N_{II}(\tau_{k_1})N_{II}(\tau_{k_2})\right\}_{\tau_{k_1}\neq\tau_{k_2}} = \int_{\tau_{k_1}}^{T_H}\int_{\tau_{k_2}}^{T_H} \mathcal{E}\left\{n_I(t_1)n_I(t_1-\tau_{k_1})n_I(t_2)n_I(t_2-\tau_{k_2})\right\}dt_1dt_2 \quad \text{(H-5)}$$

We shall approximate the integral (H-5) as the double sum

$$\mathcal{E}\left\{N_{II}(\tau_{k_1})N_{II}(\tau_{k_2})\right\}_{k_1\neq k_2} \approx (\Delta\tau)^2 \sum_{k=k_1}^{G}\sum_{m=k_2}^{G} \mathcal{E}\left\{n_I(k)n_I(k-k_1)n_I(m)n_I(m-k_2)\right\} \quad \text{(H-6)}$$

where $\Delta\tau = \tau_1 = B^{-1}$. Approximating integrals as per (H-5) by summation is a common and well-founded practice. We note that $n_I(k)$ and $n_I(k-k_1)$ are independent rv's since $k_1 \neq 0$, as are $n_I(m)$ and $n_I(m-k_2)$. Furthermore, due to the independence of the rv's involved, the expectation in (H-6) will be zero whenever all four sampling times k, $k-k_1$, m, $m-k_2$ are pairwise different, as shown in Figure H.1(a). If we assume that $k_1 < k_2$, we then observe that the three remaining cases depicted in Figure H.1 are (b) $k-k_1 = m-k_2$; in which case, $k \neq m$, or (c) $k=m$; in which case, $k-k_1 \neq m-k_2$, or (d) $k = m-k_2$; in which case, $k-k_1 \neq m$. In all those cases, the common conclusion is that at least two rv's exist which do not coincide with the others. The net result is that the expectation in (H-6) will always be zero, establishing the approximate uncorrelatedness of $N_{II}(\tau_{k_1})$ and $N_{II}(\tau_{k_2})$. The same exact argument establishes that $\mathcal{E}\left\{N_{QQ}(\tau_{k_1})\ N_{QQ}(\tau_{k_2})\right\} \cong 0$, while it is even easier to show that $\mathcal{E}\left\{N_{II}(\tau_{k_1})\ N_{QQ}(\tau_{k_2})\right\} \cong \mathcal{E}\left\{N_{QQ}(\tau_{k_1})N_{II}(\tau_{k_2})\right\} \cong 0$. Thus all of the above can be combined in (H-4) to illustrate that different samples ($\tau_{k_1} \neq \tau_{k_2}$) of the same process $N_I^{eq}(\tau)$ are approximately uncorrelated. It can similarly be demonstrated that the same is true for $N_Q^{eq}(\tau)$, defined in (5-17c).

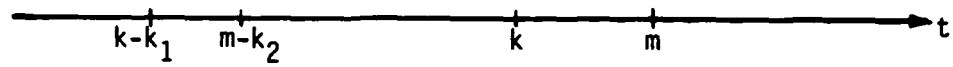

(a) All sampling times different

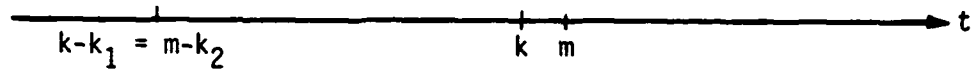

(b) $k - k_1 = m - k_2$

(c) $k = m$

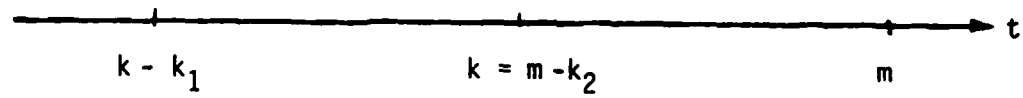

(d) $k = m - k_2$

Figure H.1. Some Possible Combinations of Sampling Times in (H-6)

Finally, we are concerned with the variance of $N_I^{eq}(\tau_k)$ and $N_Q^{eq}(\tau_k)$, i.e., (5-19). Clearly, since the respective means are zero, those variances coincide with the second moments. Furthermore,

$$\mathcal{E}\left\{\left(N_I^{eq}(\tau_k)\right)^2\right\} = \mathcal{E}\left\{N_{II}^2(\tau_k)\right\} + \mathcal{E}\left\{N_{QQ}^2(\tau_k)\right\} = 2\mathcal{E}\left\{N_{II}^2(\tau_k)\right\} \tag{H-7}$$

But,

$$\begin{aligned}\mathcal{E}\left\{N_{II}^2(\tau_k)\right\} &= \int_{\tau_k}^{T_H}\int_{\tau_k}^{T_H} \mathcal{E}\left\{n_I(t_1)n_I(t_1-\tau_k)n_I(t_2)n_I(t_2-\tau_k)\right\} dt_1 dt_2 \\ &= \int_0^{T_H-\tau_k}\int \mathcal{E}\left\{n_I(t_1'+\tau_k)n_I(t_1')n_I(t_2'+\tau_k)n_I(t_2')\right\} dt_1'\ dt_2' \end{aligned} \tag{H-8}$$

where a simple change of variables has been performed. We shall now use a familiar property of four jointly Gaussian rv's $\{x_i\}_{i=1}^4$, namely, that [15]

$$\mathcal{E}\left\{\prod_{i=1}^4 x_i\right\} = \mathcal{E}\left\{x_1x_2\right\}\mathcal{E}\left\{x_3x_4\right\} + \mathcal{E}\left\{x_1x_3\right\}\mathcal{E}\left\{x_2x_4\right\} + \mathcal{E}\left\{x_1x_4\right\}\mathcal{E}\left\{x_2x_3\right\} \tag{H-9}$$

Applying (H-9) into (H-8) results in (for any τ):

$$\begin{aligned}\mathcal{E}\left\{N_{II}^2(\tau)\right\} &= \int_0^{T_H-\tau}\int \mathcal{E}\left\{n_I(t_1'+\tau)n_I(t_1')\right\}\ \mathcal{E}\left\{n_I(t_2'+\tau)n_I(t_2')\right\}\ dt_1'dt_2' \\ &\quad + \int_0^{T_H-\tau}\int \mathcal{E}\left\{n_I(t_1'+\tau)n_I(t_2'+\tau)\right\}\mathcal{E}\left\{n_I(t_1')\ n_I(t_2')\right\} dt_1'dt_2' \\ &\quad + \int_0^{T_H-\tau}\int \mathcal{E}\left\{n_I(t_1'+\tau)n_I(t_2')\right\}\mathcal{E}\left\{n_I(t_1')\ n_I(t_2'+\tau)\right\}\ dt_1'dt_2' \\ &= R_{nn}^2(\tau)\ (T_H-\tau)^2 + \int_0^{T_H-\tau}\int R_{nn}^2(t_1'-t_2')\ dt_1'dt_2' \\ &\quad + \int_0^{T_H-\tau}\int R_{nn}(t_1'-t_2'+\tau)\ R_{nn}(t_1'-t_2'-\tau)\ dt_1'dt_2' \end{aligned} \tag{H-10}$$

where $R_{nn}(\tau) = \mathcal{E}\{n_I(t)n_I(t+\tau)\}$ is the correlation function of $n_I(t)$, as per (5-13).

Equation (H-10) can be further simplified. First, we note that, for $\tau = \tau_k = kB^{-1}$, $R_{nn}(\tau_k) = 0$, so the first term drops out. Furthermore, one can employ the even symmetry of $R_{nn}(\tau)$, i.e., the fact that $R_{nn}(\tau) = R_{nn}(-\tau)$, in order to reduce the two-dimensional integrals to one-dimensional ones (see [15], page 325 for details). The result is then

$$\mathcal{E}\{N_{II}^2(\tau_k)\} = 2\int_0^{T_H-\tau_k}(T_H-\tau_k-\rho)\left(\frac{N_0B}{2}\right)^2 \mathrm{Sa}^2(\pi B\rho)\,d\rho$$

$$+ 2\int_0^{T_H-\tau_k}(T_H-\tau_k-\rho)\left(\frac{N_0B}{2}\right)^2 \mathrm{Sa}\left[\pi B(\rho+\tau_k)\right]\mathrm{Sa}\left[\pi B(\rho-\tau_k)\right]d\rho \qquad \text{(H-11)}$$

With the change of variables

$$\rho' = \frac{\rho}{T_H-\tau_k} \qquad \text{(H-12)}$$

and defining the normalized parameter ζ_k as

$$\zeta_k \triangleq \frac{\tau_k}{T_H} = \frac{k}{BT_H} = \frac{k}{G} \qquad \text{(H-13)}$$

we can rewrite (H-11) as

$$\mathcal{E}\{N_{II}^2(\tau_k)\} = \frac{(N_0B)^2}{2}(T_H-\tau_k)^2\left[\int_0^1 (1-\rho')\mathrm{Sa}^2\left[\pi B\rho'(T_H-\tau_k)\right]d\rho'\right.$$

$$\left. + \int_0^1 (1-\rho')\mathrm{Sa}\left[\pi B\left(\rho'(T_H-\tau_k)+\tau_k\right)\right]\mathrm{Sa}\left[\pi B\left(\rho'(T_H-\tau_k)-\tau_k\right)\right]d\rho'\right]$$

$$= \frac{(N_0B)^2(T_H-\tau_k)^2}{2}(F_1(k)+F_2(k)) \qquad \text{(H-14)}$$

where

$$F_1(k) = \int_0^1 (1-\rho')Sa^2\left[\pi BT_H\left(1 - \frac{\tau_k}{T_H}\right)\rho'\right]d\rho' = \int_0^1 (1-\rho')Sa^2\left[\pi G(1-\zeta_k)\rho'\right]d\rho' \quad \text{(H-15)}$$

and

$$F_2(k) = \int_0^1 (1-\rho')\, Sa\left[\pi G\left(\rho'(1-\zeta_k) + \zeta_k\right)\right] Sa\left[\pi G\left(\rho'(1-\zeta_k) - \zeta_k\right)\right]d\rho' \quad \text{(H-16)}$$

exactly as in (5-20). Combining (H-14) with (H-7) yields (5-19a).

Quite similarly, it follows from (5-17c) that

$$\mathcal{E}\left\{\left(N_Q^{eq}(\tau)\right)^2\right\} = 2\mathcal{E}\left\{N_{IQ}^2(\tau)\right\} - 2\mathcal{E}\left\{N_{IQ}(\tau)N_{QI}(\tau)\right\} \quad \text{(H-17)}$$

But,

$$\begin{aligned}\mathcal{E}\left\{N_{IQ}^2(\tau)\right\} &= \int_\tau^{T_H}\int \mathcal{E}\left\{n_I(t_1)n_Q(t_1-\tau)n_I(t_2)n_Q(t_2-\tau)\right\}dt_1dt_2 \\ &= \int_\tau^{T_H}\int R_{nn}^2(t_1-t_2)dt_1dt_2 = \int_0^{T_H-\tau}\int R_{nn}^2(t_1'-t_2')\, dt_1'dt_2' \end{aligned} \quad \text{(H-18)}$$

since $n_I(t)$ and $n_Q(t)$ are independent, with the same correlation function. The integral in (H-18) is identical to the second term in (H-10), which corresponds to the $F_1(k)$ term in (H-14). Furthermore,

$$\begin{aligned}\mathcal{E}\left\{N_{IQ}(\tau)\, N_{QI}(\tau)\right\} &= \int_\tau^{T_H}\int \mathcal{E}\left\{n_I(t_1)n_Q(t_1-\tau)n_Q(t_2)\, n_Q(t_2-\tau)\right\}dt_1dt_2 \\ &= \int_0^{T_H-\tau}\int R_{nn}\left(t_1' - t_2' + \tau\right)R_{nn}\left(t_1' - t_2' - \tau\right)dt_1'dt_2' \end{aligned} \quad \text{(H-19)}$$

which is identical to the third term in (H-10) corresponding to the $F_2(k)$ term in (H-14). Combining the above with (H-17) (note the minus sign of the second term) results in

$$\mathcal{E}\left\{N_Q^{eq}(\tau)^2\right\} = (N_0B)^2(T_H - \tau_k)^2\left(F_1(k) - F_2(k)\right) \qquad \text{(H-20)}$$

as per (5-19b).

APPENDIX I

COMPUTER SIMULATIONS OF THE RADIOMETER AND AUTOCORRELATION TECHNIQUES FOR DETECTING FH SIGNALS IN GAUSSIAN NOISE

1.0 INTRODUCTION

Theoretical performances of the autocorrelation technique and the conventional radiometer approach in detecting frequency-hopped (FH) signals in Gaussian noise, discussed in earlier sections of this report, have been verified through computer simulation. The simulation results are summarized in this appendix. Close agreement was observed between theoretical predictions and simulation results.

2.0 SYSTEM MODEL

The system model studied here is illustrated in Figure I.1. The total spread bandwidth W_s is segmented into M B-Hz bands, where $M = W_s/B$. The received signal from each of these B-Hz bands is processed by a waveform processor which determines whether or not an FH signal is present in that segment of the spread bandwidth during the time interval of observation. The decisions made by the waveform processors are accumulated to form the final decision with respect to whether or not an FH signal is present.

Two forms of waveform processing are studied by computer simulation: (1) the radiometer, and (2) the correlation detector. In each case, the waveform processor output statistics (mean and variance) are collected under either hypothesis regardless of whether or not the signal is present. The channel is assumed to be corrupted by additive Gaussian noise in all cases under consideration herein.

Based on the waveform processor-output statistics, the detector output signal-to-noise ratio (SNR) defined here as

$$SNR_0 = \frac{\left[\mathcal{E}(Y|H_0) - \mathcal{E}(Y|H_1)\right]^2}{\mathrm{var}(Y|H_0)} \qquad \text{(I-1)}$$

is first computed as a function of the bandwidth-observation time product BT_H and the input SNR γ_{in}, which is defined by

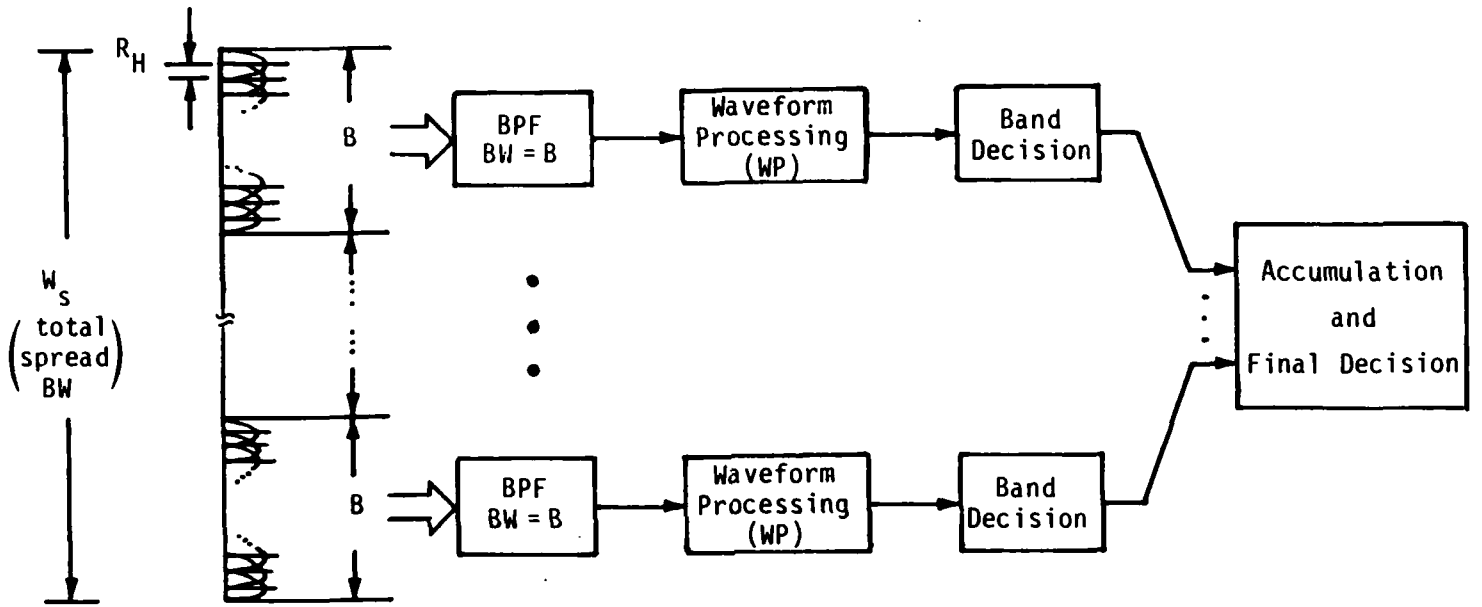

Figure I.1. Suboptimal Processing: Segmenting W_s into B-Hz Bands ($B \gg R_H$)

$$\gamma_{in} = \frac{S}{N_0 B} \tag{I-2}$$

In (I-1) and (I-2), the following notations are used:

$\mathcal{E}(Y|H_0)$ = mean value of the waveform processor output when signal is not present

$\mathcal{E}(Y|H_1)$ = mean value of the waveform processor output when signal is present

$\text{var}(Y|H_0)$ = variance of the waveform processor output when signal is absent

S = received power of the FH signal to be detected

B = input bandwidth of the waveform processor

T_H = the FH time

N_0 = one-sided noise power spectral density (PSD) of the receiver.

The input SNR (γ_{in}) is related to the hop SNR (γ_H) by the BT_H product, as follows:

$$\gamma_H = \frac{ST_H}{N_0} = (BT_H)\,\gamma_{in} \tag{I-3}$$

Also computed in this appendix are the probabilities of detection (P_D) and false alarm (P_{FA}) of each of the waveform detectors. They are related to the first two moments of Y by:

$$P_{FA} = \frac{1}{2} - \frac{1}{2}\,\text{erf}\left[\frac{\Lambda_0 - \mathcal{E}(Y|H_0)}{\sqrt{2\,\text{var}(Y|H_0)}}\right] \tag{I-4}$$

and

$$P_D = \frac{1}{2} - \frac{1}{2}\,\text{erf}\left[\frac{\Lambda_0 - \mathcal{E}(Y|H_1)}{\sqrt{2\,\text{var}(Y|H_1)}}\right] \tag{I-5}$$

In (I-4) and (I-5), Λ_0 denotes the threshold setting and erf denotes the error function

$$\text{erf}(x) = \frac{2}{\sqrt{\pi}} \int_0^x e^{-t^2}\, dt \qquad \text{(I-6)}$$

For each desired P_{FA}, the probability of detection P_D can also be determined, as follows:

$$P_D = \frac{1}{2} - \frac{1}{2}\,\text{erf}\left[\frac{\mathcal{E}(Y|H_0) - \mathcal{E}(Y|H_1) + \sqrt{2\ \text{var}(Y|H_0)}\ \text{erf}^{-1}(1 - 2P_{FA})}{\sqrt{2\ \text{var}(Y|H_1)}}\right] \qquad \text{(I-7)}$$

Gaussian approximations have been made on the waveform processor output Y in arriving at the expressions for P_D and P_{FA} in (I-4) and (I-5). This is justified by the fact that Y is the sum of a large number ($\approx BT_H$) of independent random variables (see next section) and by invoking the central-limit theorem.

3.0 RADIOMETER SIMULATION

For the case of the radiometer, the waveform processor performs the following operation on the received signal r(t) to obtain the detector-output variable Y:

$$Y = \frac{1}{T_H} \int_0^{T_H} \rho^2(t)\, dt \qquad \text{(I-8)}$$

where $\rho(t)$ is the envelope of the received bandpass signal r(t), given as

$$r(t) = \sqrt{2S}\cos\omega_0 t + \sqrt{2}\, n_I(t)\cos\omega_0 t - \sqrt{2}\, n_Q(t)\sin\omega_0 t \qquad \text{(I-9)}$$

In (I-9), ω_0 is the center frequency of the received signal and n_I and n_Q are the quadrature components of the bandpass noise process with a bandwidth B. Thus, n_I and n_Q are independent, zero-mean Gaussian processes having one-sided noise PSD N_0 and variances $N_0B/2$. We assume here that ω_0 coincides with the center frequency of the BPF with bandwidth B (see Figure I.1) so that there is no filtering loss on the received pulse. This assumption is not unduly restrictive since most channels in the bandwidth B will not experience excessive filtering loss except for the ones near the band edges.

Since r(t) is a bandpass process, it can be expressed as

$$r(t) = \mathrm{Im}\left\{\sqrt{2}\, u(t)\, e^{j\omega_0 t}\right\} \tag{I-10}$$

where Im(z) stands for the imaginary part of z and u(t) is the complex envelope

$$u(t) = \sqrt{S} + n_I(t) - j\, n_Q(t) \tag{I-11}$$

where $j = \sqrt{-1}$. The envelope $\rho(t)$ is given by

$$\rho(t) = \sqrt{2}|u(t)| = \sqrt{2\left\{\left[\sqrt{S} + n_I(t)\right]^2 + n_Q^2(t)\right\}} \tag{I-12}$$

Since n_I and n_Q (and, thus, $\rho(t)$ also) are bandpass processes with bandwidth $\pm B/2$, by invoking the (stochastic) sampling theory, they can be represented as samples taken at time intervals separated by $\Delta T = 1/B$. In other words, a valid simulation of the integration process (I-8), from which the detector output variable Y is derived, is the discrete-time summation

$$Y = \frac{1}{BT_H} \sum_{k=1}^{G} \rho^2\left(\frac{k}{B}\right) \tag{I-13}$$

where $G = BT_H$ is the number of samples to be accumulated over the hop time T_H. The discrete-time simulation (I-13) is equivalent to the actual process (I-8) in the sense that, if the sample values r(k/B) are taken from the actual band-limited analog signal r(t), the discrete system outputs at the sample time instants (in this case, after $G = BT_H$ samples have been accumulated) will be identical to the analog system output at the same instants*. The noise samples of n_I and n_Q input to the discrete-time simulation model can be taken to be uncorrelated and, thus, independent. This assumes that the impulse response of the bandpass filter preceding the waveform processor has zero crossings at 1/B. One BPF response which will satisfy this assumption is the ideal response

$$H(\omega) = \begin{cases} 1 & |\omega - \omega_0| \leq B/2 \\ 0 & \text{elsewhere} \end{cases} \tag{I-14}$$

---

*Reference A. Papoulis, Signal Analysis, McGraw-Hill Book Company, 1977, pp. 25-27.

This ideal response is closely approximated by actual BPF's with sharp cutoffs which will probably be the case in actual radiometer implementations.

Table I.1 summarizes the theoretical predictions on the radiometer output statistics which are required to compute SNR_0. They are given here as functions of BT_H and S/N_0B. The results summarized in this table are those derived from the discrete-time model, which is of interest when calibrating the accuracy of the simulation.

Table I.2 summarizes the radiometer simulation results. It is observed that the simulation results agree very well with the computed results from theory (with SNR_0 error $\leq$ 0.25 dB in 200 trials).

Based on the simulated results of the means and variances of the radiometer output under H_0 or H_1, the probability of detection (P_D) of FH signals by the radiometer technique is computed by (I-7), for each desired probability of false alarm (P_{FA}), as a function of input SNR γ_{in}. The results for BT_H = 100 and BT_H = 1000 are summarized in Figures I.2 and I.3, respectively.

4.0 AUTOCORRELATION TECHNIQUE SIMULATION

In the autocorrelation technique, the waveform processor output Y is characterized by the following operations:

$$Y = \sum_{k=1}^{G} a_k W_k \tag{I-15}$$

where W_k is the squared value of the envelope of the autocorrelation function $R_r(\tau)$ of the received signal r(t) at $\tau = k/b$, and a_k's are weighting coefficients

$$a_k \equiv \begin{cases} (T_H - k/B)^{-2} & \text{if } k \leq \lambda G \\ 0 & \text{if } k > \lambda G \end{cases} \tag{I-16}$$

where $G = BT_H$ and λ is a positive fraction < 1, which serves to truncate the sum (I-15) to (λ BT_H - 1) terms. The autocorrelation function $R_r(\tau)$ of the bandpass signal r(t) with complex envelope u(t) (see (I-9), I-10) and (I-11)) is given by

Table I.1. Threshold Relationships of Radiometer Output Statistics and SNR_0

$\mathcal{E}(Y \mid H_0)$	$2N_0B$
$\mathcal{E}(Y \mid H_1)$	$2\left[S + N_0B\right]$
$\text{var}(Y \mid H_0)$	$\frac{1}{BT_H}\left(2N_0B\right)^2$
SNR_0	$\left(BT_H\right)\left(\frac{S}{N_0B}\right)^2 = G \cdot \gamma_{in}^2$

Table I.2. Comparison of Radiometer Simulation Results to Theory; (200 Trials)

(a) $BT_H = 100$

Input SNR	-20 dB		-10 dB		-5 dB	
Theory or Simulation	Theory	Simulation	Theory	Simulation	Theory	Simulation
$\mathcal{E}(Y\|H_0)$	4.00	3.96	4.00	4.01	4.00	3.96
$\mathcal{E}(Y\|H_1)$	4.04	4.00	4.40	4.41	5.27	5.22
$\text{var}(Y\|H_0)$	16.00	15.96	16.00	15.63	16.00	15.96
$\text{var}(Y\|H_1)$	-	16.32	-	20.29	-	25.54
SNR_0	-20.00	-20.14	0.00	0.25	10.00	9.98

(b) $BT_H = 1000$

Input SNR	-20 dB		-15 dB		-10 dB	
Theory or Simulation	Theory	Simulation	Theory	Simulation	Theory	Simulation
$\mathcal{E}(Y\|H_0)$	4.00	4.003	4.00	4.003	4.00	4.003
$\mathcal{E}(Y\|H_1)$	4.04	4.044	4.126	4.132	4.40	4.407
$\text{var}(Y\|H_0)$	16.00	16.14	16.00	16.14	16.00	16.14
$\text{var}(Y\|H_1)$	-	16.20	-	16.69	-	18.57
SNR_0 (dB)	-10.00	-9.73	0.00	0.14	10.0	10.06

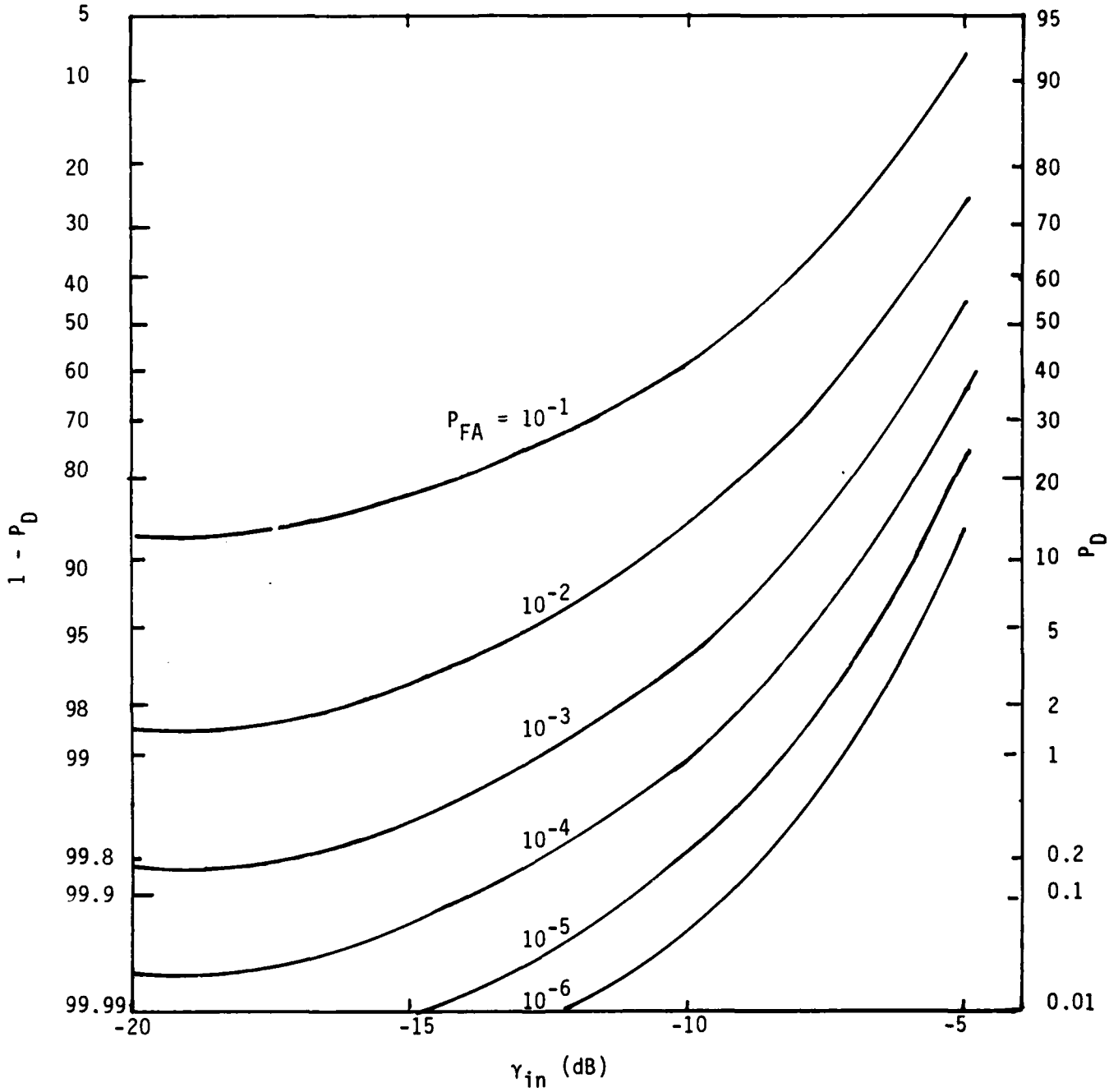

Figure I.2. Radiometer Simulation Results; $BT_H = 100$

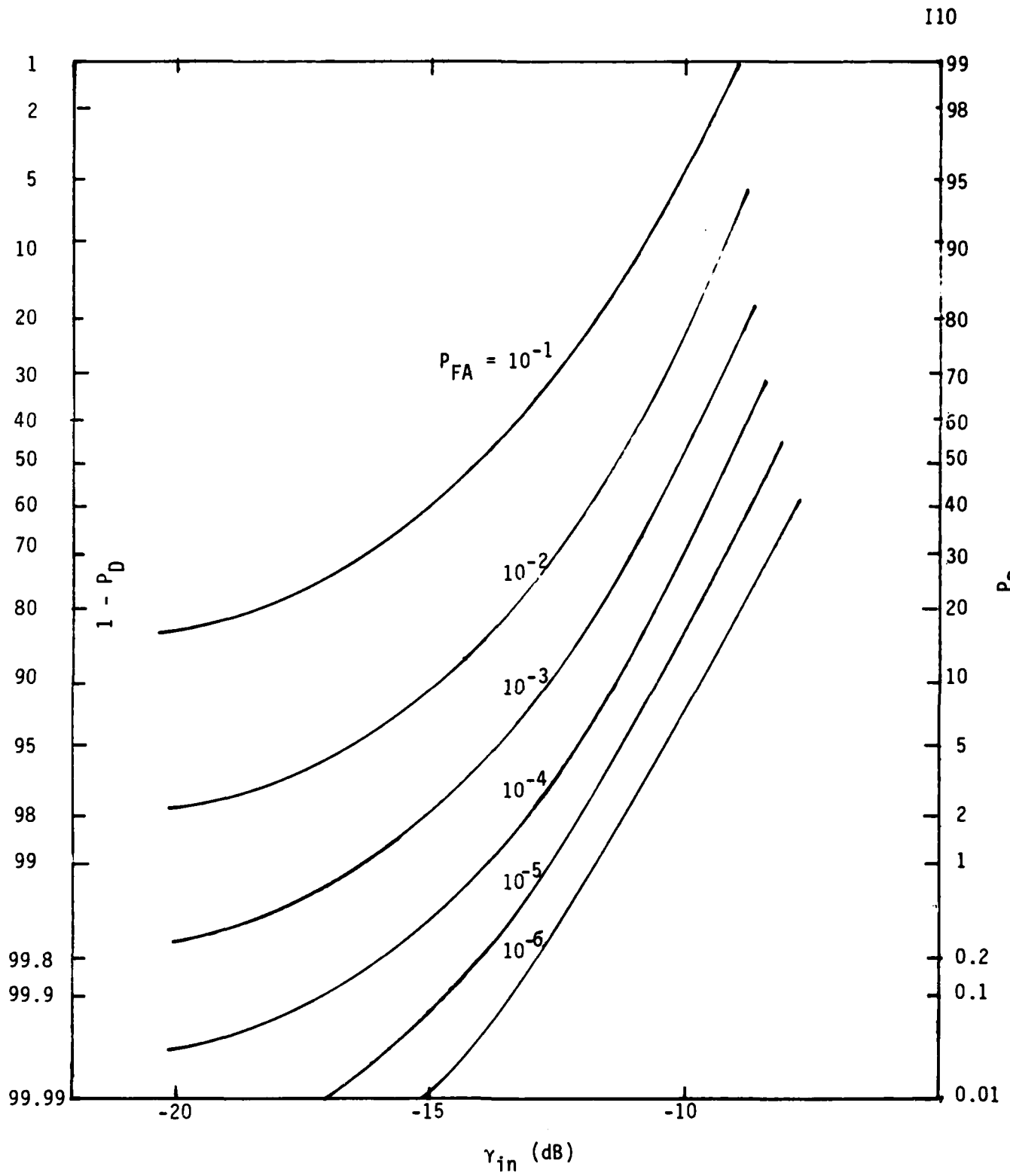

Figure I.3. Radiometer Simulation Results: $BT_H = 1000$

$$R_r(\tau) = \mathrm{Re}\left\{R_u(\tau)\, e^{j\omega_0 t}\right\} \tag{I-17}$$

where $R_u(\tau)$ is the autocorrelation function of u(t):

$$R_u(\tau) = \int_0^{T_H} u^*(t)\, u(t-\tau)dt \tag{I-18}$$

Since $R_r(\tau)$ is itself a bandpass function of τ, the envelope of $R_r(\tau)$ is $|R_u(\tau)|$. Thus, we have

$$W_k \equiv \left|R_r\left(\frac{k}{B}\right)\right|^2 = \left|R_u\left(\frac{k}{B}\right)\right|^2 = \left|\int_{k/B}^{T_H} u^*(t)\, u\left(t - \frac{k}{B}\right)dt\right|^2 \tag{I-19}$$

Now, since u(t), given by

$$u(t) = \sqrt{S} + n_I(t) - j\, n_Q(t) \tag{I-20}$$

is bandlimited to B, the simulation of (I-19) can again be performed by a discrete-time model similar to that used in the radiometer simulation. The discrete-time model is characterized by the following equations:

$$W_k = \left|\frac{1}{B}\sum_{\ell=k}^{G} u^*[\ell/B]u[(\ell-k)/B]\right|^2 \tag{I-21}$$

$$Y = \sum_{k=1}^{G} a_k W_k \tag{I-22}$$

and

$$a_k = \begin{cases} \left(\frac{B}{N-k}\right)^2 & \text{if } k \leq \lambda G \\ 0 & \text{if } k > \lambda G \end{cases} \tag{I-23}$$

The mean values of W_k and, thus, Y, under either hypotheses H_0 or H_1, can be computed relatively easily from the discrete-time equations (I-21), (I-22) and (I-23). These theoretical results are summarized in Table I.3.

The variance of W_k and, thus, Y, is difficult to compute exactly, however, due to the complexity of W_k. (Computations of expected values of products of eight Gaussian random variables are required here.) Under hypothesis H_0, the sum in W_k of (A-21) can be written as

$$\sum_{\ell=k}^{G} u^*\left(\frac{\ell}{B}\right) u\left[\frac{[\ell-k]}{B}\right] = \left(N_{II} + N_{QQ}\right) + j\left(N_{IQ} - N_{QI}\right) \qquad \text{(I-24)}$$

where N_{II}, N_{QQ}, N_{IQ} and N_{QI} are the sums defined by (with $k \geq 1$):

$$N_{II} = \sum_{\ell=k}^{G} n_I(\ell) n_I(\ell-k) \quad ; \quad N_{QQ} = \sum_{\ell=k}^{G} n_Q(\ell) n_Q(\ell-k)$$

$$N_{IQ} = \sum_{\ell=k}^{G} n_I(\ell) n_Q(\ell-k) \quad ; \quad N_{QI} = \sum_{\ell=k}^{G} n_Q(\ell) n_I(\ell-k) \qquad \text{(I-25)}$$

The above noise terms are zero mean, with variance $(G-k)(N_0B/2)^2$. They are uncorrelated. For $k \ll G$, they are sums of a large number of independent random variables. Thus, for $k \ll G$, they are, to a good approximation, Gaussian. We can therefore write W_k as

$$W_k = \left(\frac{1}{B}\right)^2 \left(\eta_A^2 + \eta_B^2\right) \qquad \text{(I-26)}$$

where η_A and η_B are given by

$$\eta_A = N_{II} + N_{QQ} \quad ; \quad \eta_B = N_{IQ} - N_{QI} \qquad \text{(I-27)}$$

and are, to a good approximation, independent Gaussian random variables themselves, with mean zero and variance $2(G-k)(N_0B/2)^2$. Thus, W_k is a squared Rayleigh random variable, to a good approximation. The mean square of W_k is equal to

Table I.3. Theoretical Relationships of the Mean Autocorrelation Detector Outputs as Functions of $G = BT_H$

$\mathcal{E}(W_k \mid H_0)$	$\left(\frac{1}{B}\right)^2 (G-k)(N_0B)^2$
$\mathcal{E}(W_k \mid H_1)$	$\left(\frac{1}{B}\right)^2 S^2\left\{(G-k)^2 + (G-k)\left(\frac{S}{N_0B}\right)^{-1}\left[2 + \left(\frac{S}{N_0B}\right)^{-1}\right]\right\}$
$\mathcal{E}(Y \mid H_0)$	$(N_0B)^2 \sum_{k=1}^{\lambda G} \frac{1}{G-k}$
$\mathcal{E}(Y \mid H_1)$	$S^2\left\{\lambda G + \left(\frac{S}{N_0B}\right)^{-1}\left[2 + \left(\frac{S}{N_0B}\right)^{-1}\right]\sum_{k=1}^{\lambda G}\left(\frac{1}{N-k}\right)\right\}$
$\mathcal{E}(Y \mid H_1) - \mathcal{E}(Y \mid H_0)$	$\lambda G S^2 + 2SN_0B \sum_{k=1}^{\lambda G}\left(\frac{1}{G-k}\right) \cong S^2\left\{\lambda G + 2\left(\frac{S}{N_0B}\right)^{-1} \ln\left(\frac{1}{1-\lambda}\right)\right\}$

$$\mathcal{E}\left(W_k^2\right) = 32(G-k)^2\left(\frac{N_0B}{2}\right)^4\left(\frac{1}{B}\right)^4 = 2\left(\frac{1}{B}\right)^4 (G-k)^2(N_0B)^4 \qquad \text{(I-28)}$$

The variance of W_k under H_0 can thus be written as (see Table I.3):

$$\text{var}(W_k) = \mathcal{E}\left(W_k^2\right) - \left[\mathcal{E}(W_k)\right]^2 = \left(\frac{1}{B}\right)^4 (G-k)^2 (N_0B)^4 \qquad \text{(I-29)}$$

It can also be shown that W_k's are uncorrelated (thus, independent). Based on this approximation, the variance of Y in (I-22) can be written for H_0 as:

$$\text{var}(Y|H_0) = \sum_{k=1}^{\lambda G}\left(\frac{B}{G-k}\right)^4 \text{var}(W_k) = \sum_{k=1}^{\lambda G}\left(\frac{1}{G-k}\right)^2 (N_0B)^4 \qquad \text{(I-30)}$$

Combined with the results in Table I.3, we finally obtain an approximated formula for the autocorrelation detector output SNR (for the discrete-time model):

$$SNR_0 = \frac{\left[\lambda GS^2 + 2SN_0B\sum_{k=1}^{\lambda G}\left(\frac{1}{G-k}\right)\right]^2}{(N_0B)^4\sum_{k=1}^{\lambda G}\left(\frac{1}{G-k}\right)^2} \qquad \text{(I-31)}$$

$$\approx \frac{G\,\gamma_{in}^2\left[\lambda G\gamma_{in} + 2\ell n\left(\frac{1}{1-\lambda}\right)\right]^2}{\left[\frac{\lambda}{(1-\lambda)}\right]} \qquad \text{(I-32)}$$

Again, these results are summarized in Table I.4 for easy reference. For cases when $G\gamma_{in} \gg 2/\lambda\ \ell n(1/(1-\lambda))$, where $0 \leq \lambda \leq 1$ (i.e., large BT_H products), the improvement of the autocorrelation technique over the radiometer approach is given by the ratio

$$\frac{SNR_0^{\text{correlation}}}{SNR_0^{\text{radiometer}}} \approx \lambda(1-\lambda)\left(G\gamma_{in}\right)^2 \qquad \text{(I-33)}$$

Table I.4. Autocorrelation Technique Detector-Output SNR; Theory for the Discrete-Time Model

$\mathcal{E}(Y\|H_1) - \mathcal{E}(Y\|H_0)$	$\cong S^2\left\{\lambda G + 2\left(\frac{S}{N_0B}\right)^{-1} \ell n\left(\frac{1}{1-\lambda}\right)\right\}$
$\text{var}(Y\|H_0)$	$\cong \frac{1}{G}\left(\frac{\lambda}{1-\lambda}\right)(N_0B)^4$
Autocorrelation Output SNR_0	$\cong \frac{G\,\gamma_{in}^2\left[\lambda G\gamma_{in} + 2\,\ell n\left(\frac{1}{1-\lambda}\right)\right]^2}{\left[\frac{\lambda}{(1-\lambda)}\right]}$
Radiometer Technique Output SNR	$G\,\gamma_{in}^2$
$\frac{(SNR_0)^{\text{Autocorr}}}{(SNR)_0^{\text{Radiometer}}}$	$\left(\frac{1-\lambda}{\lambda}\right)\left[\lambda G\,\gamma_{in} + 2\,\ell n\left(\frac{1}{1-\lambda}\right)\right]^2$

It is of interest to note that, for these cases, the optimum choice of λ (the summation truncation factor) is approximately $\approx 1/2$. For $\lambda = 1/2$, the improvement of the autocorrelation technique over the radiometer approach is given by

$$\left.\frac{SNR_0^{\text{correlation}}}{SNR_0^{\text{radiometer}}}\right|_{\lambda=1/2} \simeq \frac{1}{4}\left(G\,\gamma_{in}\right)^2 \qquad \text{(I-34)}$$

(The exact result is given in Table I.4 for all λ.)

Tables I.5 and I.6 compare the simulation results to the theoretical predictions with Gaussian approximations on variance calculations. The following observations can be made:

(1) Simulation results agree exceptionally well with theory for the mean values of the correlator detector outputs for all values of G, γ_{in} and λ. This is true since the theory for this part of the calculations is exact.

(2) Simulation results show that the variance of the detector output Y under H_1 can be quite a bit larger than that under H_0 for high γ_{in} values. Also, simulation results on the variance of Y is generally larger than the approximated theoretical predictions for $\lambda > 0.1$, where Gaussian approximations used in computing the variance of Y began to lose validity.

Based on the autocorrelation detector mean and variance simulation results, the probability of detection versus γ_{in} for various P_{FA} settings are computed. These results are summarized in Figures I.4 and I.5. The improvement in performance of the autocorrelation technique as BT_H increases from 100 (Figure I.4) to 1000 (Figure I.5) is apparent. The truncation factor λ in Figure I.4 is 0.5, while that in Figure I.5 is 0.1. The performance is relatively insensitive with respect to λ as long as λ is > 0.1 and is < 0.8. This λ dependence is illustrated in Figure I.6, where the probability of detection is plotted against λ for various P_{FA} (10^{-2}, 10^{-4} and 10^{-6}) settings and at various γ_{in} (-5, -10, and -20 dB) for the case $BT_H = 100$. Thus, we can regard Figures I.4 and I.5 to be the representative performance of the autocorrelation technique for $BT_H = 100$ and 1000, respectively.

Table I.5. Comparison of Autocorrelation Detector Simulation Results to Approximated Analysis

(a) $BT_H = 100$; $\lambda = 0.01$

γ_{in} (dB)	-20 dB		-10 dB		-5 dB	
Theory or Simulation	Theory	Simulation	Theory	Simulation	Theory	Simulation
$\mathcal{E}(Y\|H_0)$	0.38	0.378	0.38	0.392	0.38	0.384
$\mathcal{E}(Y\|H_1)$	0.39	0.390	0.82	0.826	4.2	4.24
$\text{var}(Y\|H_0)$	0.016	0.0251	0.016	0.0215	0.016	0.021
$\text{var}(Y\|H_1)$	-	0.0274	-	0.0235	-	4.1
Autocorrelation Detector SNR_0 (dB)	-21.1	-22.5	10.74	9.42	29.64	28.57

(b) $BT_H = 100$; $\lambda = 0.5$

γ_{in} (dB)	-20 dB		-10 dB		-5 dB	
Theory or Simulation	Theory	Simulation	Theory	Simulation	Theory	Simulation
$\mathcal{E}(Y\|H_0)$	2.7	2.76	2.7	2.69	2.7	2.695
$\mathcal{E}(Y\|H_1)$	2.786	2.84	5.22	5.22	24	23.75
$\text{var}(Y\|H_0)$	0.156	0.6	0.156	0.633	0.156	0.708
$\text{var}(Y\|H_1)$	-	0.665	-	6.22	-	91.4
Autocorrelation Detector SNR_0 (dB)	-14.56	-19.5	16.0	10.04	34.6	28

Table I.5. Comparison of Autocorrelation Detector Simulation Results to Approximated Analysis

(c) $BT_H = 1000$; $\lambda = 0.1$

γ_{in} (dB)	-20 dB		-15 dB		-10 dB	
Theory or Simulation	Theory	Simulation	Theory	Simulation	Theory	Simulation
$\mathcal{E}(Y\|H_0)$	0.417	0.419	0.417	0.419	0.417	0.42
$\mathcal{E}(Y\|H_1)$	0.47	0.472	0.84	0.863	4.46	4.57
$\text{var}(Y\|H_0)$	1.76×10^{-3}	2.61×10^{-3}	1.76×10^{-3}	2.6×10^{-3}	1.76×10^{-3}	2.61×10^{-3}
$\text{var}(Y\|H_1)$	-	4.97×10^{-3}	-	5.34×10^{-2}	-	1.41
Autocorrelation Detector SNR_0 (dB)	1.16	0.17	20.06	18.76	39.7	38.2

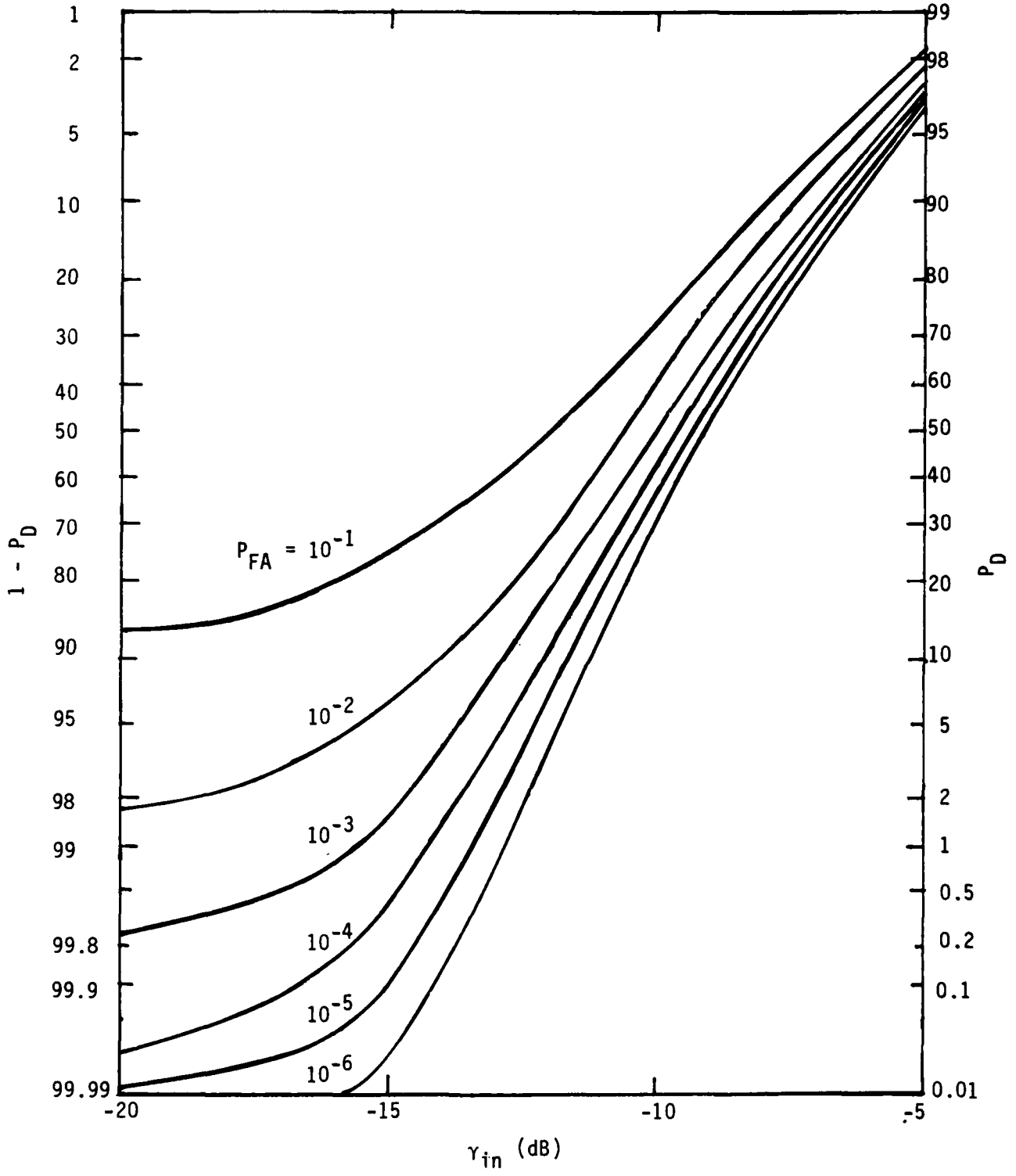

Figure I.4. Autocorrelation Method Simulation Results:
BT = 100; λBT = 50

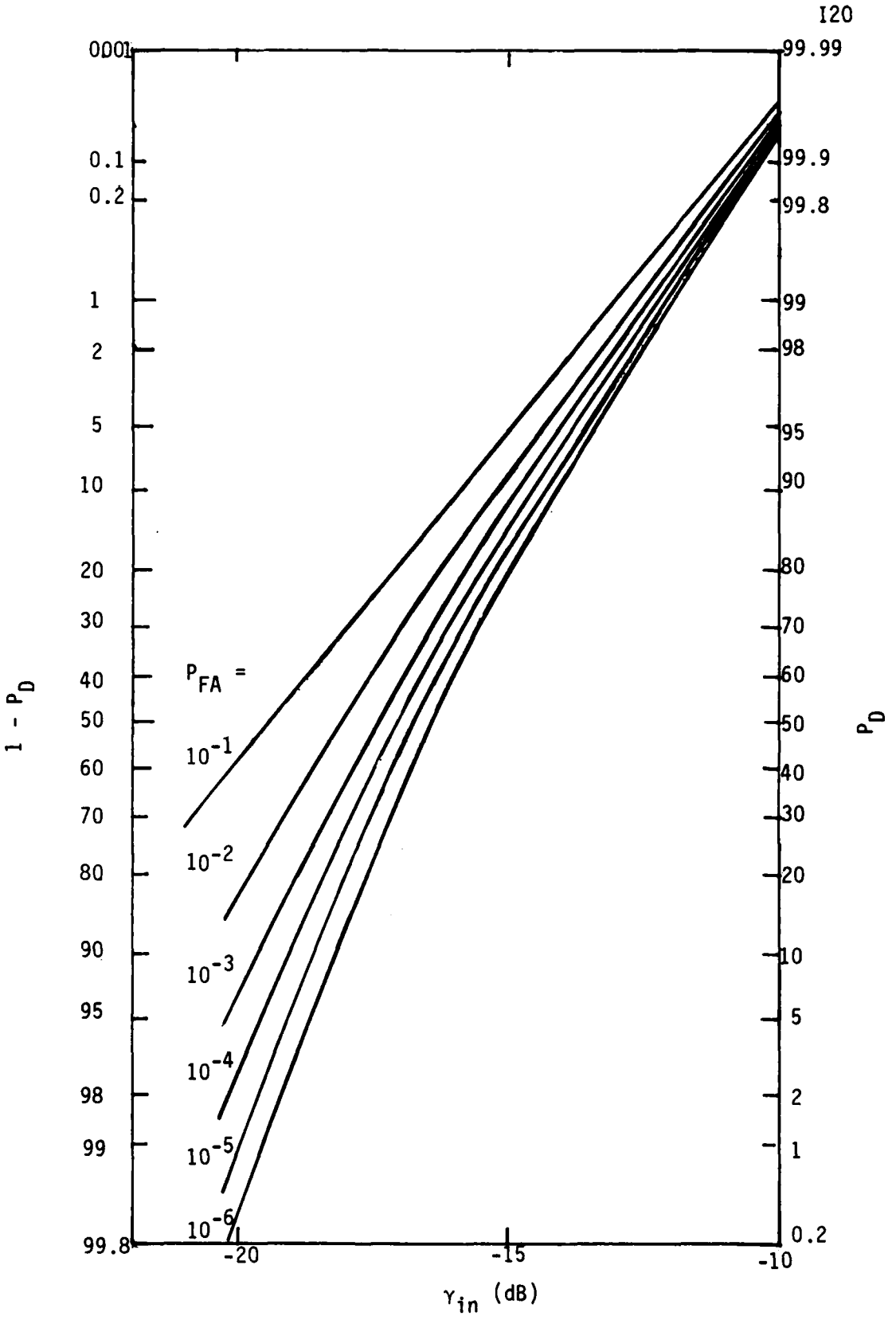

Figure I.5. Autocorrelation Method Simulation Results: BT = 1000; λ = 0.1

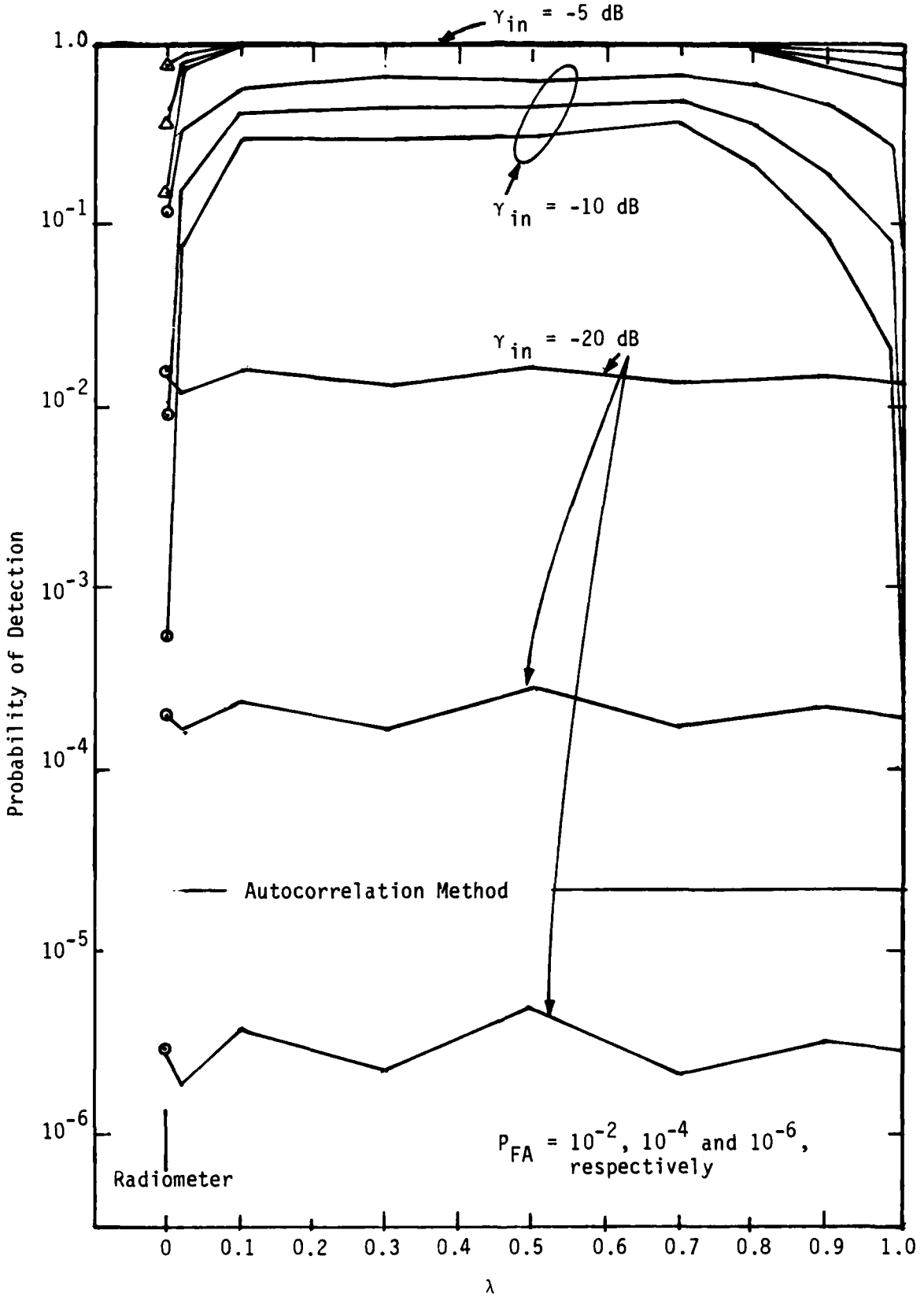

Figure I.6. Simulation Results: Effect of λ on Detector Performance; BT = 100

5.0 RELATIVE COMPARISON OF RADIOMETER AND AUTOCORRELATION TECHNIQUES IN DETECTING FH SIGNALS

Relative performances of the radiometer and autocorrelation techniques in detecting FH signals can be compared two different ways: (1) their detector output SNR (as defined in (I-1)), or (2) their operating characteristics P_D and P_{FA} (in particular, in terms of the required input SNR γ_{in} for the specified P_{FA} and P_D).

Table I.6 compares the two techniques in terms of their respective output SNR's as functions of BT_H and γ_{in}. As shown in Table I.6, the SNR_0 of the autocorrelation technique is significantly improved over that of the radiometer, especially in large BT_H cases and with high γ_{in}. In typical systems, BT_H is large while γ_{in} is small ($BT_H = 1000$, $\gamma_{in} = -20$ dB). In that case, the autocorrelator's output SNR_0 is still $\approx$ 10 dB over that of the radiometer. As shown in Table I.6, the theoretical prediction on SNR_0 improvement agrees very well with simulation results. Thus, this relationship can be described, to a very good approximation, by the equation (see Table I.4):

$$\frac{SNR_0{}^{\text{autocorrelator}}}{SNR_0{}^{\text{radiometer}}} \cong \left(\frac{1-\lambda}{\lambda}\right)\left[\lambda G \gamma_{in} + 2\,\ell n\left(\frac{1}{1-\lambda}\right)\right]^2 \qquad \text{(I-35)}$$

Equation (I-35) indicates that this improvement, for a fixed λ, is essentially $\sim(G\,\gamma_{in})^2$, or $\gamma_H{}^2$.

A more detailed evaluation of the relative performances of these two approaches, which is probably more useful in terms of actual system design, is to compare their respective required input SNR (γ_{in}) for a specified set of P_{FA} and P_D. These data can be extracted from Figures I.2, I.3, I.4 and I.5. The results are plotted in Figures I.7 and I.8. The relative improvements of the autocorrelation approach over that of the radiometer, in terms of required γ_{in} to give specified P_{FA} and P_D, are summarized in Table I.7.

Table I.6. Relative Comparisons of Detector Output SNR's

(a) $BT_H = 100$; $\lambda = 0.1$

γ_{in} (dB)	Simulation			Theoretical Prediction of Autocorrelation SNR_0 Improvement Over Radiometer
	Radiometer SNR_0 (dB)	Autocorrelation SNR_0 (dB)	Improvement of Autocorrelation over Radiometer in SNR_0	
-20	-20.14	-22.5	-2.36 (dB)	-1.1 (dB)
-10	0.25	9.42	9.17	10.74
-5	9.98	28.57	18.6	19.64

(b) $BT_H = 1000$; $\lambda = 0.1$

γ_{in} (dB)	Simulation			Theoretical Prediction of Autcorrelation SNR_0 Improvement Over Radiometer
	Radiometer SNR_0 (dB)	Autocorrelation SNR_0 (dB)	Improvement of Autocorrelation Over Radiometer in SNR_0	
-20	-9.73	0.17	9.9 (dB)	11.6 (dB)
-15	0.14	18.76	18.62	20.06
-10	10.06	38.2	28.14	29.7

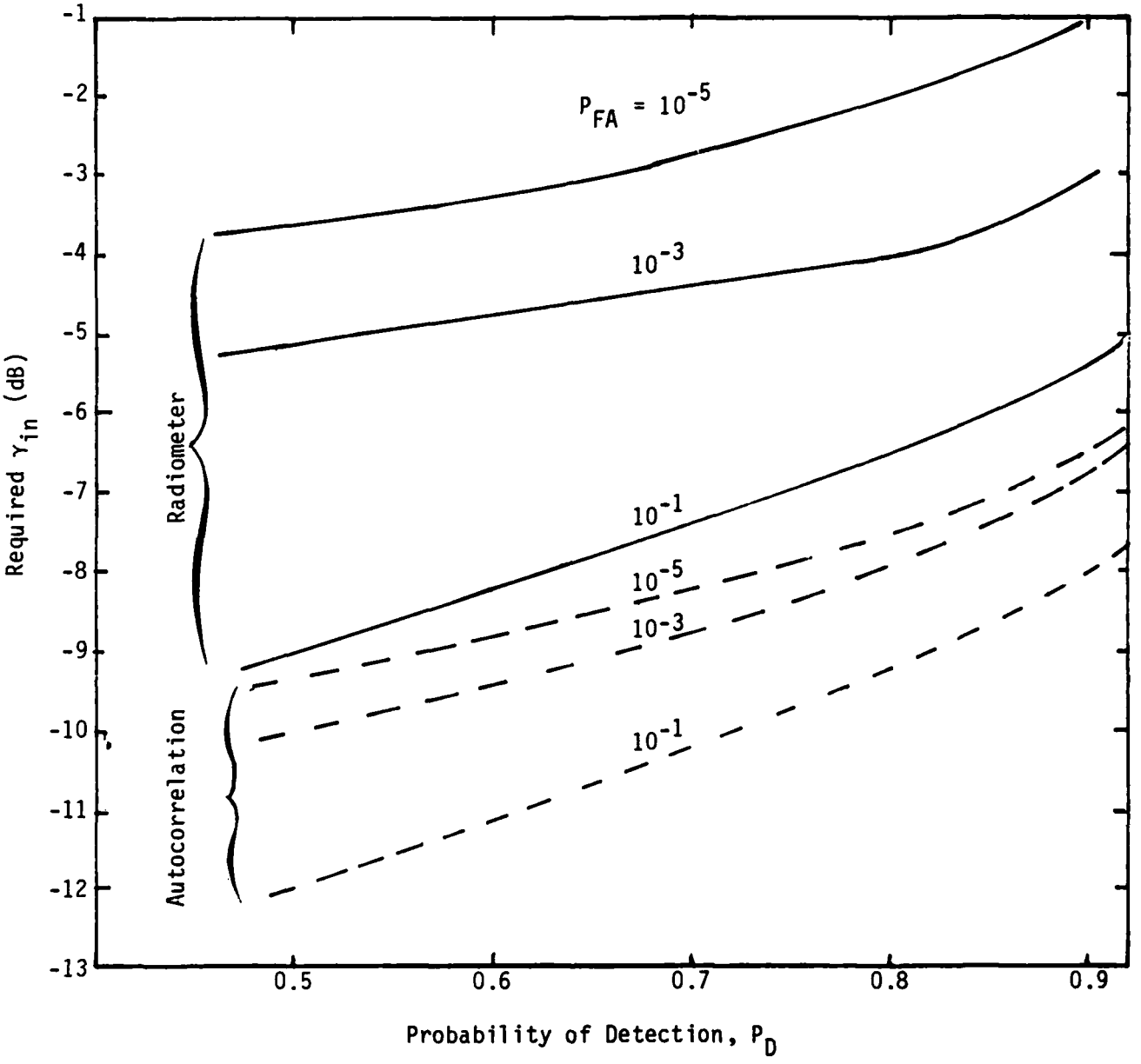

Figure I.7. Relative Comparison of Radiometer and Correlation-Detector Performance; $BT_H = 100$; $\lambda = 0.1$

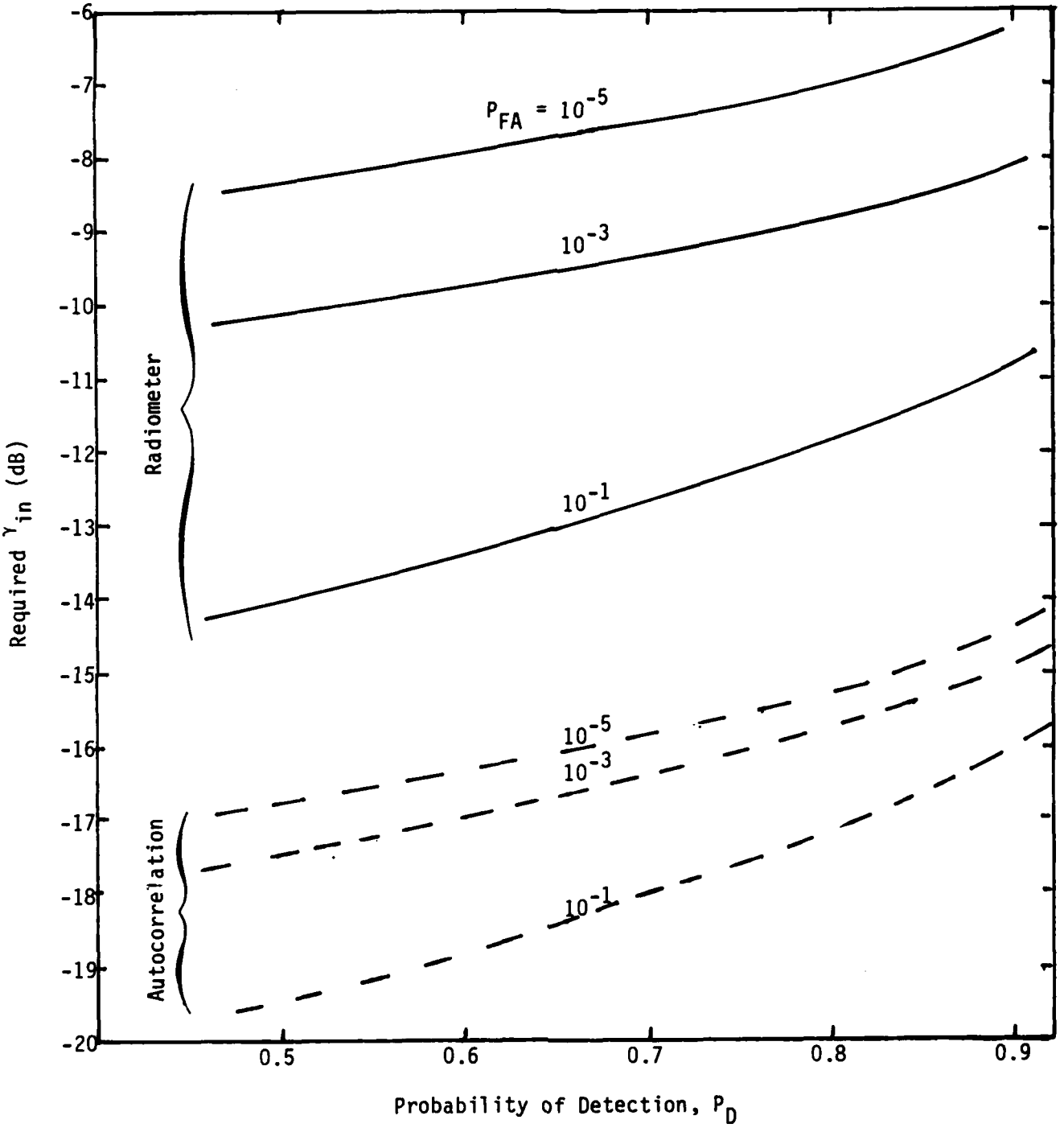

Figure I.8. Relative Comparison of Radiometer and Correlation-Detector Performances; $BT_H = 1000$; $\lambda = 0.1$

Table I.7. Relative Improvement of the Autocorrelation Technique Over the Radiometer Approach in terms of Required Input SNR γ_{in} For Desired P_D and P_{FA} Performances

BT_H	P_{FA}	Improvement of Autocorrelation Technique over Radiometer (dB)				
		$P_D = 0.9$	$P_D = 0.8$	$P_D = 0.7$	$P_D = 0.6$	$P_D = 0.5$
100	10^{-5}	5.4	5.5	5.5	5.6	5.7
	10^{-3}	3.8	4.0	4.4	4.6	4.8
	10^{-1}	2.6	2.7	2.8	2.9	3.0
1000	10^{-5}	8.3	8.3	8.4	8.4	8.5
	10^{-3}	6.8	7.0	7.1	7.3	7.5
	10^{-1}	5.2	5.3	5.4	5.4	5.5

APPENDIX J

STATISTICAL CHARACTERIZATION OF NOISE PROCESSES $n_k^{\alpha}(\tau)$ AND $n_0^{\beta}(\tau)$

Let

$$n_k^{\alpha}(\tau) = \alpha_k^I(\tau) \cos \omega_k \tau - \alpha_k^Q(\tau) \sin \omega_k \tau; \; k=1,\ldots,M \tag{J-1}$$

and

$$n_0^{\beta}(\tau) = \left(\sum_{k=1}^{M} \beta_k^I(\tau) \right) \cos \omega_0 \tau + \left(\sum_{k=1}^{M} \beta_k^Q(\tau) \right) \sin \omega_0 \tau \tag{J-2}$$

where

$$\alpha_k^I(\tau) = \int_{\tau}^{T_H} c(t) \cos\left(\Delta\omega_k t - \phi_k\right) dt \tag{J-3a}$$

$$\alpha_k^Q(\tau) = \int_{\tau}^{T_H} c(t) \sin\left(\Delta\omega_k t - \phi_k\right) dt \tag{J-3b}$$

$$\beta_k^I(\tau) = \int_{\tau}^{T_H} c(t-\tau) \cos\left(\Delta\omega_k t - \phi_k\right) dt \tag{J-3c}$$

and

$$\beta_k^Q(\tau) = \int_{\tau}^{T_H} c(t-\tau) \sin\left(\Delta\omega_k t - \phi_k\right) dt \tag{J-3d}$$

with $\Delta\omega_k = \omega_0 - \omega_k$. Equations (J-1) through (J-3) are also given by (5-42) and (5-43). First, since c(t) is a random code with $\mathcal{E}\{c(t)\} = 0$, it follows that the noise processes in (J-1) and (J-2) are zero mean, and that

$$\text{var}\left\{\alpha_k^j(\tau)\right\} = \text{var}\left\{\beta_k^j(\tau)\right\} = \mathcal{E}\left\{\left(\alpha_k^I(\tau)\right)^2\right\} \tag{J-4}$$

We shall first establish (5-47), i.e., claim (a) in section 5.2.2. We have from (J-3a) that

$$\alpha_k^I(mT_c) = \int_{mT_c}^{T_H} c(t) \cos\left[(\Delta\omega_k)t - \phi_k\right] dt = \sum_{n=m}^{N-1} c_{n+1} \int_{nT_c}^{(n+1)T_c} \cos\left[(\Delta\omega_k)t - \phi_k\right] dt$$

$$\triangleq \sum_{n=m}^{N-1} c_{n+1}\, I_{n+1} \qquad \text{(J-5)}$$

where c_{n+1} is the $(n+1)^{th}$ code chip and

$$I_{n+1} \triangleq \int_{nT_c}^{(n+1)T_c} \cos\left[(\Delta\omega_k)t - \phi_k\right] dt \qquad \text{(J-6)}$$

Let $\underline{c} = \left[c_1, \ldots, c_N\right]$. Then,

$$\mathcal{E}\left\{\left(\alpha_k^I(mT_c)\right)^2\right\} = \mathcal{E}_{\phi_k}\left\{\mathcal{E}_{\underline{c}|\phi_k}\left\{\left(\alpha_k^I(mT_c)\right)^2 \middle| \phi_k\right\}\right\}$$

$$= \mathcal{E}_{\phi_k}\left\{\mathcal{E}_{\underline{c}|\phi_k}\left\{\sum_{n=m}^{N-1}\sum_{n'=m}^{N-1} c_{n+1}\, c_{n'+1}\, I_{n+1}\, I_{n'+1}\right\}\right\} \qquad \text{(J-7)}$$

But

$$\mathcal{E}\left\{c_{n+1}\, c_{n'+1}\right\} = \delta_{nn'} = \begin{cases} 1 & , \text{ if } n=n' \\ 0 & , \text{ otherwise} \end{cases}$$

which reduces (J-7) to

$$\mathcal{E}\left\{\left(\alpha_k^I(mT_c)\right)^2\right\} = \mathcal{E}_{\phi_k}\left\{\sum_{n=m}^{N-1} I_{n+1}^2\right\} = \sum_{n=m}^{N-1} \mathcal{E}_{\phi_k}\left\{I_{n+1}^2\right\} \qquad \text{(J-8)}$$

However,

$$\mathcal{E}_{\phi_k}\left\{I_{n+1}^2\right\} = \mathcal{E}_{\phi_k}\left\{\left(\cos\phi_k \int_{nT_c}^{(n+1)T_c} \cos(\Delta\omega_k t)dt + \sin\phi_k \int_{nT_c}^{(n+1)T_c} \sin(\Delta\omega_k t)dt\right)^2\right\}$$

$$= \left(\frac{1}{2}\right)\left[\left(\int_{nT_c}^{(n+1)T_c} \cos(\Delta\omega_k t)dt\right)^2 + \left(\int_{nT_c}^{(n+1)T_c} \sin(\Delta\omega_k t)dt\right)^2\right] \quad \text{(J-9)}$$

But

$$\int_a^b \cos(\Delta\omega_k t)dt = \left(\frac{1}{\Delta\omega}\right)\sin x\Big|_{(\Delta\omega)a}^{(\Delta\omega)b} = \left(\frac{1}{\Delta\omega}\right)\left[\sin(\Delta\omega)b - \sin(\Delta\omega)a\right] \quad \text{(J10-a)}$$

and

$$\int_a^b \sin(\Delta\omega_k t)dt = \left(\frac{1}{\Delta\omega}\right)\left[\cos(\Delta\omega)a - \cos(\Delta\omega)b\right] \quad \text{(J10-b)}$$

Upon inserting (J-10) into (J-9) and combining with (J-8), it follows that

$$\mathcal{E}\left\{\left(\alpha_k(mT_c)\right)^2\right\} = \frac{1}{2(\Delta\omega_k)^2}\sum_{n=m}^{N-1}\left[\left(\sin(n+1)(\Delta\omega_k)T_c - \sin n(\Delta\omega_k)T_c\right)^2 + \left(\cos n(\Delta\omega_k)T_c - \cos(n+1)(\Delta\omega_k)T_c\right)^2\right]$$

$$= \frac{1}{2(\Delta\omega_k)^2}\sum_{n=m}^{N-1}\left[2 - 2\cos(\Delta\omega_k)T_c\right] = \frac{2\sin^2\left[\frac{\Delta\omega_k T_c}{2}\right]}{(\Delta\omega_k)^2}(N-m)$$

or

$$\mathcal{E}\left\{\left(\alpha_k^I(mT_c)\right)^2\right\} = \frac{(N-m)T_c^2}{2}\,Sa^2\left[(\Delta\omega_k)\frac{T_c}{2}\right] \quad \text{(J-11)}$$

which is (5-47).

We shall now proceed to prove claim (b), namely, that each noise process $n_k^{\alpha}(\tau);k=1,\ldots,M$ and $n_0^{\beta}(\tau)$ have uncorrelated (and, by the Gaussian assumption, independent) inphase and quadrature components. From (J-3a) and (J-3b), we can write

$$\alpha_k^I(\tau) = A_k^I \cos \phi_k + A_k^Q \sin \phi_k \tag{J-12a}$$

and

$$\alpha_k^Q(\tau) = A_k^Q \cos \phi_k - A_k^I \sin \phi_k \tag{J-12b}$$

where we define the random variables A_k^Q and A_k^I as

$$A_k^I = \int_{\tau}^{T_H} c(t) \cos \Delta\omega_k t \, dt \tag{J-13a}$$

and

$$A_k^Q = \int_{\tau}^{T_H} c(t) \sin \Delta\omega_k t \, dt \tag{J-13b}$$

Thus, from (J-12),

$$\begin{aligned} \mathcal{E}\left\{\alpha_k^I(\tau)\alpha_k^Q(\tau)\right\} &= \mathcal{E}_{\underline{c}}\left\{\mathcal{E}_{\phi_k|\underline{c}}\left\{\alpha_k^I(\tau)\alpha_k^Q(\tau)\right\}\right\} = \mathcal{E}_{\underline{c}}\left\{A_k^I A_k^Q \, \mathcal{E}_{\phi_k}\left\{\cos^2\phi_k - \sin^2\phi_k\right\}\right. \\ &\qquad \left. + \left[\left(A_k^Q\right)^2 - \left(A_k^I\right)^2\right] \cdot \mathcal{E}_{\phi_k}\left\{\sin\phi_k \cos\phi_k\right\}\right\} \\ &= \mathcal{E}_{\underline{c}}\left\{A_k^I A_k^Q\right\} \mathcal{E}_{\phi_k}\left\{\cos 2\phi_k\right\} + \frac{\mathcal{E}_{\underline{c}}\left\{\left(A_k^Q\right)^2 - \left(A_k^I\right)^2\right\}}{2} \mathcal{E}_{\phi_k}\left\{\sin 2\phi_k\right\} = 0 \end{aligned} \tag{J-14}$$

which proves the uncorrelatedness of $\alpha_k^I(\tau)$ and $\alpha_k^Q(\tau)$. In a similar manner, $\beta_k^I(\tau)$ and $\beta_k^Q(\tau)$ are shown to be uncorrelated. Furthermore, $\beta_k^I(\tau)$ and $\beta_m^Q(\tau)$ for $k \neq m$ are also uncorrelated since they correspond to independent phases ϕ_k and ϕ_m. This implies that the random variables

$$\sum_{k=1}^{M} \beta_k^I(\tau) \qquad \text{and} \qquad \sum_{k=1}^{M} \beta_k^Q(\tau)$$

which constitute the inphase and quadrature components of $n_0^{\beta}(\tau)$, are uncorrelated. This concludes the proof of claim (b).

The proof of claim (c) is based on the simple fact that

$$\mathcal{E}\left\{\alpha_k^j(\tau)\ \alpha_m^j(\tau)\right\} = 0\ ;\ k\neq m; j=I,Q \tag{J-15}$$

since ϕ_k and ϕ_m are independent (see (J-3)). Finally, in order to substantiate claim (d), we look at $n_k^{\alpha}(\tau)$ at $\tau = 0$ and $\tau = T_c$. Then,

$$\alpha_k^I(0) = \int_0^{T_H} c(t)\cos\left(\Delta\omega_k t - \phi_k\right)dt = \int_0^{T_c} c(t)\cos\left(\Delta\omega_k t - \phi_k\right)dt + \alpha_k^I(T_c)$$

$$\approx \alpha_k^I(T_c) \tag{J-16}$$

since the first term (integral from 0 to T_c) is negligible compared to the $(N-1)T_c$ integration involved in $\alpha_k^I(T_c)$. Thus, $\alpha_k(0)$ is almost equal to (i.e., very correlated with) $\alpha_k^I(T_c)$, and the same holds for $a_k^Q(\tau)$. It follows that $n_k^{\alpha}(\tau)$ is a highly correlated noise with respect to the T_c time interval. On the other hand,

$$\beta_k^I(0) = \int_0^{T_c} c(t)\cos\left(\Delta\omega_k t - \phi_k\right)dt \tag{J-17a}$$

while

$$\beta_k^I(T_c) = \int_{T_c}^{T_H} c(t - T_c)\cos\left(\Delta\omega_k t - \phi_k\right)dt$$

$$= \int_0^{T_H - T_c} c(t')\cos\left(\Delta\omega_k t' + \Delta\omega_k T_c - \phi_k\right)dt'$$

$$\approx \beta_k^I(0)\cos\left(\Delta\omega_k T_c\right) - \beta_k^Q(0)\sin\left(\Delta\omega_k T_c\right) \tag{J-17b}$$

Thus, the degree of correlation between $n_k^I(0)$ and $\beta_k^I(T_c)$ depends on the phase shift $\Delta\omega_k T_c$. If, for instance, $(f_0-f_k)T_c = 0$ or 1/2 or 1, then $\beta_k^I(0)$ and $\beta_k^I T_c$ are highly correlated while, if $(f_0-f_k)T_c = 1/4$ or 3/4, then $\beta_k^I(T_c) \approx \beta_k^Q(0)$, which is uncorrelated with $\beta_k^I(0)$! Since similar rules hold for $\beta_k^Q(\tau)$, we conclude that the correlation time of the noise $n_0^\beta(\tau)$ varies with $(\Delta f_k)T_c$. For the particular case of one interfering tone on the signal frequency, i.e., $f_1 = f_0$, it is concluded that $n_1^\beta(0) \approx n_1^\beta(T_c)$, resulting in a highly correlated noise (which is a favorable case here).

APPENDIX K

PROOF OF EQUATION (5.52)

From (5-50), we have that

$$\Delta = \frac{(ST_H)^2}{2}\left[1 + 2\gamma_I^{-1}\left(1 + 2\sqrt{\gamma_I}\, a_{1,norm}\right)\right] \tag{K-1}$$

where

$$a_{1,norm} = \left(\frac{T_c}{T_H}\right)\cos\phi_1 \sum_{n=1}^{N} c_n \tag{K-2}$$

Clearly, $\mathcal{E}\{a_{1,norm}\} = 0$; which, upon substitution in (K-1), immediately yields (5-52a). Furthermore, from (K-1) and (5-52a),

$$\text{var}\{\Delta|H_1\} = \text{var}\left\{2(ST_H)^2\,\gamma_I^{-1/2}\,a_{1,norm}\right\} = 4(ST_H)^4\,\gamma_I^{-1}\,\text{var}\{a_{1,norm}\}$$

$$= 4(ST_H)^4\,\gamma_I^{-1}\left(\frac{T_c}{T_H}\right)^2\left(\frac{1}{2}\right)\cdot N \tag{K-3}$$

since $\text{var}\{\cos\phi_1\} = 1/2$ and the c_n's are independent, so that

$$\text{var}\left\{\sum_{n=1}^{N} c_n\right\} = N\cdot\text{var}\{c_n\} = N$$

If we recall that $N \triangleq T_H/T_c$, we conclude from (K-3) that

$$\text{var}\{\Delta|H_1\} = \frac{2(ST_H)^4}{N\gamma_I} \tag{K-4}$$

i.e., (5-52b).

APPENDIX L

RADIOMETER PERFORMANCE FOR THE FH/DS CASE WITH RANDOM TONE INTERFERENCE

The radiometer output $Y_{rad} = y(0)$ can be written as

$$Y_{rad} = ST_H + MI_1T_H + 2\sqrt{SI_1}\left[\sum_{k=1}^{M} \alpha_k^I(0)\right] \tag{L-1}$$

where I_1 is the power per tone, so the total power for M tones is $I = MI_1$. In our formulation, M is a random variable, taking values in the set $[1,2,\ldots,M_{max}]$ with equal probability in each hop. Conditioned on M, the mean and variance of Y_{rad} are

$$\mathcal{E}\{Y_{rad}|M\} = ST_H + MI_1T_H = (S + MI_1)T_H \tag{L-2}$$

and

$$\text{var}\{Y_{rad}|M\} = 4SI_1\,\mathcal{E}\left\{\left(\sum_{k=1}^{M} \alpha_k^I(0)\right)^2 \middle| M\right\} = 4SI_1 \sum_{k=1}^{M} \mathcal{E}\left\{\left(\alpha_k^I(0)\right)^2\right\} \tag{L-3}$$

where we have used the fact that $\alpha_k^I(0)$ and $\alpha_m^I(0)$ are uncorrelated for $k \neq m$. (See Appendix J.) Furthermore, the second moment of $\alpha_k^I(0)$ is given by equation (5-47) which, upon substitution in (L-3) for m=0 yields

$$\text{var}\{Y_{rad}|M\} = 2SI_1\,NT_c^2 \sum_{k=1}^{M} \text{Sa}^2\left[\pi(f_0-f_k)T_c\right] = 2SI_1\,T_H\,T_c\,L(M) \tag{L-4}$$

where

$$L(M) \triangleq \sum_{k=1}^{M} \text{Sa}^2\left[\pi(f_0-f_k)T_c\right] \tag{L-5}$$

and the fact that $T_H = NT_c$ has been used.

Under the Gaussian assumption for Y_{rad} (conditioned on M), we can easily derive the conditional detection probability under hypothesis H_1 as

$$P_{D|M}^{rad} = Pr\left\{ Y_{rad} > Y_0 \middle| M, H_1 \right\} = Q\left[\frac{Y_0 - (S+MI_1)T_H}{\sqrt{2SI_1T_HT_cL(M)}} \right] \qquad \text{(L-6)}$$

where Y_0 is the detection threshold and equations (L-2) through (L-5) have been used. Clearly, under H_0, the first and third terms in (L-1) disappear, so that

$$Y_{rad} = MI_1T_H \qquad \text{under } H_0 \qquad \text{(L-7)}$$

with probability 1. This implies that the conditional false-alarm probability is two valued:

$$P_{FA|M}^{rad} = \begin{cases} 1 \text{ , if } MI_1T_H > Y_0 \\ 0 \text{ , if } MI_1T_H \leq Y_0 \end{cases} \qquad \text{(L-8)}$$

In deriving (L-8), we have implicitly assumed that the detector decides H_0 whenever the radiometer output Y_{rad} is exactly equal to the threshold Y_0.

If we now insert the equidistribution assumption about M between 1 and M_{max}, we can average (L-6) or (L-8) with respect to M in order to obtain the overall P_D^{rad} and P_{FA}^{rad}. Thus,

$$P_D^{rad} = \mathcal{E}_M\left\{P_{D|M}^{rad}\right\} = \frac{1}{M_{max}} \sum_{M=1}^{M_{max}} Q\left[\frac{Y_0 - (S+MI_1)T_H}{\sqrt{2SI_1T_HT_cL(M)}} \right] \qquad \text{(L-9)}$$

while

$$P_{FA}^{rad} = 1 - \frac{M_{Y_0}}{M_{max}} \qquad \text{(L-10a)}$$

where M_{Y_0} is the largest integer not exceeding Y_0/I_1T_H, i.e.,

$$M_{Y_0} = \begin{cases} \left\lfloor \frac{Y_0}{I_1 T_H} \right\rfloor & \text{if} \quad \frac{Y_0}{I_1 T_H} \leq M_{max} \\ M_{max} & \text{if} \quad \frac{Y_0}{I_1 T_H} > M_{max} \end{cases} \tag{L-10b}$$

In (L-10b), $\lfloor \cdot \rfloor$ denotes "integer part of." Furthermore, for a desired P_{FA}^{rad} level, M_{Y_0} can be calculated. Then, Y_0 should be chosen at the lowest allowable level in order to maximize P_D^{rad}. Clearly, this choice is

$$Y_0 = M_{Y_0} I_1 T_H = M_{max}\left(1 - P_{FA}^{rad}\right) I_1 T_H \tag{L-11}$$

We note that, in the case treated here, i.e., no thermal noise, P_{FA}^{rad} can assume only discrete (quantized) values, as dictated by (L-10a). In other words, P_{FA}^{rad} can only be of the form

$$P_{FA}^{rad} = k \cdot \frac{1}{M_{max}} \; ; \; k=0,1,\ldots, M_{max} \tag{L-12}$$

We can now combine (L-9) with (L-11) in order to get the radiometer's operating characteristic as

$$P_D^{rad} = \frac{1}{M_{max}} \sum_{M=1}^{M_{max}} Q\left[\frac{M_{max}\left(1 - P_{FA}^{rad}\right) - M - \left(\frac{S}{I_1}\right)}{\sqrt{2\left(\frac{S}{I_1}\right) T_c \, L(M)}} \sqrt{T_H} \right] \tag{L-13}$$

If we let γ_1 denote the signal to single-tone power ratio

$$\gamma_1 \triangleq \frac{S}{I_1} \tag{L-14}$$

and recall that $N \triangleq T_H/T_c$, we conclude that

$$P_D^{rad} = \frac{1}{M_{max}} \sum_{M=1}^{M_{max}} Q\left[\frac{M_{max}\left(1 - P_{FA}^{rad}\right) - \gamma_1 - M}{\sqrt{2\gamma_1 \cdot N^{-1} \cdot \sum_{k=1}^{M} Sa^2\left[\pi(f_0 - f_k)T_c\right]}}\right] \qquad \text{(L-15)}$$

$$\text{with } P_{FA}^{rad} = k/M_{max};\ k=0,\ldots,M_{max}$$

As an interesting side result, let us consider the limiting case where $N \to +\infty$, i.e., the DS code rate is much larger than the FH rate. Since this would correspond to $T_c \to 0$ (for a fixed T_H), we conclude that

$$\lim_{N\to+\infty} \sum_{k=1}^{M} Sa^2\left[\pi(f_0 - f_k)T_c\right] = \sum_{k=1}^{M} \lim_{T_c\to 0} Sa^2\left[\pi(f_0 - f_k)T_c\right] = M \qquad \text{(L-16)}$$

since $\lim_{x\to 0} Sa^2(x) = 1$. Therefore, the whole *denominator of the $Q(\cdot)$ functions in* (L-15) tends to zero,

$$\lim_{N\to\infty} \frac{2\gamma_1 \cdot M}{N} = 0$$

which implies that

$$\lim_{N\to+\infty} Q(\cdot) = \begin{cases} 1 & \text{if } M > M_{max}\left(1 - P_{FA}^{rad}\right) - \gamma_1 \\ 0 & \text{if } M < M_{max}\left(1 - P_{FA}^{rad}\right) - \gamma_1 \end{cases} \qquad \text{(L-17)}$$

Therefore, from (L-16) and (L-17),

$$\lim_{N\to+\infty} P_D^{rad} = \frac{M_{max} - M_D + 1}{M_{max}} = 1 - \frac{M_D - 1}{M_{max}} \qquad \text{(L-18)}$$

where M_D is the minimum M such that $M > M_{max}\left(1 - P_{FA}^{rad}\right) - \gamma_1$. Equation (L-18) can be rewritten in the final, more compact, form, i.e.,

$$\lim_{N\to+\infty} P_D^{rad} = 1 - \frac{\max\left(\left\lfloor M_{max}\left(1 - P_{FA}^{rad}\right) - \gamma_1 \right\rfloor + 1, 1\right) - 1}{M_{max}} \qquad \text{(L-19)}$$

So, for instance, for $M_{max} = 2$, it is easily derived from (L-19) that

$$\lim_{\substack{N\to+\infty \\ \gamma_1\to 0}} P_D^{rad} = \begin{cases} 1/2 & \text{if } P_{FA} = 0 \\ 1 & \text{if } P_{FA} = 1/2 \end{cases}$$

as expected. More generally, for an arbitrary M_{max},

$$\lim_{\substack{N\to+\infty \\ \gamma_1\to 0}} P_D^{rad} = P_{FA}^{rad} + \frac{1}{M_{max}}$$

The case treated in the text, $M_{max} = 1$, is slightly different from that which is presented in this appendix. In particular, let us assume that in each hop, either none or one interfering tone can be present with equal probability, i.e.,

$$Pr[M=0] = Pr[M=1] = 1/2 \qquad \text{(L-20)}$$

Then,

$$P_{D|1}^{rad} = Q\left[\frac{M_{max}\left(1 - P_{FA}^{rad}\right) - \gamma_I - 1}{\sqrt{2\gamma_I N^{-1}}}\right] = 1 - Q\left[\frac{\gamma_I + 1 - M_{max}\left(1 - P_{FA}^{rad}\right)}{\sqrt{2\gamma_I N^{-1}}}\right] \qquad \text{(L-21)}$$

where

$$\gamma_I \triangleq \gamma_1 \triangleq \frac{S}{I} \qquad \text{(L-22)}$$

and we have assumed that $f_1 = f_0$ (interference centered on signal frequency). Here, $M_{max} = 1$. Furthermore, if we wish to have $P_{FA}^{rad} = 0$, we should set the

threshold $Y_0 = IT$. Then, under signal present (H_1) but tone absent $(M = 0)$ conditions, it follows that

$$Y_{rad} = ST_H \qquad (M = 0) \tag{L-23}$$

Clearly, this output will result in an H_1 (correct) decision if and only if:

$$ST_H > Y_0 = IT_H \Leftrightarrow S > I \Leftrightarrow \gamma_I > 1 \tag{L-24}$$

Thus,

$$P_{D|M=0}^{rad} = \begin{cases} 1, \text{ if } \gamma_I > 1 \\ 0, \text{ otherwise} \end{cases} \tag{L-25}$$

For the same desired level $P_{FA}^{rad} = 0$, (L-21) yields

$$P_{D|1}^{rad} = 1 - Q\left[\sqrt{\frac{N\gamma_I}{2}}\right] \tag{L-26}$$

The final detection performance is the average between (L-25) and (L-26), and is given by

$$P_D^{rad} = \frac{1}{2}\left(P_{D|M=1}^{rad} + P_{D|M=0}^{rad}\right) = \begin{cases} 1 - \frac{1}{2} Q\left[\sqrt{\frac{N\gamma_I}{2}}\right] & \text{if } \gamma_I > 1 \\ \frac{1}{2}\left(1 - Q\left[\sqrt{\frac{N\gamma_I}{2}}\right]\right) & \text{if } \gamma_I < 1 \end{cases}$$

$$P_{FA}^{rad} = 0$$

as per (5-55).

APPENDIX M

SIMULATION OF THE FH/DS CASE IN RANDOM TONE INTERFERENCE

The received signal is given by

$$r(t) = \sqrt{2S}\, c(t) \cos \omega_0 t + \sqrt{2I} \cos(\omega_1 t + \phi_1) \tag{M-1}$$

Recall from the text that

$$N = R_c/R_H \tag{M-2}$$

with R_c representing the code rate and R_H being the hop rate. The real-time autocorrelator is specified by

$$y(\tau) = \int_{\tau}^{T_H} r(t)\, r(t-\tau)dt \qquad 0 \leq \tau \leq T_H \tag{M-3}$$

Letting $\omega_0 = \omega_1$ with unknown phase difference ϕ_1 and putting (M-1) in (M-3) yields

$$y(\tau) = S\, y_c(\tau) \cos \omega_0 \tau + I(T_H - \tau)\cos \omega_1 \tau + \sqrt{SI}\, \left(n_1^{\alpha}(\tau) + n_0^{\beta}(\tau)\right) \tag{M-4}$$

with

$$n_1^{\alpha}(\tau) = \alpha_1^I(\tau) \cos \omega_1 - \alpha_1^Q(\tau) \sin \omega_1 \tau \tag{M-5}$$

$$n_0^{\beta}(\tau) = \beta_1^I(\tau) \cos \omega_0 \tau + \beta_1^Q(\tau) \sin \omega_0 \tau \tag{M-6}$$

$$\alpha_1^I(\tau) = \cos \phi_1 \int_{\tau}^{T_H} c(t)dt \tag{M-7}$$

$$\alpha_1^Q(\tau) = -\sin \phi_1 \int_{\tau}^{T_H} c(t)dt \tag{M-8}$$

$$\beta_1^I(\tau) = \cos \phi_1 \int_{\tau}^{T_H} c(t-\tau)dt \tag{M-9}$$

$$\beta_1^Q(\tau) = -\sin \phi_1 \int_{\tau}^{T_H} c(t-\tau)dt \tag{M-10}$$